Targeting the complexity of the mouse olfactory system

Thesis submitted for the degree of Philosophiæ Doctor

International School for Advanced Studies

S.I.S.S.A. / I.S.A.S.

Candidate

Giovanni Pascarella

Supervisor

Prof. Stefano Gustincich

2008

Declaration

I declare that this thesis was composed by me and the research presented is my own unless otherwise stated.

Giovanni Pascarella, 2008

Abstract

In recent years the research on the olfactory system has entered a phase of deep innovation, regardless of the animal model taken as a reference.

While the advancements achieved in different fields have provided answer to old questions, the striking evidences that have emerged in this new olfactory landscape have brought new ideas, new hypothesis and new scientific problems that necessarily need to be approached with adequate tools and strategies. The work presented in this thesis has targeted three different issues among the more intriguing ones concerning the murine olfactory system.

The project described in the first section has confronted with the molecular identity of the Calcium-activated chloride channel responsible for the amplification of cationic currents in olfactory sensory neurons, a key mechanism for the triggering of action potentials after binding of odour molecules with their specific receptors.

Olfactory microvillar cells constitute a cell population largely represented in the main olfactory epithelium, but their role is still poorly understood mostly because a precise genomic characterization of this cell-type has never been undertaken; the project presented in the second section has tried to reveal the genomic fingerprint of microvillar cells through a custom gene expression profiling.

The data presented in the third section of this thesis are the result of a deep genomic investigation that has targeted the entire transcriptome of the olfactory sensory epithelium exploiting a newly developed high-throughput tagging approach derived from the Cap-Analysis of Gene Expression (CAGE) technology. The potential of this workflow has allowed revealing new details about the expression of pheromone vomeronasal receptors in the main olfactory epithelium.

Table of contents

Introduction

Examples of how the complexity of the surrounding environment has driven the evolution of species are very easy to be found in nature.
Every single component of a living unit can be interpreted as a reflection of its need for adaptation to this complexity, but if a deep comprehension of this need has to be achieved there is no better way than the one that goes through the mysteries of animal senses.
No living organism may miss the ability to sense changes in the environment and adapt to them. For the more complex, multiorgans species, the development of keen specialized structures designed to collect crucial cues from the environment has represented the key to their survival, proliferation and colonization of water and land.

While the common meaning given to the word ”olfaction” refers to the sensitiveness to volatile chemical substances (chemoreception), animals living in the aquatic world like fishes and crustaceans have sensory structures resembling the anatomy of olfactory systems in land-based species (1-2).
The complexity of the outer world is reflected at the molecular level by a rich and yet unexplored array of odorous compounds. Different classes of odour signals convey information on the presence of food, water or an environmental danger (environmental odours), serve to communicate with conspecific mates and to ignite inborn behaviours (pheromones), help to locate a prey and to deter a predator, or are used for territorial marking, metamorphosis and growth (allelochemicals).
This wide landscape of different activities that could seem very difficult to be approached from an experimental point of view is further expanded by two considerations; the first one is that odour molecules rarely exist as single units: it is well established that complete biological responses are stimulated by complex multi-compound mixtures of odours, and that slight concentration differences of a single component between two almost identical mixtures can elicit different responses (3).
The latter is that, not considering microbes and small eukaryotes, odour mixtures are spread from point sources through turbulent air and water flow so that the recipient olfactory system will only be intermittently exposed to the stimulus in a way that is dependent on a high number of parameters which can be very difficult to control and reproduce in a laboratory environment (4).
Nevertheless, during the last twenty years some of the fundamental questions about olfaction have received landmark answers, including the molecular identity of olfactory receptors, the organization of their gene families in genomes of different species, the interpretation of how the olfactory

information is coded in discrete brain centres, the role of vomeronasal organ in species-specific communication. All of these discoveries have put a solid basis that can now be used to climb up to a more complete consciousness of what olfaction is, and that could eventually tell us something more about the role of this sense in our everyday life.

1. The olfactory system in mice: general overview.

Like all other mammalian species, mice have an olfactory system that is anatomically divided in two main functional units: the main olfactory epithelium (MOE) and the vomeronasal organ (VNO). The receptors responsible for sensing odour mixtures brought by the airflow are expressed in specialized neurons (olfactory sensory neurons and vomeronasal sensory neurons, OSNs and VSNs) that are localized in restricted areas within these two structures (fig. 1)

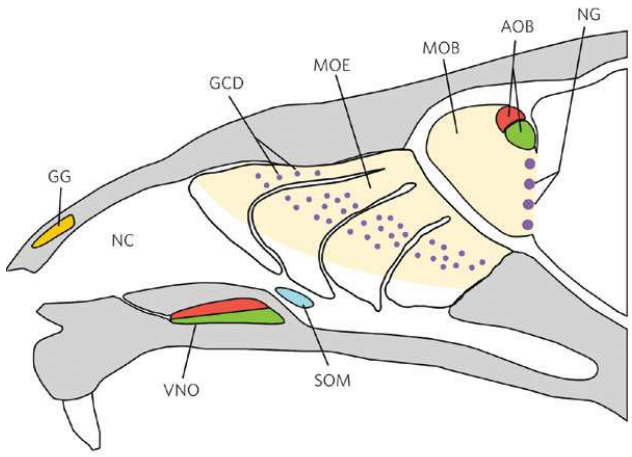

Figure 1: Mouse olfactory system. This picture shows a sagittal section of the head and highlights the foremost olfactory substructures. NC: nasal cavitiy; MOE: main olfactory epithelium; VNO: vomerosanal organ; GG: Grueneberg ganglion; SOM: septal organ of Masera; GCD: guanylate cyclase-D neurons; MOB: main olfactory bulb; AOB: accessory olfactory bulb; NG: necklace glomeruli. (Adapted from Brennan A., Zufall F, *Nature*, 2006).

The main olfactory epithelium is located in the posterior nasal cavity where it is arranged over multiple cartilaginous structures (turbinates); it can be morphologically distinguished from the pseudostratified non-sensory respiratory epithelium by its thickness.

Historically, the MOE has been considered the only component of the olfactory system responsible for volatile odours recognition; it is composed by at least four different cell populations (5) and each of these cell types occupies a specific position in the neuroepithelium (fig.2).

The basal layer of MOE is mainly composed by two populations of stem cells, defined as globose cells (GCs) and horizontal basal cells (HBCs). The olfactory epithelium is the only known district of the central nervous system which is capable of regeneration: being directly and continuously exposed to insults coming from the outer environment, the ability of this tissue to renew itself throughout the life of an individual is fundamental to prevent a loss of the sense of smell due to death of OSNs.

At present the olfactory epithelium is the best known model to study the differentiation of stem cells into neurons. This is mainly due to the fact MOE structurally resembles the embryonal differentiating neuroepithelium which gives rise to the central nervous system, but as far as it is known it contains only one type of sensory neuron, thus constituting a key system for the study of neurodifferentiation (6).

Olfactory sensory neurons, which occupy the middle layer of the MOE, are bipolar neurons with a specialized apical dendritic end which protrudes on the surface of the epithelium; in the superficial district, OSNs dendrites form a typical button-like structure (knob) that is covered by specialized membranous cilia.

Receptors for odour molecules (odorant receptors, ORs) are located on these tiny ciliary structures following the distinguishing feature that only one gene out of 1.400 coding for odour receptors is expressed in a given single OSN from a single allele (7-9).

On the basal side, every OSN sends an unbranched axon towards the basal lamina where it is fasciculated with axons coming from other OSNs and then redirected to the main olfactory bulb (MOB).

Supporting cells (SCs) and olfactory microvillar cells (OMCs) compose the apical layer of olfactory neuroepithelium that is in contact with the air flow circulating through the nasal cavities. SCs are functionally similar to glial cells in CNS; they are excitable and electrically coupled (10, 11) and they have a foot-like process that extends to the basal lamina and which is also ramified in order to communicate with neighbouring cells (12). Their principal role is to regulate the composition of the overlaying surface fluid and to metabolize odorants and other xenocompounds (13, 14).

Microvillar olfactory cells have been described for the first time in 1967 but generally they are not mentioned in textbooks that describe the cell composition of olfactory epithelium (15). Recently, they have grabbed the attention of the scientific community because some of their intriguing molecular features have been revealed, but a complete characterization of this cell type is still missing and its function is not yet understood.

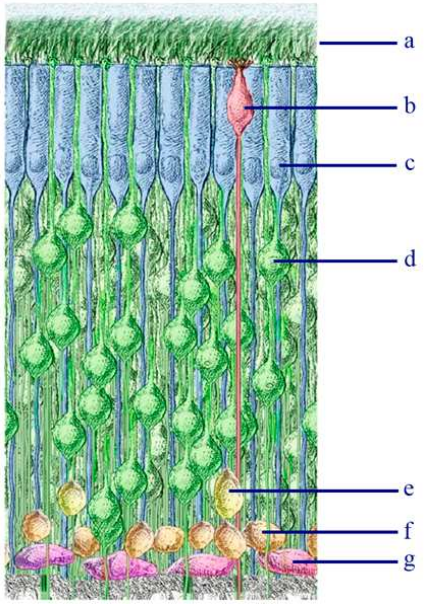

Figure 2: Cellular architecture of main olfactory epithelium; a: outer superficial layer; b: a microvillar cell; c: sustentacular cells; d: a mature olfactory sensory neuron; e: an immature OSN; f: globose cells; g: horizontal basal cells. (Adapted from Elsaesser R., *J. Neurocyt*., 2005).

The vomeronasal organ is usually considered as a specialized structure responsible for detecting pheromones and other chemical signals emitted by other animals which convey information concerning species, gender, identity and a variety of social cues. The VNO can be easily recognized because of its peculiar anatomy: it is composed by a blind-ended tube filled with mucus that is encapsulated in a bony structure located on the anterior nasal septum. In mice, this tube is closed in the posterior region and it is open anteriorly towards the nasal cavity to allow the entry of both volatile and non-volatile chemical cues following sniffing and licking.

Vomeronasal sensory neurons (VSNs) are distributed within a crescent-shaped sensory epithelium located on the medial concave surface of the vomeronasal cavity and they are morphologically similar to OSNs: they are bipolar neurons with an apical dendrite extending to the surface of the epithelium, but the tips of their dendrites form a knob that is covered, differing from OSNs, with numerous microvilli. On the basal side they have a single unbranched axon that reaches the basal lamina and is then directed to the accessory olfactory bulb (AOB).

The murine olfactory system comprises also other two structures that have been recently identified and that are generally considered as minor olfactory subsystems, although their specific function is not clearly defined.

The septal organ of Masera (SO) is composed by two islands of sensory tissue located on each side of the nasal septum but its consistency and position slightly vary among individuals; the cellular architecture of this organ is very similar to that of MOE but the thickness of the medial layer occupied by OSNs is more restricted. Neurons contained in the SO respond to a broad range of olfactory stimuli and their specific connections to the MOB support the hypothesis that this sensory tissue is an ectopic part of MOE or VNO and a chemosensory unit with a precise identity (16, 17).

The Grueneberg ganglion (GG) is situated in the rostro-dorsal area of the nasal cavities, in the corner formed by the nasal septum and the nasal roof and it apparently lacks direct access to the lumen of the nasal cavity. Cells located in GG express the olfactory marker protein (OMP), a typical feature of OSNs, and are endowed with modified cilia which resemble those of crypt sensory cells in the OE of fish; these atypical neurons project on a limited number of glomeruli located in a region of the MOB that is activated during suckling behaviour of pups. It has been recently demonstrated that, given the expression of a vomeronasal receptor and of some components of the OSNs transduction pathway, the molecular profile of GG neurons is similar to both VSNs and OSNs (17) and that this olfactory substructure is involved in the fast response to a specific class of alarm pheromones (18).

2. Odorant receptors, signal transduction and connectivity in MOE.

A fundamental discovery in the field of olfaction is the one that revealed the molecular identity of odour receptors.

In 1991 Linda Buck and Richard Axel identified in rats an extremely large multigene family of transmembrane proteins that were hypothesized to be ORs on the basis of their typical expression pattern, restricted to the MOE (19); further studies confirmed that OR genes form the largest multigene family ever found in vertebrates (20). For their research activity in ORs, the two scientists have been awarded with the Nobel Prize for Physiology or Medicine in 2004.

The number of genes coding for odorant receptors largely varies in genomes of different species, and each gene repertoire is composed by a definite proportion of functional genes and pseudogenes degenerated during the course of evolution.

In the mouse genome the total number of OR genes is approximately 1.400, out of which the 20-25% are pseudogenes. Human genome contains 800 OR genes, but only half of them preserve an intact open reading frame (ORF): having developed trichromatic colour vision that is very powerful

in detecting environmental signals, it is likely that olfaction has become less important for primates confronted to other dichromatic mammalian species.

OR genes are present as genomic clusters scattered on many different chromosomes. Despite the difference in the number of genes between humans and mice, the organization of ORs clusters is well conserved between the two species (21).

Following a distinguishing genomic feature, all vertebrates OSNs express only one OR gene from the entire genome repertoire; moreover, in a given OSN a specific OR is expressed only from a single allele, and OSNs expressing the maternal or paternal allele coexist mosaically in the MOE (22).

The molecular mechanism that stands behind this selectivity has been only partially revealed; it is well accepted that a levelled hierarchy of elements and events are involved in the selection of a given OR including the gene coding sequence, short DNA sequences upstream of OR coding sequences, locus control regions (LCR)-like conserved elements (as in the case of globins gene cluster) and feedback signals given by the expression of a full-length OR protein. Nevertheless, how an OSN determines whether it is expressing an OR, the nature of the feedback signal that ensures continuous expression of a definite OR while keeping all other OR genes silent and what features of an OR coding sequence are recognized to assist this complex regulation are still pending questions (23).

Considering the patterns of OR genes expression, the MOE can be seen as a complex receptorial map in which OSNs expressing a specific receptor are interspersed among neurons expressing other ORs: this expedient increases the likelihood that a particular odour molecule transported by the airflow can encounter its cognate receptor along its travel through the nasal cavities. According to the distribution of OSNs populations expressing the same OR gene, the MOE can be divided into four zones (I-IV) even though this classical topographical organization has recently been questioned and reinterpreted (24).

All ORs belong to the superfamily of G-protein coupled receptors (GPCRs) that comprises a variety of receptorial proteins responsive to a multitude of stimuli. The structural fingerprint of GPCRs is represented by seven segments mostly composed by hydrophobic amino acid residues that are predicted to form α-helix structures buried in the lipid bilayer membrane; these seven hypothetic transmembrane domains are interconnected by segments of hydrophilic residues that form water-stable loops. On the basis of molecular dynamics simulations, in ORs structure the α-helices should pack one against each other to form a bundle assembly containing an odorant binding site on the extracellular side (corresponding to the mucus layer in the nose) and a cytoplasmic domain coupled with a heterotrimeric guanine nucleotide binding protein (25, 26). The high variability in the

aminoacidic sequence of the 3rd, 4th and 5th α-helices among the different ORs suggests an involvement in the formation of the odorant binding site (fig. 3).

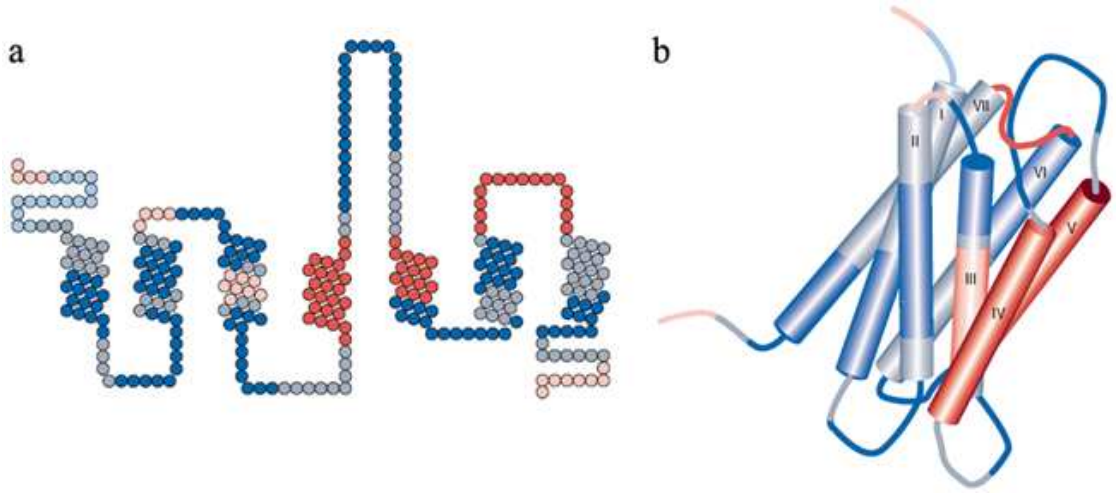

Figure 3: Schematic representation of odor receptors. **a**: snake diagram of M71 odor receptor showing most conserved amino acidic residues (shades of blue) and most variable residues (shades of red). **b:** proposed 3D-structure of the receptor with conserved (blue) and variable regions (red). (Adapted from Firestein S., *Nature*, 2001)

Olfactory transduction begins with the binding of an odorant molecule to a receptor protein on the ciliary membrane of OSNs. As a result of this event, the OR undergoes a structural change that triggers the exchange of GDP by GTP on the *α*-subunit of the olfactory G protein, $G_{\alpha olf}$, and activates an adenylyl cyclase type III (ACIII or AC3), leading to elevated intraciliary concentrations of cAMP (27, 28). The consequent opening of the olfactory cyclic nucleotide-gated (CNG) channel lets Ca^{2+} and Na^{+} flow into the cilia (29, 30) thus depolarizing the cell. This depolarization is amplified by a substantial excitatory Ca^{2+}-activated Cl^{-} current at the ciliary membrane due to the aperture of a specific Ca^{2+}-activated Cl^{-} channel (31-35, fig. 4). The excictatory Cl^{-} current is sustained by a high intracellular Cl^{-} concentration maintained mostly by constitutive Cl^{-} uptake through a Na^{+}-K^{+}-Cl^{-} cotransporter (36).

If enough CNGs are gated by cAMP for a sufficient time, the depolarization of OSNs membrane reaches a threshold that culminates in the generation of an action potential that is propagated through the axons to the main olfactory bulb.

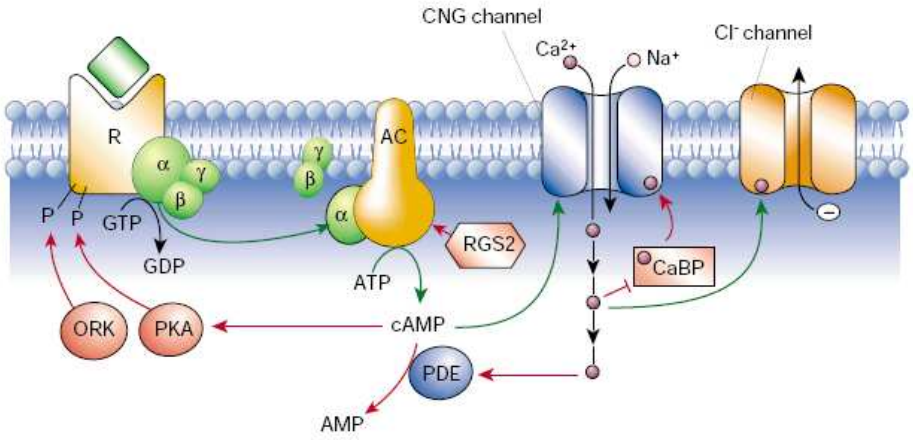

Figure 4: Signal transduction in OSNs. This picture schematically represents the signal transduction pathway adopted by the major part of OSNs in the MOE; green arrows indicate stimulatory pathways, red arrows indicate inhibitory pathways. R: odor receptor; AC: adenylyl cyclase; CNG: cyclic nucleotide gated channel; PDE: phosphodiesterase; PKA: protein kinase A; ORK: olfactory receptor kinase; RGS: regulator of G-proteins; CaBP: calmodulin binding protein. (Adapted from Firestein S., *Nature*, 2001)

The Ca^{2+} influx through the CNG channels also leads to olfactory adaptation. One mechanism of Ca^{2+}-mediated adaptation involves, through Ca^{2+}-calmodulin, a reduction in the CNG channel's sensitivity to cAMP (37-39). Another adaptation mechanism involves an inhibition, via Ca^{2+}-calmodulin and calmodulin-dependent protein kinase II, of the adenylyl cyclase (40, 41). The termination of the OSN response requires all components of the signal transduction cascade to be inactivated. This begins with the separation of the odourant from the receptor, which occurs quickly (42). The GTP bound to $G_{\alpha olf}$ is hydrolyzed to GDP, deactivating $G_{\alpha olf}$ and allowing the adenylyl cyclase to return to its basal activity. The generated cAMP is hydrolysed by a phosphodiesterase (PDE) (43, 44). Finally, the excess intracellular Ca^{2+} is removed from the ciliary space via Na^{+}-Ca^{2+} exchange (45) or a Ca^{2+}-ATPase (46) in order for the Ca^{2+}-activated Cl^{-} channel to close.

The MOB is the most rostral part of the brain; it is composed by two identical hemispheres with a multi-layered cellular architecture. OSNs axons course through the outer layer (olfactory nerve layer) and once inside the second layer they reach their synaptical targets in structures defined as *glomeruli*, considered as the functional units of MOB: they are neuropil-networks of synaptic interactions between the axon terminals of OSNs and the dendritic trees of mitral/tufted cells, which are the projection neurons of olfactory bulb. A network of interneurons is comprised and participates in these glomerular synaptic facilities.

In the MOB, the apparent random punctuate expression of different OR genes within one of the four regions of MOE turns into an stunning precision: axons belonging to a discrete OR-specific OSNs population target a medial glomerulus and a lateral glomerulus in each hemisphere, forming a mirror-symmetric pair of glomerular maps on both sides of the MOB. This peculiar axonal convergence onto distinct mirrored glomeruli generates a chemospecific map which is considered as the basis for a combinatorial processing of odour signals (47, fig. 5).

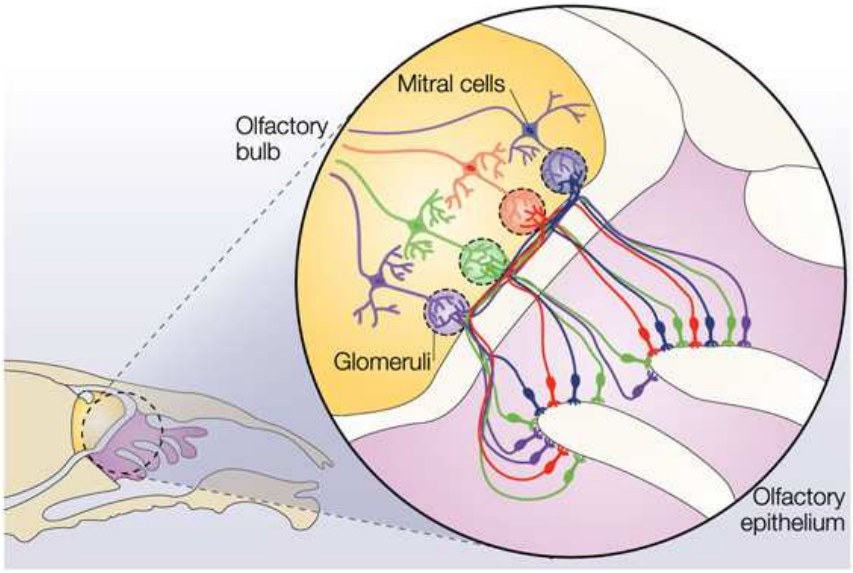

Figure 5: Functional connections between the MOE and the MOB. This picture illustrates the axonal convergence of OSNs populations expressing specific ORs to distinct glomeruli in the MOB. (Adapted from Dulac C. and Torello AT., *Nat. Neurosci.*, 2005).

What makes the olfactory system even more unique is the fact that, differing from other sensitive pathways, it does not relay most information through the thalamus, but it passes signals directly from receptor neurons to the olfactory cortex through the OB.

Projections leaving from the olfactory cortex target several regions, including the orbitofrontal cortex, the amygdala, the entorhinal cortex, and the ventral striatum. Only the orbitofrontal cortex receives information via a secondary indirect thalamic pathway. The few steps of processing suggest that olfactory information requires less pre-processing than other sensory modalities. Nevertheless, the diversity and complexity of synaptic interactions in the OB attest to a critical and active role of this structure in the translation of peripheral olfactory information into a language intelligible to the rest of the brain (48).

The topographical organization of MOE in four zones has been recently challenged since new studies have proposed that olfactory neurons are rather organized in overlapping zonal positions that are coherently arranged along the central-to-peripheral axis (49-51). Within these zones, they can be further subdivided in two groups on the basis of their axonal convergence on medium or lateral glomeruli in the MOB.

Even though the logic of this OSNs distribution is not completely understood, its importance is emphasized by the selective expression of surface molecules such as semaphorins and ephrins in homogeneous OSNs subpopulations (52, 53). Far from being casual, it is likely that every OSNs subset expressing a given OR occupies in the sensory epithelium a position set to optimize the possibilities of binding with its specific odour ligand; since the entire surface of MOE is covered with mucus, odours transported by turbulence of the airflow are first of all dissolved in this mucus and this process will follow different dynamics according to chemical nature of odour molecules (faster for hydrophilic molecules, slower for more hydrophobic molecules).

This hypothesis is confirmed by the observation that all the ORs expressed in the dorsal zone of the sensory epithelium belong to class I receptors that are the most related to those found in aquatic vertebrates and which are expected to have a higher affinity for hydrophilic odorants (54, 55).

3. The MOE presents other sensory subsystems in addition to the canonical OR/OSNs-mediated chemoreception.

3.1 GC-D olfactory sensory neurons subfamily.

It was already known since 1997 that not all OSNs rely on cAMP pathway for the transduction of odour signal, and that there is a subset of OSNs that selectively express on their plasma membrane the receptor guanylate cyclase-D; GC-D do not rely on well-known components of the canonical OSN odour transduction cascade, including $G\alpha_{olf}$, type III adenylyl cyclase, the Ca^{2+}/calmodulin-dependent phosphodiesterase PDE1C2, the cAMP-specific phosphodiesterase PDE4A, and the cAMP-sensitive CNG channel subunits CNGA2 and CNGB1b. Instead, these atypical OSNs express a cGMP-specific CNG channel subunit, CNGA3, and a cGMP-stimulated phosphodiesterase, PDE2. Axonal projections of this subpopulation of neuron innervate a particular set of glomeruli in the MOB (necklace glomeruli) that are thought to be involved in the processing of pheromone-induced responses (56-58).

A recent work has de-orphanized GC-D demonstrating that it recognizes natural urine stimuli and that it selectively binds two natriuretic peptides, uroguanylin and guanylin, suggesting the

possibility that GC-D neurons represent an olfactory subsystem that contributes to maintenance of salt and water homeostasis and to the detection of cues related to hunger, satiety or thirst (59).

On another hand, a work by Luo and colleagues identified in GC-D neurons subsystem a fine-tuned control mechanism for environmental CO_2 concentration (60). CO_2 has a fundamental role as an olfactory environmental cue for a number of animal species; for example in *Drosophila Melanogaster* CO_2 is able to activate a single population of sensory neurons thus activating avoidance behaviour (61). CO_2 emissions derived from newly opened and nectar-rich flowers indicate food-source profitability, and this may represent an important signal in the foraging behaviour of nectar-feeding insects (62); blood-feeding insects use highly specialized and sensitive olfactory systems to detect and follow air plumes containing the volatile emissions from their hosts, and in 2007 Leslie Vosshall and colleagues have revealed the molecular identity of CO_2 receptors involved in this olfactory pathway (63). Luo and colleagues demonstrated that in mice GC-D neurons are responsible for highly sensitive innate avoidance behaviour in response to environmetal CO_2 concentration changes. It is likely that this mechanism has been developed during evolution by all terrestrial species as a result of the adaptation to atmospheric low-CO_2 concentrations.

3.2 TAARs-expressing olfactory sensory neurons.

Among the most important recent findings in the field of olfaction, in 2006 Linda Buck and Stephen Liberles discovered the expression of a second class of OR-unrelated chemosensory receptors in MOE (64). The authors found several members of trace amine-associated receptors (TAARs) to be expressed like ORs in unique patterned subsets of OSNs that co-express also $G_{\alpha olf}$, thus indicating that also TAARs-OSNs use cAMP as a second messenger. TAARs are related to biogenic amine receptors, and in their work Buck and Lieberles proved that at least three murine TAARs expressed in MOE recognize small amine found in urine that may elicit innate responses; in particular, mTAAR4 is responsive to β-phenylethylamine, a compound whose elevation in urine is correlated with increases in stress and stress responses in both rodents and humans (65-67), and mTAAR3 and mTAAR5 have been demonstrated to detect isoamylamine and trimethylamine, two compunds that are enriched in male versus female mouse urine. Furthermore, because of its ability to accelerate puberty onset in female mice isoamylamine contained in male urine is reported to act as a pheromone (68, 69).

3.3 Trpm5-expressing olfactory sensory neurons.

The transient receptor potential channel M5 is a well-known component of the transduction pathway for sweet, amino acid and bitter perception; in taste cells, it is functionally coupled to taste receptors and components of the phospholipase C (PLC) and phosphoinositides (IP) pathways. In 2006 Diego Restrepo and colleagues highlighted the expression of TRPM5 in a subset of OSNs, and they also showed that in these neurons it co-localizes with the olfactory CNG and the β2 isoform of PLC, a data that would suggest the coexistence of canonical cAMP and PLC transduction machineries.

Glomeruli innervated by TRPM5-OSNs have been found in a ventral region of the MOB that may constitute an elaboration unit specific for pheromones and other molecular social cues; the same work also attested the expression of TRPM5 in a class of olfactory microvillar-like cells, and this evidence is further supported by a study concerning the expression of TRPM5 in a large number of chemosensory cells published in the same year by Silke Kaske and colleagues (70).

4. Vomeronasal receptors, signal transduction and connectivity in VNO.

Like ORs, vomeronasal receptors (VRs) belong to the superfamily of seven-transmembrane G-protein coupled receptors.

The first family of VRs (V1R) was discovered by Catherine Dulac and Richard Axel in 1995 by comparative hybridization of cDNA libraries constructed from single rat VSNs. Expression of V1Rs was observed in cell bodies of VSNs located in the apical part of the sensory epithelium (71). In 1997 independent researches conducted by Catherine Dulac, Linda Buck and Roberto Tirindelli showed that VSNs in the middle-basal layer of sensory VNO epithelium express an unrelated second family of VRs that was later defined as V2R (72-74); another class of vomeronasal receptors was identified in 2000 by Catherine Dulac and initially defined as a third family, but afterward it was integrated in the V1R family (75).

V1R and V2R receptor families are functionally coupled with different G-proteins and their expression characterizes two different sets of VSNs; it has been hypothesized and partially demonstrated that these two neuronal populations recognize chemically distinct pheromones, as also underlined by their anatomical segregation in the apical (V1R-expressing VSNs) and basal (V2R-expressing VSNs) layers of VNO sensory epithelium (76-78).

V1R genes are scattered in clusters across several chromosomes and they have no introns in their coding sequences, but similarities between VRs and ORs families are no further extended: in fact, despite V1R genes are reminiscent to OR genes, the encoded receptors do not share any sequence homology with ORs. Furthermore, V1Rs belong to subgroup A of GPCRs superfamily and they are weakly related to T2R taste receptors with an amino acid sequence identity varying from 15% to 20%.

A recent data mining has identified 308 V1R sequences in the mouse genome, out of which 191 are seem to be intact genes (79). V1R-expressing VSNs respond to volatile compounds that are able to elicit pheromonal activity in phenomena such as puberty delay, oestrus induction and intermale aggression.

Multi-exonic V2Rs belong to subgroup C of GPCRs and are related to Ca^{2+}-sensing and metabotropic glutamate receptors as well as to T1R taste receptors (80). The total number of identified V2Rs sequences in the more recent mouse genome assembly is 280, of which 70 seem to have an intact ORF (81); they can be classified into four subfamilies (V2Rs A-D), with family A, B and D representing the 95% of the entire V2Rs repertoire. V2Rs are structurally characterized by a long and highly variable N-terminal domain encoded by multiple exons, a molecular feature that is not shared with V1Rs and that has been hypothesized to constitute the ligand binding domain (fig. 6).

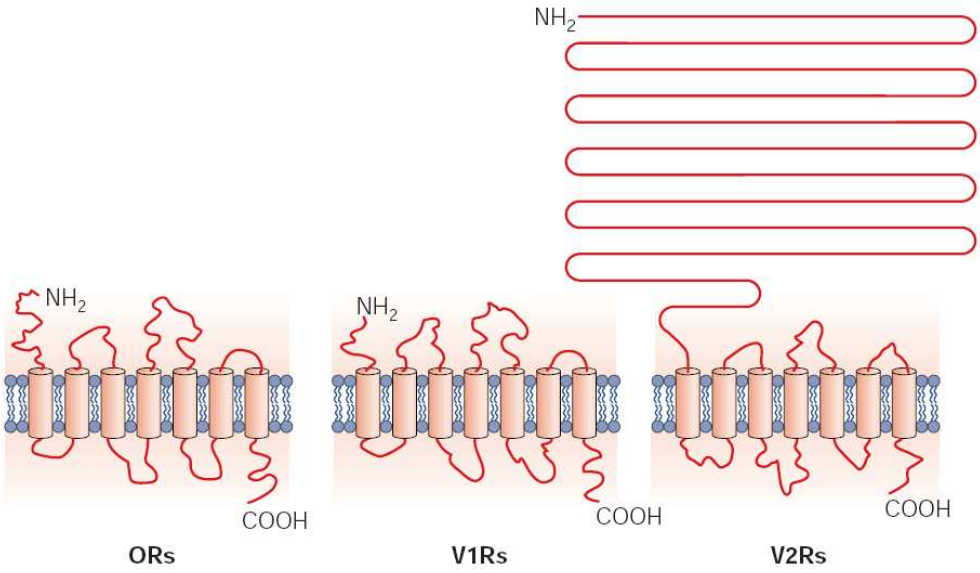

Figure 6: Structural differences of the best-known sensory receptors in mouse olfactory system. ORs: odor receptors; V1Rs: vomeronasal receptors, type 1; V2Rs: vomeronasal receptors, type 2. (Adapted from Mombaerts P., *Nat. Neurosci*., 2004)

V2R-expressing VSNs have been demonstrated to be responsive to non-volatile pheromonal cues such as major histocompatibility Mhc class I peptides, which convey information on individuality and are involved in mate recognition, ESP1, a male-specific peptide secreted from the extraorbital lachrymal gland, and a class of proteins isolated from urines (major urinary proteins, MUPs) that are responsible for the triggering of aggressive behaviours (82).

An intriguing feature of V2R-neurons is the selective expression of another multigene family, named "H2-Mv", which includes nine nonclassical class I genes of the major histocompatibility complex (MHC). In 2003 Peter Mombaerts and Tomohiro Ishii, searching for genes that are expressed in the mouse VNO but not in the main olfactory epithelium, demonstrated that the nine H2-Mv genes are expressed differentially in subsets of V2R-vomeronasal neurons in a complex and non-random pattern of combinatorial expression (82); in the same year the group leaded by Catherine Dulac reached the same conclusions and in their work they hypothesized a role for H2-Mv gene products as escort molecules in transport of V2Rs to the neuron surface (83). Mombaerts and Ishii have recently reported that H2-Mv genes are not expressed in all of the V2R-VSNs, thus revealing a tripartite neuronal organization of the VNO featuring $V1R^{+}$VSNs, $V2R^{+}$/H2-Mv^{-} VSNs, and $V2R^{+}$/H2-Mv^{+} VSNs and confirming that the role of H2-Mv genes remains unclear (84).

In VSNs the gene expression rule one neuron-one receptor that is commonly accepted for the OR genes has been recently discarded following the finding that each basal V2R-specific VSNs co-express two different V2Rs, although this has been demonstrated only for V2R receptors belonging to a small subfamily (Vmn2r1-7, subfamily C) (85).

VNO size and functionality and VR gene families vary according to species-specific differences. When comparing mouse and human gene repertoire of VRs the pseudogenization occurred in primates during evolution is even more evident than the one observed for ORs; mice have 191 potentially functional V1R genes versus only five in humans (86), and the count for intact V2R genes is 70 in mice versus none in humans. As for the case of ORs, it seems that deterioration of VNO and VR genes in primates coincided with the development of trichromatic colour vision suggesting that vision became more important than chemical communication in these clades. Human vomeronasal receptors throughout the genome have undergone a massive degeneration as a result of missense mutations, frameshift mutations and Alu sequences insertion.

Among the five human V1Rs with an intact ORF no cases of functionality have been reported yet, although a V1R-like gene (V1RL1) has been found to be expressed in human olfactory mucosa

(87). Moreover, if human MOE and MOB are proportionally reduced compared to their rodent counterpart, VNO in humans seems to be little more than a vestigial leftover: it is developed during early phases of gestation, but its nervous connections with the olfactory bulb are apparently lost during development between week 14 and 28. Although some evidences indicate that portions of the human vomeronasal duct possess a highly differentiated epithelium resembling that of the functional chemoreceptive organ, in different individuals it exhibits considerable variability in size, shape, detectability and even presence (88, 89).

Signal transduction in VSNs is not well-characterized. Transduction components characteristic of most OSNs, such as ACIII and $G_{\alpha olf}$, are absent from VSNs, but a member of the transient receptor potential (TRP) channels family, TRPC2, is widely expressed in both basal and apical regions of VNO and its critical role in VSNs activation has been demonstrated by gene knockout studies (90-92). According to the latest theories, when pheromones bind their specific V1R or V2R receptors the corresponding G-proteins ($G_{\alpha i2}$ and $G_{\alpha o}$, respectively) are activated by a receptorial conformational change. G-proteins in turn activate TRPC2 which mediates both receptor- and store depletion-triggered Ca^{2+} entry through the modulation of phospholipase C and phosphoinositides pathway (93). This molecular cascade initiates an action potential that through VSNs axon terminals is projected to the accessory olfactory bulb (AOB) (fig. 7).

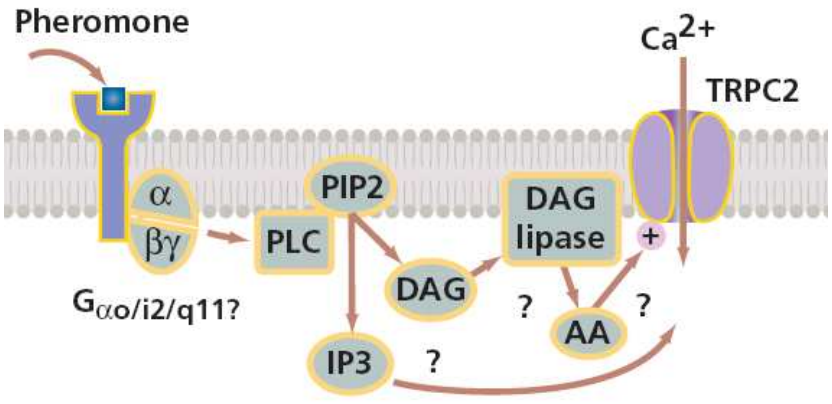

Figure 7: Proposed signal transduction in VSNs. As shown in this picture, the sensory transduction pathway activated by pheromones in VSNs has been only partially characterized. PLC: phospholipase C; PIP2: phosphatidyl inositol di-phosphate; IP3: inositol tri-phosphate; DAG: diacylglycerol; AA: arachidonic acid; TRPC2: transient receptor potential channel, C2 (Adapted from Rodriguez I., Nat. Neurosci., 2003).

The spatial segregation of V1R-VSNs and V2R-VSNs in the VNO is conserved in the structural organization of the AOB in that the two neuronal subsets project their axons to the anterior and posterior regions, respectively.

The basic connectivity of AOB resembles that of the MOB: the axons of VSNs terminate in the glomerular layer forming synapses with apical dendrites of mitral and tufted cells. However, while axons of OSNs target a pair of mirrored specific glomeruli in MOB, axons belonging to a specific population of VSNs converge on up to 30 small glomeruli but the apparent divergent pheromonal information is converged at the level of every single mitral cell that seem to innervate only glomeruli targeted by a given VSNs population (94, 95).

The high selectivity of VSNs suggests that each pheromonal compound would activate a small and exclusive subset of AOB mitral cells, but only a few verified pheromonal compounds are available thus reducing the likelihood of finding an effective stimulus for a specific AOB neuron. From the AOB, the output olfactory information is carried first to the amygdala and then to higher cortical cognition centres, where it is transformed into complex innate behaviours that arise from a blend of diverse pheromonal and non-pheromonal stimuli.

5. The functional separation between MOE and VNO is questioned.

The different locations and anatomical structures of the MOE and VNO have direct consequences for stimulus access. Whereas the MOE has access to stimuli in the nasal airstream, the VNO is connected to the nasal cavity by a narrow duct. Stimuli are thought to gain access to the VNO by a vascular pumping mechanism that is activated in arousing situations. This scheme has longly fed the model that the main olfactory system is specialized for detecting volatile, airborne molecules, while the vomeronasal system is specialized for the detection of non-volatile chemosignals, such as those in urine, skin, scent glands and reproductive secretions, after direct contact with the stimulus source (“dual olfactory hypothesis”) (96).

This dichotomy between VNO and MOE has often been associated to the idea of pheromones as non-volatile substances and general odorants as volatile compounds, but the latest experimental evidences have highlighted the absence of definite boundaries between the two molecular categories and have surprisingly revealed that both VNO and MOE can sense volatile plus non-volatile compounds and pheromonal plus non-pheromonal cues, thus sketching a new, wide and complex sensorial landscape where the view of a mammalian olfactory system organized in sealed compartments has been definitively challenged.

5.1 Odorants sensitivity and OR expression in VNO.

In 2001 Sam and colleagues discovered that subfamilies of VSNs were responsive to several mixes of odorants. Furthermore, they observed an ability to discriminate between highly related molecules differing only in a functional group, which is a distinguishing sensorial feature of OR-expressing OSNs. The sensitivity of VSNs to these odorants was found to be more similar to that of classical VSNs to pheromones than the one of OSNs towards general odorants (97).

In 2003 Kien Trinh and Daniel R. Storm used an ACIII knock-out mouse model to demonstrate that, in a condition in which the classical OSNs transduction pathway is disrupted, the VNO was able to detect a number of non-pheromonal odorants. In wild type mice, the response to these same odorants was found to be intact in MOE, and following this observation the authors hypothesized that the existence of a redundancy in the two sensory systems might underline the necessity to detect in a different way some molecules that are more important than others for survival (98).

As a confirmation to these observations, in 2006 a study published by Lèvai and colleagues identified 44 ORs expressed in VNO by canonical VSNs projecting in the anterior AOB and positive also for the expression of TRPC2 and $G_{\alpha i2}$ (ref). The same OR genes were found regularly expressed also in MOE with a carachteristical zonal distribution that was not observed in VNO (99).

5.2 Pheromones sensitivity in MOE.

Evidences for an involvement of MOE in pheromonal perception have been accumulating for years. For example, survival of newborn rabbits during the first two days of life depends on mother’s milk intake, and it is known that to trigger the conventional nipple-search behaviour and for nipple attachment the pups rely on a pheromone present on the mother's belly (100).

In 1986 Hudson and Distel reported that surgical removal of the VNO had no effect on pups’ ability to respond to the pheromone when tested on a lactating female, nor on their ability to obtain milk in the normal nursing situation (101). Similarly, in 1997 Dorries and colleagues demonstrated that in domestic pig the effects of androstenone and androstenol on sexual behaviour are unaffected by VNO lesions (102). Moreover, urinary attractant methylthio-methanethiol (MTMT), a potent and previously unknown semiochemical present only in male urine, is able to selectively excite mitral cells in the MOB, although its activity has been tested through direct interaction with OB neurons and the components of the MOE mediating its attractant effects are still unknown (103).

A mouse model in which the canonical OSNs transduction pathway had been disrupted through the genetic ablation of CNGA2 was used in 2004 by Diego Restrepo and colleagues to reveal that

knockout mice showed behavioural deficits comparable to those observed in animals with a lesioned VNO; whereas these observations cannot be confuted, the authors underestimated the possibility that an intact MOE could have a role in triggering behaviours resulting in the activation of the vomeronasal pump. Furthemore, other CNGA2-unrelated sensory systems integrated in the MOE may contribute to the residual pheromonal behaviours observed in CNGA2$^{-/-}$ mouse, which therefore cannot be completely attributed to the VNO function (104).

The functional structures and subsystems responsible for pheromonal sensitiveness in the MOE have been recently brought out of the shadows, at least in mice, although details about their sensorial contribution are sometimes only partial.

5.3 Vomeronasal receptors in MOE.

Goats have a well-developed vomeronasal (VN) system that lacks the spatial and functional segregation given by $G_{\alpha o}$ and $G_{\alpha i2}$ proteins which has been observed in mouse VNO, presenting an even $G_{\alpha i2}$ layer that occupies the entire vomeronasal sensory epithelium. Differences between goat and mouse extend also to the VRs repertoire; in fact, all V2Rs identified in goat genome contain stop codons and/or frameshift mutations in their deduced coding region, an evidence that is consistent with the lack of $G_{\alpha o}$ expression. Like goats, other mammals such as dogs, horses, cows, and marmosets also have only $G_{\alpha i2}$-expressing VSNs (105, 106).

In 2002 a member of the V1R goat family, gv1ra1, was reported to be expressed in the MOE, and the characteristics of the OSNs expressing this receptor have been investigated by the same research group in 2007. The results of their analyses have confirmed that in goat MOE two different kinds of OSNs coexpress $G_{\alpha i2}$-g1ra1 or $G_{\alpha olf}$-gv1ra1. The first OSN type does not express OMP, thus constituting a rather atypical and new class of sensory neuron, but since these neurons are located on the basal side of the MOE authors have not excluded that, although unlikely, they could represent classical OSNs undergoing an immature phase (107, 108).

Recently, 21 potentially functional amphibians V1Rs have been identified in the latest genome assembly of *Xenopus Tropicalis* (109). Amphibians are phylogenetic intermediates between fish and mammals and are adapted for both aquatic and terrestrial life, therefore their olfactory organs reflect this dualism and the MOE is divided in two districts, the PC and MC: the first one is responsible for detecting airborne odorants, while the latter detects water-soluble odorants. The fish-like olfactory receptors (OR1) and the mammalian-like olfactory receptors (OR2) are specifically expressed in the MC and PC, respectively. Amphibian species presents also an atypical VNO that expresses only $G_{\alpha o}$ and is devoid of $G_{\alpha i2}$-positive cells. Surprisingly, Atsuko Date-Ito and

colleagues have reported in 2008 that Xenopus V1R repertoire is selectively expressed in both MC and PC subunits of MOE but not in VNO, a result that may suggest that amphibians use both volatile and non-volatile molecules as pheromones although volatile pheromones specific for this clade have never been identified.

In 2006 Delicia Karunadasa and colleagues have highlighted for the first time the expression of a V1R receptor with an intact coding sequence, v1rd, in scattered unidentified cells within the MOE in both embryonic and post-natal mice. Their work did not investigate further the identity of the V1R-positive cells, and this is as far the only direct existing evidence of the expression of vomeronasal receptors in mouse MOE (110).

A provocative work published in 2000 by Ivan Rodriguez and Peter Mombaerts demonstrated that the spliced mRNA encoding for receptor V1RL1 (one out of the group of five V1R receptors conserving an intact ORF in human genome) is represented in cDNA derived from human olfactory mucosa (87). Although the presence and/or functionality of human VNO is still controversial, this evidence re-opened the door to the theories arguing that in primates some vomeronasal-specific functions might have been integrated in MOE during the course of evolution, but under the light of recent discoveries attesting in rodents the fundamental role of the MOE in complex innate behaviours that have been for long time exclusively and/or erroneously attributed to the VNO, it seems that this hypothesis of evolutionary integration is not anymore needed to speculate about the existence of dedicated pheromone-sensing subsystems also in human species.

5.4 VNO and MOE are involved in reproductive behaviours.

In the central nervous system, neurons that synthesize and secrete the luteinizing hormone-releasing hormone (LHRH), also known as gonadotropin-releasing hormone (GnRH) integrate a variety of internal and external stimuli that affect mating behavior and fertility (111, 112). In the CNS of mice they are mainly located in the rostral hypothalamus, in the medial preoptic area (MPOA) and in the basal forebrain. LHRH secretion regulates the synthesis and secretion of the luteinizing hormone (LH) and the follicular-stimulating hormone (FSH) by the anterior pituitary gland; LH and FSH, in turn, control the development and the function of the male and female gonads and the release of steroids into the bloodstream. Steroids coordinate the development of sexual traits and organs and act centrally on brain structures to modulate LHRH secretion to facilitate sexual behaviour. In addition to its role as a neurohormone, LHRH is detected in axonal projections in the amygdala and

the midbrain, where it is thought to act directly as a neurotransmitter facilitating sexual receptivity and mating behavior (113).

In 2005 Hayan Yoon and colleagues demonstrated that a discrete population of OSNs targets the hypothalamus via a major projection pathway from the primary olfactory cortex (114). In the same work, authors used selective chemical ablation of the MOE without affecting the VNO and documented that MOE-lesioned mice displayed little to no interest at all towards females, resulting in dramatic reduction in the time spent investigating females and in the number of mounting attempts. Their data are in agreement with results obtained from the genetic ablation of VNO function in the TRPC2$^{-/-}$ mutant (91, 92). TRPC2$^{-/-}$ male mice seem perfectly able to reproduce, with no reduction in courtship and mating behaviour with females, but they display mating behaviour towards both males and females with equal frequency. Taken together, these data provide a new model of integration between the VNO and the MOE, according to which non-VNO cues are sufficient to trigger mating behaviour, while VNO function ensures the sex specificity of reproduction.

However, it has to be noted that in the VNO the loss of TRPC2 has a little influence on the transduction of MHC peptides by basal V2R-neurons (115) and it can be therefore difficult to discriminate between a residual VNO activity and a MOE involvement in TRPC2$^{-/-}$ mice mating behaviours.

Moreover, the molecular fingerprint of receptors involved in these mechanisms and transduction pathways of the OSNs targeting the hypothalamus remain unknown.

5.5 MHC peptides are involved in pheromonal communication in VNO and MOE.

The classical class I antigens of the major histocompatibility complex (MHC) are cell-surface glycoproteins that were originally discovered because of their role in rapid rejection of cells or tissues grafted between unrelated individuals. These molecules are encoded by the *K*, *D* and *L* loci of the mouse MHC (and analogous loci in other species) which show extreme species-specific polymorphism and a large number of alleles. This high level of polymorphism ensures that the cells and tissues of each unrelated individual are uniquely identified by their class I membrane-bound antigens. Like other membrane bound proteins, these class I molecules are anchored in the lipid bilayer by a hydrophobic domain; in 1987 Prim Singh and colleagues reported for the first time that in rats classical polymorphic MHC class I molecules are constitutively excreted in the urine (116). Peptide/MHC complexes can be cleaved from cell surface and released into the extracellular space,

thus appearing in the urine and other bodily secretions; exploiting this mechanism, any information contained in MHC chemical complexity becomes a property of the entire individual and it can be used for interindividual communication.

Starting from these findings, the role of MHC in influencing behaviours such as mate choice and parent-offspring interaction has been then well-documented. For example, laboratory mice are more likely to mate with individuals of dissimilar MHC genotype from their own (117); in mother-pups recognition, female show a preference in retrieving pups having the same MHC background as themselves (118). Moreover, mice can be trained to discriminate between urine odours of congenic mice that differ genetically only at their MHC H2 locus (119), implying that MHC genotype influences the volatile constituents of urine. MHC peptides have been hypothesized to be capable of binding small volatile molecules (although a direct evidence of this binding is still missing), thus the urine of a single individual may contain a unique genetic signature directly related to its genetic MHC background.

One of the most interesting discoveries made in recent years is that MHC class I peptides can act as chemosignals: in 2004 Trese Leinders-Zufall and colleagues proved that MHC peptides are recognized as activating ligands by V2R-VSNs located in the basal layer of VNO. This has been as a matter of fact the first evidence of V2R-VSNs sensitiveness to any kind of molecular cue, and given the peculiar structure of V2R receptors it was proposed that the binding with MHC peptides might happen through the long and variable V2R N-terminal domain. Authors demonstrated that peptides must meet precise structural specifications for VSN activation, and peptides of random sequence were found unlikely to function as ligands for the receptors on VSNs. For example, the peptide AAPDNRETF elicited an action potential in an individual VSN, but not its scramble version ANPRAFDTE. Given that MHC peptides activate VSNs in a sequence-specific manner, authors concluded that they could potentially function as individuality signals during social recognition. Considering the limited diversity of amino acid residues occupying the two anchor positions of mouse MHC class I peptides, they estimated that about 50 different receptors should be sufficient to discriminate ligands from all known mouse MHC class I molecules (120).

The newly identified chemosensory function of MHC peptides provided a direct link between MHC diversity and MHC-related behavior, converting a MHC genotype into an olfactory detectable quality.

Two years after the key discovery of MHC peptides action on V2R-VSNs, it was reported that non-volatile immune system MHC molecules exert a direct function also in mouse olfactory epithelium, thus questioning the longly held theory that OSNs can only be stimulated by volatile chemosignals (121). Starting from the conclusions published in 2004, their work was based on the evidence that

the MOE also participate in MHC-related behaviours (122). Using a dye-tracing approach, the authors managed to prove that non-volatile cues can enter the MOE after direct contact with bodily secretions through sniffing and licking of facial and anogenital areas; the sensitivity to MHC peptides was found to be spread on all of the four endoturbinates, although with some areas that failed to respond to the stimuli and that were consistent with the theory of mosaical topography of different OSNs families. Moreover, testing the MHC sensitivity in the MOE of a CNGA2$^{-/-}$ mouse model, the authors proved that MHC class I molecules are transduced by OSNs in a CNGA2-dependent way, most likely through the canonical cAMP transduction pathway. This was not the only difference they found compared to the situation in the VNO, in fact the specificity of OSNs towards MHC peptides was also found to be different to that of VSNs: whereas VSNs did not show any response to elevated concentrations of MHC peptides in which the characteristic anchor residues are mutated, OSNs recognized such peptides and the measured sensitivity to normal and mutated peptides was 2 order of magnitudes higher than VSNs sensitivity to normal MHC peptides.
This work published in 2006 by Frank Zufall and colleagues obviously leaves some blanks that are still waiting for their respective fillings; for example, the identity of the OSNs involved in MHC peptides responsiveness is still unknown, as well as the molecular features of the receptors specific for this peculiar class of peptides. Authors suggested that it is unlikely that the same receptors are used for MHC peptides recognition in both the VNO and the MOE, but even with a shared receptorial repertoire the fact that MHC peptides signalling rely on different transduction pathways in the two olfactory susbsytems could imply a non-redundant function, with the final effect that the same social cues may mediate different conspecific behaviours through the activation of each system.

6. The post-genomic era.

The advent of post-genomics era has ushered forth the barriers of knowledge, giving rise to a revolution that is touching and influencing the biological scientific world in almost all of its perspectives.
The availability of new tools and techniques has represented a way to obtain new answers to old questions. On one hand these new answers have rapidly turned into an array of exciting and somewhat overwhelming challenges that is probably requiring new and/or updated technologies and altered points of view.
Without the development of adequate bioinformatics tools, the scientific community couldn’t have fully exploited the completion of genomes annotation for human, mouse and a number of other

species. The need for the integration of these data has in turn produced more sophisticated algorithms for predicting gene structures which have fundamentally expanded our knowledge of genomes complexity.

The transition from genomic to post-genomic era has been based on the spreading of high-throughput technologies that has produced a consistent reduction of experimental costs, and a massive availability of data. The first and more evident outcome of this process has been the shifting of genomic research towards the annotation of functional elements and transcribed regions. One of the most striking findings that genomic research has lately brought is that the genomes are widely transcribed; in the first instance, this evidence has somehow given an answer to the paradox that the increase of complexity in different organisms at the phenotypical level is not paired by an increase in the number of protein-coding genes. For example, the number of protein-coding genes in mice and humans is 20.000-25.000, 13.000 in drosophila, 19.000 in C. Elegans, but all of the previous species are surpassed by a simple rice grain having 46.000 protein-coding genes.

The old idea of "transcriptome" as a context-specific group of protein-coding mRNAs sharing distinctive features (capped 5'-end, 5'-untranslated region, coding sequence, 3'-untranslated region and a polyA tail) has thus been replaced by a more dynamic and still not completely characterized landscape of transcripts. Only a small portion of them contains information to encode for proteins, while the rest is composed by a wide array of non-structural and non-coding RNAs, both $polyA^+$ and $polyA^-$. These transcripts then may be subdivided in multiple categories displaying a number of diverse features. The ratio between non-protein coding RNAs and protein-coding RNAs has then been found to increase going from bacteria to primates.

On the other hand, in recent years it has become evident that the protein-coding portion of the transcriptome displays an unexpected intrinsic complexity which can arise from a number of mechanisms including alternative splicing, multiple transcription start sites (TSSs) and termination sites (TTSs); transcriptional diversity can also be generated by variations of the untranslated regions (UTRs) located at 5' or 3' and which can influence mRNA turnover, transcription and subcellular localization.

In order to organize this multitude of data, several collections of clones have been realized exploiting different approaches, among which the efforts of the RIKEN mouse gene encyclopaedia project have been particularly fruitful, aimed at creating a detailed description of mammalian genome through isolation and sequencing of full-length mouse cDNAs. Through the years, the RIKEN cDNA clone collection has undergone several phases of improvements in the strategies adopted for collecting and annotating the entire mammalian transcriptome and proteome. The latest release (FANTOM3) includes a total number of 181.047 independent transcripts isolated from a

variety of mouse tissues in a total of 237 libraries, and it has been completed through a strategy comprising full-length cDNA enrichment obtained through an mRNA cap-trapping approach, subtraction, sequencing and bioinformatics analyses.

This work has also introduced novel computational and unequivocal definitions to describe the emerging new view of the transcriptome; a transcriptional unit (TU) identifies a group of mRNAs whose exons overlap with at least one nucleotide in the genome and have the same orientation. Similarly, a transcriptional framework (TK) is composed of mRNAs that share common expressed regions, splicing events, TSSs or TTSs. Thus, TKs are contained within TU, and mRNAs lying within the same TK are expected to be functionally related. The analysis of RIKEN FANTOM3 cDNA library has identified a number of independent transcripts encoded from mouse genome which is at least one order of magnitude larger than previous estimates. Moreover, a total number of 16.274 new protein sequences have been introduced, and the 65% of all the TUs have been found to encode multiple splice variants (123).

However, approaches like the FANTOM3 library and others directed at creating large collections of cDNA clones do not fit the necessity to describe the dynamical aspects of transcriptome and other regulatory principles, like alternative splicing or alternative promoter usage.

Tagging technologies, which includes for example SAGE, CAGE and tiling arrays, are aimed at the description of new transcripts and their TSSs. Being the strategy of tagging methods related in no way to pre-existing sequence information or prediction, their main advantage is the complete transcriptional scanning of a target genome or, as in the case of tiling arrays, discrete portions of a genome.

By definition, tiling arrays are microarrays designed to cover at regular interval whole chromosomes or genomes, regardless of the genome annotation. The outcome of tiling arrays experiments so far published is striking; for example, a tiling array on human chromosome 20 and 22 has revealed that the number of detectable transcribed exons in at least one out of ten human cell lines tested is tenfold greater than the number of exons that are currently annotated, although this phenomenon has resulted to be highly cell- and condition-specific (124). In 2005, Cheng and colleagues combined in their tiling arrays on human chromosome 10 the use of $polyA^+$ and $polyA^-$ fractions from either the nucleus or the cytoplasm of HepG2 cells, and surprisingly they reported that 41.7% of all the RNA transcripts examined were confined to the nucleus. Moreover, in cytoplasmatic-RNAs, less than a third was polyadenylated, suggesting that transcripts constituting the remaining 2/3 are commonly cut out by procedures that use the presence of polyA tails for transcript purification (125). The total number of detectable RNAs that have emerged from these

experiments exceeds the whole fraction of annotated protein-coding exons by one order of magnitude.

6.1 CAGE and NanoCAGE technologies.

CAGE (Cap-Analysis of Gene Expression) is a powerful tagging technique set up at RIKEN Institute in Japan. It is based on the production of short tag sequences close to the 5'-end of the transcript and the ligation of tags into groups of concatamers, followed by cloning and sequencing of ligation products (126, 127).

CAGE requires the synthesis of cDNA from isolated RNA using either an oligo-dT or a random primer at high temperature (55°C–60°C) in presence of trehalose and sorbitol, which confer thermal stability to the reverse transcriptase. After the first strand cDNA synthesis, the cap site on the 5'-end of full length mRNAs is biotinylated and subsequently RNaseI is used to digest any single-strand RNA, including the biotinylated cap from non full length cDNA-mRNA partial hybrids. The biotinylated cap remains on the mRNAs-full length cDNAs hybrids only. After selection with streptavidin magnetic beads followed by RNA hydrolysis, a linker containing a restriction site for the class II restriction enzyme MmeI is ligated to the 5'-ends of first strand cDNA and used to prime second strand cDNA. MmeI recognizes the linker, but cleaves 20-21bp inside the 5'-ends of cDNAs. After ligation of a second linker to the 3'-end and various PCR and purification steps, these 20-21bp fragments are concatenated with DNA ligase and cloned into a plasmid vector for large-scale sequencing. Depending on concatenation efficiency, up to 15 of the 20bp long CAGE tags per clone are ligated, but usually 50 000-1 000 000 tags are sequenced (128).

The CAGE tags sequences are mapped to a unique location using a BLAST search against sequences in the databases (with 65% to 70% efficacy). Ambiguously mapped tags map to more than one location (mostly to two or to three), and a large proportion of these tags correspond to transcribed repeats. The enrichment over non-capped molecules (and so not full length or fragments) has been calculated to be about 330-fold (129). As when assessing cDNA mappings, new terminology had to be introduced to analyze CAGE-defined TSSs; CAGE tags are grouped into "Tag clusters" (TCs) including tags mapping on the same genomic region and that are overlapping for at least one base pair. The observed slight variations in the position of tags belonging to the same TC are likely to be due to the inherent variability of TSSs; putative TSSs indicated by the presence of a TC are defined as CAGE-tag starting sites (CTSSs).

TCs differ from transcriptional units (TUs) identified in RIKEN clone collection because alternative promoter usage can create more than one TC along a single gene or transcriptional unit.

The reliability of TCs as pointers of putative TSSs has been confirmed by classic data validation methods such as 5'-RACE; an extensive validation assay has demonstrated that in selected mouse genomic loci of specific biological interest where CAGE tags identified putative novel transcripts, RACE has confirmed the existence of TSSs in more than 90% of cases (127). Moreover, through statistical calculations assessing the number of tags related to a specific transcripts normalized per million of sequenced tags (tags per million, TPM) the information derived by CAGE data may be quantitative.

The sequencing of 145 CAGE libraries derived from a variety of mouse tissues has identified a total number of 729.504 CTSSs and 593.290 TCs. 159.075 TCs contained in independent libraries comprised at least one or two CAGE tags, and when these data were matched with the RIKEN clone collection a total of 236.000 TCs found a correspondence with either full length cDNAs or expressed sequence tags (ESTs). One of the most surprising evidences that have derived from various CAGE experiments is that initiation of transcription within transcriptional units is more diverse than expected; only 13.767 out of 20.639 mouse protein-encoding transcriptional units (67%) are supported by CAGE tags within 20 nucleotide from the annotated 5'-end of a full-length cDNA. In some cases, the increase of TSSs detected by CAGE in the 3'-UTR of protein-coding genes has been significantly related to the presence of a downstream gene on the opposite strand. A considerable number of CAGE tags (34.000) map into intronic regions or more generally inside coding sequences; it is not clear at present whether these atypical TSSs may generate truncated coding transcripts or non-functional transcripts, but the evidence that transcription in these loci is conserved between mouse and human suggests that the shorter transcripts or transcription itself may be functional.

The advantages of CAGE over other methodologies such as microarrays in identifying new promoters and new TSSs are becoming more evident as the sequencing technologies become more affordable; the CAGE approach has been recently adapted (DeepCAGE) to exploit the latest high-throughput sequencing technologies in a study that has revealed the differential usage of promoters in various regions of mouse brain (Eivind Valen et al., submitted). The transcriptional complexity of biological systems, such as the brain, can hardly be dissected using approaches that are limited right from the design phase because of inherent deficiencies; in the case of microarray, the main issue is that probes extension and variety are not adequate to cover the emerging transcriptional heterogeneity of genomes. Since 5'-end tags can capture a relevant number of details, including additional splice variants generated by alternative promoter usage, the information about the expression of a given transcriptional unit obtained by grouping all of its 5'-end tags is far more accurate.

A major issue of classic CAGE technology was the need for a huge amount of starting RNA from the target tissue of cell type; recent advancements in 5'-end tagging and sequence technologies have made possible to develop a new CAGE protocol suitable for starting total RNA quantities as low as 50 nanograms. This new technique, named "NanoCAGE", has a tremendous potential in the analyses of transcriptomes and promotomes of small RNA samples, for example those derived from Laser Cutting Microdissection (LCM), Fluorescence-Activated Cell Sorters (FACS) and similar technologies.

The NanoCAGE technique starts with a random primed first strand cDNA synthesis in the presence of a strand switching RNA-DNA oligonucleotide. This allows the introduction of a tag at the 3'-end of all the cDNA synthesized taking advantage of the well known terminal deoxynucleotide transferase activity of the reverse transcriptase. Then, a second strand cDNA is sythesized in the presence of primers that are used in a few cycles PCR reaction. Primers contain the site for EcoP151 that allows the post-PCR endonuclease digestion at 27 nucleotides 3' from the 5'-end of the double-stranded cDNA. Fragments are then ligated to an adaptor containing primers for sequencing, and after purification the 120 bp cDNAs collection is sequenced without cloning on a flow-cell system (Solexa) that allows obtaining a final tags number of about 20-30,000,000.

NanoCAGE protocol introduces a reduction in the number of purification steps in which a certain amount of starting material is usually lost. Moreover, first-strand cDNAs are synthesized using random primers so that polyA$^-$ RNAs are also reverse-transcribed; since this technology is unpublished and currently under patenting procedure it is not possible to reveal major technical details.

6.2 Genomic approaches to MOE.

The research on olfaction has recently started to take advantage of genomic large-scale technologies.

When Linda Buck and Richard Axel identified the OR genes family, their work was partly based on a one-gene-at-a-time approach and on the observation that OR genes were expressed in the olfactory epithelium, but were not detected in other tissues. In the following years additional OR genes were recognized in genomic sequences by their similarity to the first set of identified OR genes and by the presence of predicted protein motifs, but a homogeneous view of the number of genes coding for ORs and their distribution on chromosomes has been gained only when the analyses of complete mammalian genomes have been made available.

In 2004 Stuart Firestein and colleagues designed a custom high-density oligonucleotide array containing all known mouse OR and V1R genes deducted from the Celera mouse genome to empirically demonstrate the specific expression in the olfactory epithelium of 817 OR genes previously designated as "ORs" solely on the basis of their genomic sequences; the array was also used to monitor for the first time the spatial and temporal distribution of gene expression for the entire OR gene family in the olfactory epithelium (130). Interestingly, a subset of OR genes was found to be expressed only in non-olfactory tissues. The ectopic expression of olfactory receptor genes has been supported in 2006 by a work published by Doron Lancet and colleagues in which the expression of hundreds of human and mouse OR transcripts was analyzed via EST and microarray data but to date, apart from some unconfirmed hypothesis as mediators of sperm chemotaxis, their function is still unknown (131).

Using the same approach of Stuart Firestein group, in 2007 Yoav Gilad and colleagues detected the expression of 437 predicted human OR genes in human olfactory epithelium, in support of their functional annotation as odorant receptors. They also detected an abundant ectopic expression of some human OR genes but, even though an additional function of OR proteins was not excluded, on the basis of evolutionary analyses they suggested that this phenomenon could be due to a leaky activity of ORs promoters (132).

In the same year Timothy McClintock and his group published a gene expression profiling experiment on a pure population of OSNs isolated from the olfactory epithelium of a transgenic mouse model in which the expression of the green fluorescent protein (GFP) was driven by the promoter of OMP. Thanks to this approach they were able to assess the average expression of more than 10.000 genes in OSNs; the analysis of biological processes in which these genes are involved confirmed and expanded previously reported evidences that chromatin remodelling and gene silencing are highly active in OSNs and their progenitors, a data that may reflect the molecular activities needed for the process of neurogenesis that continuously takes place in the olfactory epithelium (133).

The first study that demonstrates a role for noncoding RNA transcripts in MOE has been published in 2008 by Catherine Dulac and colleagues; exploiting the advantages of a microRNA (miRNA) microarray platform, they have characterized the repertoire of miRNA expressed in the MOE of mouse and zebrafish, demonstrating that in both species a particular subset of noncoding RNAs belonging to the miRNA 200 family is required for terminal differentiation of olfactory precursors, even though they are not essential for the proper function of mature OSNs. This work has strengthened the evidence that vertebrate tissue differentiation is controlled by conserved subsets of organ-specific non-coding RNA (134).

Large-scale approaches such as microarrays have indeed represented in the past few years a way to gain new exciting insights of the olfactory world. In spite of that, to dissect the emerging structural complexity of the transcriptional world that is most likely to be paired by a functional complexity, the scientific community will have to look at new adequate technologies.

7. Aims, theoretical basis and experimental approach of this thesis.

This Ph.D. thesis has been concentrated on three separate projects aimed to unveil the molecular basis of unsolved biological issues in MOE:

1. The molecular identity of the calcium-activated chloride channel involved in the canonical cAMP transduction pathway in OSNs;
2. The description of the molecular repertoire of genes expressed in microvillar cells;
3. Taking advantage of the new high-throughput NanoCAGE technology developed in collaboration between the laboratory directed by Prof. Gustincich at SISSA, Trieste, and the laboratory directed by Dr. Piero Carninci at RIKEN Institute, Japan, the transcriptome of the main olfactory epithelium has been described.

The following sections will present the theoretical basis of these three biological problems.

7.1 The molecular identity of chloride channels involved in olfactory transduction.

The identification of the molecular players involved in olfactory transduction has gone through a long road (135).

The first hypothesis concerning the involvement of a signalling cascade in olfactory neurons was made in 1976 by Bert Menco and Adnan Menevse. Their work claimed that the production of olfactory potentials was stimulated by an adenylyl cyclase activity leading to production of cAMP as a second messenger. In the following years, Gloria Adamek demonstrated that the recording of MOE electrical activity (electro-olfactogram, EOG) was dependent on the presence of cilia in physiological preparations. This observation led to the development of a protocol for the isolation of cilia by Solomon Snyder and Doron Lancet representing a key step for the understanding of

cAMP induction by most odours in preparations of isolated cilia. In 1987 a cyclic nucleotide gated cation conductance was observed in the membrane of cilia, supporting the idea that odour molecules could trigger receptor potentials by opening ion channels through the activation of an adenylyl cyclase. The olfactory-specific subunit A2 of the CNG channels responsible for this conductance was cloned from olfactory epithelium in 1990. The olfactory G-protein $G\alpha_{olf}$ was characterized in 1985 and cloned in 1989 by Randall Reed which, one year later, together with Heather Bakalyar identified adenylyl cyclase III as an olfactory-specific enzyme. The identification of olfactory transduction pathway components culminated with the revolutionary discovery of G-protein coupled odorant receptors by Linda Buck and Richard Axel in 1991.

In 1993 Steven Kleene postulated the use of an amplification system by OSNs in order to improve the detection of weak stimuli (136).

Stimuli amplification is a device often found in sensory systems and its importance is fundamental since following amplification steps weak stimuli become able to trigger action potentials.

Differing from other sensory mechanisms, in the olfactory transduction signal amplification is not introduced by the production of many molecules of the second messenger cAMP; following activation of ACIII, the production of cAMP in the ciliary lumen follows a fine-tuned and highly efficient energy conversion set to optimize the consumption of ATP that is broadly used for a number of cellular processes. The high surface/volume ratio of the ciliary structure further refines this calibration. Signal amplification in this system is actually introduced only in its final stage; interacting with CNGs, cAMP causes an increase of cytoplasmatic concentrations of Na^+ and Ca^{2+} that results in a multiple activation of Ca-activated chloride channels. Using a complex of membrane transporters, OSNs maintain an unusual high concentration of intraellular Cl^- ions. When chloride channels are activated, the Cl^- efflux from the cells further depolarizes the overall membrane potential, thus increasing the transduction current approximately 10-fold over the CNG current alone. The Cl^- ions stock in OSNs represents an evolutionary adaptation to the fact that mucus-embedded cilia are surrounded by an ionically unstable environment if compared to interstitial spaces.

Although it has been possible through years to determine the electrophysiological properties of currents involved in this mechanism, the molecular identity of the olfactory Ca-activated chloride channel has always remained elusive.

The family of bestrophins constitutes a novel set of calcium-activated chloride channels whose contribution to diverse physiological processes is currently under investigation; bestrophin-1 (vmd2) is the most characterized member of the family because mutations in the human variant are

linked to various kinds of macular degeneration, including Best's vitelliform macular distrophy (BVMD) from which the name of this channel proteins family derives (137).
The vmd2 gene was isolated by positional cloning in 1998, but the function of its encoded protein has remained enigmatic for a long time. Bestrophin-1 is homologous to at least 3 other proteins encoded within the human genome, 4 in the *Drosophila Melanogaster* genome, and 24 in the *Caenorhabditis elegans* genome, but they show no detectable homology to any protein of known function. In 2002, Hui Sun and colleagues demonstrated for the first time that all bestrophin family members expressed in heterologous system were able to produce a calcium-sensitive chloride conductance with distinct features in terms of current properties and ion selectivity (138). Bestrophins were also showed to form tetramers or pentamers, and on the basis of their peculiar structure and physiological properties of the measured chloride currents, bestrophins were found to define a new family of Cl^- channels. In a work published a year later by the same group, it was proposed that bestrophins might coassemble with other subunits in physiological conditions (139).

Combining RT-PCR from single isolated olfactory sensory neurons, molecular cloning and immunohistofluorescence techniques the data presented in this Ph.D. thesis contributed to the identification of bestrophin-2 as a calcium-activated chloride channel candidate to be a component of the native olfactory chloride channel. These data has led to the publication enclosed in the final section.

This project was a collaborative effort with the laboratory directed by Prof. Anna Menini at SISSA.

7.2 The investigation on the nature of olfactory microvillar cells.

Olfactory microvillar cells (OMCs, MCs) are flask-shaped cells with an apical end that gives rise to a tuft of microvilli projected into the mucus layer lining the nasal cavity. They have been identified in the olfactory epithelia of various species and their microvilli are morphologically different from those covering supporting cells.
The first description of microvillar cells (MCs) dates back to 1975 when they were observed in an electron microscopy study by François Jourdan; because of the lack of details about their function they have been usually discarded from reviews concerning the cellular architecture of the olfactory epithelium (140).
Nevertheless, MCs are quite frequent in OE: in 1989 a ratio of 1 MC for 10 OSNs in humans and 1 MC for 20 OSNs in rodents was calculated by Rowley and colleagues, but these numbers have

recently been reconsidered and it is now accepted that in rodent MOE there are 50 MCs for every olfactory neuron expressing a given odour receptor (135).

MCs are localized in the superficial layer of the epithelium, surrounded by OSNs axons directed to the luminal surface and by cell bodies of supporting cells; on the basal side they have a thin process that reaches the basal lamina.

A number of studies have identified at least two types of MCs in different species. One of these types resembles brush cells, a specialized cell type endowed with microvilli which can be found throughout the respiratory and gastro-intestinal epithelium (141).

Aside from this morphological similarity, very controversial data can be found in literature about neuronal or epithelial nature of MCs.

In 1982 Moran and colleagues identified MCs in biopsies of human olfactory epithelium taken from normal individuals and, on the basis of the observed frequency and morphology, they hypothesized that MCs might have been a new type of bipolar sensory neuron in the olfactory epithelium (142). Seven years later the same group tested this hypothesis by injecting the cytochemical tracer macromolecule horseradish peroxidase (HRP) into the olfactory bulb of the rat, and observing its pattern of uptake in the olfactory epithelium by light and electron microscopy (143). In these experiments, OSNs and microvillar cells backfilled with HRP while supporting and basal cells did not. These data seemed to demonstrate that MCs, together with OSNs, could project their axons to the OB. However in 1991 by Carr and colleagues showed that resection of olfactory bulb did not cause the degeneration of MCs, but only that of OSNs challenging previously released data. Moreover, immunoreactivity for OSNs classical marker olfactory marker protein (OMP) in MCs was negative (144).

In the attempt of clarifying the role of second messenger inositol triphosphate (IP3) in olfactory transduction, Rebeccea Elsaesser and colleagues found a specific and selective expression of phospholipase C-β2 in the microvilli of a distinct cell population defined as PLC-β2 cells. Further investigations confirmed that they did not express OMP or degenerate following unilateral bulbectomy, but in initial Ca^{2+} imaging experiments these cells showed a transient increase of Ca^{2+} intracellular concentration following exposure to some odour mixes. Besides PLC-β2, these cells were found to express also other fundamental components of the PLC/IP transduction pathway: a transient receptor potential channel, type 6 (TRPC6) and an intracellular receptor for inositol triphosphate, type 3 (IP3R-3).

On the basis of their data, the authors suggested that those cells might represent a second type of microvillar sensory cell in the olfactory epithelium, more similar to taste cells than to classical OSNs (145). In 2006 the same group demonstrated the selective expression of neuropeptide Y

(NPY) in MCs and they suggested a role for these cells in the interplay between degenerating OSNs and olfactory stem cells, which concurs to control neuronal proliferation in the postnatal OE (146).

To deepen the knowledge of this cellular type MCs have been harvested with a custom immunofluorescence-laser capture microdissection protocol (IF-LCM) and their transcriptional landscape has been analyzed by means of a two-channel custom cDNA microarray based on the FANTOM2 RIKEN full-length cDNA clone collection.

7.3 NanoCAGE of the mouse MOE.

The NanoCAGE protocol adapted CAGE technique to small samples of total RNA and taking advantage of the most recent high-throughput sequencing technologies. The availability of this technique in our laboratory has represented a unique opportunity to investigate for the first time the transcriptome of MOE with an open tagging methodology and high-throughput sequencing technology.

The emerging global view of mouse olfactory system has revealed that both the VNO and the MOE are capable of sensing volatile as well as non-volatile pheromonal and non-pheromonal cues; the resulting role of the MOE, the VNO and others olfactory subsystems must therefore be interpreted as a cooperation aimed at driving the behaviour through different social and environmental contexts, and this observation is supported by the recent findings that some areas of rat telencephalon are target sites for convergent olfactory and vomeronasal inputs (147).
However, the molecular components that stand behind the pheromonal responses in MOE are unknown. In this Ph.D. thesis NanoCAGE data analyses showed for the first time the expression of vomeronasal receptors belonging to class 2 in the MOE.

Materials and Methods

Part 1: mBest2 as a candidate Calcium-activated chloride channel involved in olfactory transduction.

1.1 Animals, tissue preparation and RT-PCR.

Adult C57Black/6J mice were killed by carbon dioxide inhalation and decapitated; the olfactory epithelium was dissected from the head, immediately snap-frozen in liquid nitrogen and stored at -80°C. To extract total RNA, each OE sample was added with 0.5ml of TRIzol reagent (Invitrogen, CA, USA) and homogenized in a glass potter kept on ice; RNA was extracted according to the manufacturer's instructions and the pellet was resuspended in nuclease-free water (Ambion, TX, USA). A fraction of the total RNA sample was treated with DNase I (Ambion) at 37°C for 1 hour, and the sample was then purified on RNAeasy mini kit columns (Qiagen, Germany). The final quality of RNA sample was tested on agarose gel. The oligonucleotide primer pairs used for each mouse bestrophin (mBest) gene, are listed in the following table:

Gene name	Accession number (GenBank)	Sequences (5'→3')	Expected PCR product size (basepairs)
mBest1	AY450427	Fw: GCATCTACAAGCTGCTGTATGG Rev: CGAAGGATATAGGGATGAGCTG	191bp
mBest2	BC019528	Fw: CCTCGTCTACACCCAGGTAGTC Rev: GCGGTCAATAAGAAAGTTGGTC	240bp
mBest4	AY450426	Fw: GAAACCTGCAGGTCTCTCTCTT Rev: CCAGGATGCTCGTGGGTACTCA	279bp
Clca1	NM009899	Fw: GCACTTCCGGTTCTGAGATCGT Rev: GGCATAGAAACGAAGCCCTCCT	171bp
Clca2	NM030601	Fw: GGTGGTCCACGAGTGTCAGAGA Rev: TGCTTCTGCGATTGCACATTTT	205bp
Clca3	NM017474	Fw: AGAGAGCAGCACCTCCGAAGAA Rev: GCTGGCCTTCAGGTCAGTGATT	198bp
Clca4	NM139148	Fw: TTGCTGAGACAGGCACTTGGAC Rev: CCAGAACAGGCAAAAACCCTTG	184bp
Clca5	NM178697	Fw: CTCAGAAGCACTTGGGACGTGA Rev: CTCTGCCATCTTCCTGGACACA	187bp

Commercial mouse total RNA from testis and heart for positive controls was purchased from Ambion. First strand cDNA synthesis was carried out by adding 2µg of DNase digested OE total RNA to a mix containing 10mM dNTPs mix (Invitrogen), 30ng of random primers (Invitrogen) and water to a volume of 10µl; sample was gently mixed, briefly centrifuged, put in a thermocycler at 70°C for 5 minutes and left on ice for 1 minute; a mix containing 5X First strand buffer, 0.1M DTT, 20u Superscript RTII (all three reagents from Invitrogen) or 1µl of nuclease-free water (Ambion) in the RT- sample, and 20u SuperaseIn RNase inhibitor (Ambion) was added to the sample and the tubes were put in a thermocycler at 50°C for 1 hour followed by 15 minutes at 70°C. Polymerase chain reaction mix was prepared by adding 2µl of first strand reaction with 0.5µl Platinum Pfx DNA polymerase (Invitrogen), 10mM dNTPs mix, 10x buffer, 10mM of each oligonucleotide primer, 50mM $MgSO_4$ and water to a final volume of 50µl.

To clone the full coding sequence of mBest2, we used the oligonucleotide primers couple Best2ORF-FWD (5'-ATGGCACTAAGCGCCGCCTATC-3') and Best2ORF-REV (5'-TCAGGCCGGACTCTCTTCCTC-3'). The PCR reaction was carried out with the same protocol used to amplify the short mBest2 fragment; the cycler program was modified according to DNA polymerase guidelines but a further increase of the annealing temperature to 72°C was necessary in order to obtain the desired full-length mBest2 target amplicon. All PCR products were cloned in ZeroBlunt TOPO cloning kit for sequencing (Invitrogen), the clones were processed with SequiTerm Excel II DNA sequencing kit (Epicentre biotechnologies, WI, USA) and sequenced with a 4200 sequencer from LI-COR.

1.2 Single Cell RT-PCR custom protocol.

Dissociated cells were prepared from OE as previously described (148, 149). A micromanipulator system for patch-clamp was used for picking up individual olfactory sensory neurons (OSNs) or supporting cells, selected using morphological criteria under an Olympus IX70 inverted microscope (Olympus, Germany). Cells were collected in TRIzol reagent, immediately snap-frozen in liquid nitrogen and stored at -80°C. Total RNA was extracted from OSNs or supporting cells with Absolutely RNA nanoprep kit (Stratagene, CA, USA) according to manufacturer's protocol. The entire eluate (~7µl) was used in subsequent steps. First strand cDNA synthesis and 40 cycles of PCR were performed with Superscript One-step RT-PCR system (Invitrogen, CA, USA) according to manufacturer's protocol. A second round of amplification (30 cycles) was carried out by using 2µl of the first-step samples added with RedTaq DNA polymerase (Sigma-Aldrich, MO, USA), 10×

reaction buffer, 10mM dNTPs, 10mM Best2-FWD/Best2-REV primers in a final volume of 50μl. PCR samples were loaded and analyzed on agarose gel.

1.3 Production of an Anti-mBest2 Polyclonal Antibody.

Full-length mBest2 cDNA (clone identification: IRAVp968E0673D) cloned in pCMV-Sport6 mammalian expression plasmid was obtained from the RZPD collection (Deutsches Ressourcenzentrum für Genomforschung, Berlin, Germany). A C-terminal 431-bp fragment was amplified by PCR and ligated to GST sequence in the isopropyl β-D-thiogalactoside (IPTG)-inducible pGEX vector (Amersham Pharmacia Biosciences, NJ, USA) to generate a GST-mBest2 344-C end fusion. Protein production was achieved in BL21 bacteria after a 0.5mM IPTG induction for 2 h at 30°C. GST-mBest2 was affinity-purified on GSH-Sepharose resin (Amersham Pharmacia Biosciences), following the manufacturer's protocols. Purified protein was used to immunize two rabbits with consecutive bursts of increasing protein quantities, after which the blood of the animals was collected at selected timepoints; sera isolated from the last bleedings were used for purification of the α-mBest2 antibody by flowing 10mL of sera on a column containing the purified GST-mBest2 purified protein cross-linked with a CNBr-activated sepharose resin (Amersham Pharmacia Biosciences). The antibody was eluted with 0.1M glycine pH2.7, osmotically transferred in a PBS-based buffer and stored at -80°C.

1.4 Cell Culture, Transfections, and Immunoblot.

HEK-293 cells were grown in DMEM (GIBCO-Invitrogen, CA, USA) supplemented with 10% FBS (Sigma-Aldrich, MO, USA), 100 units per ml penicillin, and 100μg/ml streptomycin (Sigma-Aldrich) at 37°C in a humidified CO_2 incubator. Transfection of HEK-293 cells with RZPD clone of mBest2 in pCMV-Sport6 was performed by using FuGENE 6 reagent (Roche Applied Science, Germany) according to the manufacturer's protocol; in electrophysiological experiments, transfected cells were identified by cotransfection with EFGP in pGFP (Clontech, CA, USA). Cells were lysed in 300mM NaCl/50mM Tris, pH7.5/0.5% Nonidet P-40/10% glycerol, supplemented with complete EDTA-free protease inhibitor mixture (Roche Applied Science) for 1 hour at 4°C. Lysates were cleared at 15,000 $\times$ g for 20 minutes, and supernatant was assayed for protein concentration with Bradford reagent (Sigma) according to manufacturer's protocol. For Western blot, samples were resolved on 10% and 12% SDS/PAGE, and proteins were transferred to nitrocellulose membrane (Schleicher & Schuell, Florham Park, NJ). Membrane was blocked with

5% nonfat milk in Tris buffer saline solution (TBST), then incubated overnight with primary antibodies at 4°C, and proteins were detected by horseradish peroxidase-conjugated secondary antibodies (DakoCytomation, Glostrup, Denmark) and ECL reagents (Amersham Pharmacia Biosciences).

1.5 Preparation of membrane fractions enriched in cilia.

Membrane fractions enriched in olfactory cilia were obtained by using the calcium-shock method already described in literature (32, 136). 20 adult C57Bl/6 mice were killed by carbon dioxide inhalation. The olfactory epithelium was dissected from the head and after a short wash in ice-cold saline solution (120mM NaCl/5mM KCl/1.6mM K_2HPO/25mM $NaHCO_3$/7.5mM glucose, pH7.4), the tissue was incubated in a saline solution containing 10mM $CaCl_2$ and gently stirred for 5 minutes at 4°C. Detached cilia were isolated by three sequential centrifugation steps for 5 minutes at 7,700 × *g*. The supernatants containing the cilia were collected, and pellets were resuspended in the same above 10mM $CaCl_2$ saline solution. The cilia preparation was obtained after a final centrifugation step of all of the pooled supernatants for 15 minutes at 27,000 × *g*. The pellet containing the cilia was resuspended in hypotonic buffer (10mM Tris/3mM $MgCl_2$/2mM EGTA, pH7.4) and stored at -80°C.

1.6 Immunofluorescence.

OE from postnatal day 15 (P15) and adult mice was fixed in 4% formaldehyde/15% aqueous saturated picric acid/150mM sodium phosphate, pH7.4, for 1 hour at 4°C, washed in PBS1X, equilibrated in 30% sucrose/PBS1X overnight (for OE from adult mice: tissues were previously decalcified by overnight incubation in 0.2 M EDTA pH8.0), and 30µm-thick coronal sections were cut on a cryostat. Sections were air-dried overnight, treated for 15 minutes with 0.5% SDS in PBS1X for antigen retrieval, incubated in blocking solution (2% normal goat serum, 0.2% Triton X-100 in PBS1X) for 90 minutes, and incubated overnight at 4°C in primary antibodies diluted in blocking solution (our anti-mBest2 was diluted 1:50). After rinses in 0.1% Triton X-100 in PBS1X, sections were incubated with fluorophore-conjugated secondary antibodies (Molecular Probes-Invitrogen, CA, USA) in blocking solution for 2 hours at room temperature, washed and mounted with Vectashield mounting medium (Vector Laboratories, CA, USA). The staining was analyzed with an Olympus Fluoview 300 confocal microscope (BX51WI). Primary antibodies were: mouse

monoclonal anti-CNGA2 (58) and goat anti-OMP (150) used at 1:200 and 1:500, respectively. Secondary antibodies were: Alexa 488-conjugated donkey anti-goat, Alexa-594-conjugated chicken anti-rabbit, Alexa 488-conjugated goat anti-rabbit and Alexa 594-conjugated goat anti-mouse diluted at 1:200.

Part 2: Genomic investigation on olfactory microvillar cells.

2.1 Laser Catapulting Microdissection (LCM).

LCM has been created by the fusion of two different technologies, Laser Microbeam Microdissection (LMM) and Laser Pressure Catapulting (LPM); in LMM the high photonic energy of a nitrogen laser channelled through a microscope objective is focused on the same plane of the specimen to isolate single cells, a specific cell cluster or a small tissue region from the surrounding tissue. Circumscription of the target sample operated with the laser results in a gap, free from any biological material, which can have a width of 1 to 10 microns, depending on the chosen objective and the power of the laser. Following microdissection, the focus of the laser is centred slightly below the microdissected target specimen and the energy is increased to about twice the level used for microdissection. By using discrete laser shots the microdissected sample is ejected from the glass slide and catapulted directly into the cap of a common microcentrifuge tube; cells or tissue areas can be catapulted at a distance of up to 8mm, depending on the energy of the laser. If the target tissue slices are mounted on normal glass slides, this process results in a fragmentation of the microdissected area, even though it is demonstrated that this disruption does not have a negative impact on post-processing of the sample. However, it is possible to preserve the morphology of the microdissected target by transferring the slices immediately after cryostat cutting on special glass slides coated with a polymeric membrane, whose function is to give a mechanical support to the microdissected sample during the phase of catapulting. Membrane-coated slides are particularly useful in case of large microdissected ares, and with this approach is possible to catapult samples up to 1mm in diameter (151).

2.2 Animals, tissue preparation, immunofluorescence and microvillar cells harvesting.

20-22 days old C57Bl/6 mice were sacrificed by inhalation of carbon dioxide After decapitation, the skin and the lower jaw were removed and the head was included in frozen section medium Neg-50 (Richard Allan scientific, MI, USA) and frozen on liquid nitrogen-iced isopentane for 2 minutes. The frozen block was brought into cryostat (Microm International, Germany) and left at -21°C for 30-120 minutes. Coronal sections of olfactory epithelium (14μm) were cut with a clean blade, transferred on Superfrost Plus glass slides (Menzel-Glaser, Menzel GmbH & co KG, Germany), immediately fixed with ethanol absolute for 1 minute and with acetone for another minute (both reagents from Carlo Erba Reagents, Italy). Sections were circled with liquid-repellent slide marker pen Super Pap Pen (Invitrogen, CA, USA) and incubated with 50μl of primary antibody solution containing 1X PBS diluted in nuclease-free water (both reagents from Ambion, TX, USA), α-IP_3R3 antibody (1:50, BD Transduction Laboratories, BD Biosciences, CA, USA), RNA*later* (diluted at 1:5, Ambion) and 0.1% Triton X-100 (Sigma-Aldrich, MO, USA). After 30 minutes the first solution was replaced with 50μl of secondary antibody solution containing 1X PBS diluted in nuclease-free water, Alexa Fluor 594-conjugated goat α-mouse IgG (1:250, Invitrogen Molecular Probes, Oregon, USA), RNA*later* (diluted at 1:7.5) and 0.1% Triton X-100. The incubation was carried on for additional 30 minutes, then the secondary antibody solution was removed and fluorescent microvillar cells were identified and marked on wet tissue with a Zeiss P.A.L.M. LCM microscope (Carl Zeiss Inc., Germany); once the tissue sections ran dry microvillar cells were microdissected, collected in adhesive caps (PALM Microlaser Technologies GmbH, Germany) and immediately processed.

Some of the slides containing the OE coronal sections were used for total RNA quality controls and were taken away during consecutive steps of the immunofluorescence-LCM protocol. The sections were scraped from the slides with a clean blade and collected in a clean tube containing 0.5ml of TRIzol reagent (Invitrogen). RNA was extracted following manufacturer's protocol and the quality of total RNA was tested on agarose gel.

2.3 mRNA processing for two-channel custom microarray experiments.

Messenger RNA from microdissected microvillar cells was extracted, isolated, purified and amplified with μMACS SuperAmp kit (Miltenyi Biotec, Germany) according to manufacturer's protocol to produce a GlobalPCR sample. GlobalPCR product was purified with High Pure PCR Product Purification Kit (Roche diagnostics GmbH, Germany) and DNA concentration in the

sample was measured with ND-1000 spectrophotometer (Nanodrop technologies, DE, USA). For hybridization on two microarray slides (SISSA1/SISSA2), 350 nanograms of globalPCR were labelled with μMACS SuperAmp kit with the addition of Klenow Fragment (20 units, Fermentas Inc., MD, USA) and 25nmol cy3-dCTP (GE Healthcare, UK) according to manufacturer's protocol. Once labelled the probe was purified with Illustra CyScribe GFX Purification kit (GE Healthcare); incorporation of dye and DNA concentration were measured with ND-1000 spectrophotometer.

2.4 Standard RNA processing for two-channel custom microarray experiments.

For hybridization on two microarray slides (SISSA1/SISSA2) 10μg of Universal mouse reference RNA (Stratagene, CA, USA) were mixed with 200ng of random primers and 100mM of smart T7-24 primer; after 5 minutes at 70°C the pre-mix was added with 4μl of 5X First Strand Buffer, 2μl of DTT (both reagents from Invitrogen, CA, USA), 2μl of amino allyl dUTP-dNTPs, 1μl of SuperScript II (Invitrogen) and 0.5μl of RNAse Out (Invitrogen). The reaction mix was incubated for 2 hours at 37°C and for 5 minutes at 70°C to inactivate the enzyme. After the addition of 1μl of 0.5M EDTA pH 8.0 and 10μl of 1M NaOH the reaction was incubated at 70°C for 10 minutes and then 20μl of 1M HEPES were added. The standard probe was precipitated at 4°C for 30 minutes by adding 3M NaOAc to a final concentration of 0.3M, 1μl of Linear Acrylamide (Ambion), 150μl of nuclease-free water (Ambion) and 150μl of Isopropanol. The sample was centrifuged for 30 minutes at 15000 x g and the isopropanol was carefully removed; the pellet was washed once with 70% EtOH, resuspended in 4.5μl of water and 4.5μl of 0.1M $NaHCO_3$ and it was incubated for 15 minutes at RT. Cy5 dye (GE Healthcare) resuspended in 2μl of DMSO was added to the sample and the coupling between the probe and the dye was performed overnight at RT.

The coupling reaction was quenched with 4.5μl of 4M hydroxyamine followed by incubation at RT in the dark for 15 minutes and then 35μl of 100mM NaOAc pH 5.2 were added to the sample.

The labelled probe was purified with PCR purification kit (Qiagen, Germany); incorporation of Cy5 and DNA concentration were measured with ND-1000 spectrophotometer.

2.5 Two-channels microarray hybridization.

In the pre-hybridization steps SISSA1/SISSA2 slides were incubated for 1 hour at 55°C in 0.2X SSC buffer filtered through a 0.22μm filter, briefly washed in ddH_2O and centrifuged at 2000 rpm for 5 minutes.

For each couple of slides 2µg of microvillar cells Cy3-probe were mixed with 2µg of standard RNA probe and the resulting sample was added with 1.3µl of Salmon Sperm (Sigma-Aldrich, MO, USA), 1.3µl of Cot-1 mouse (Invitrogen, CA, USA), 6.6µl of 10mg/ml Polyadenylic acid (Sigma-Aldrich) and 6.6µl of 10.8mg/ml tRNA (Sigma-Aldrich). The total volume of the sample was brought to 150µl with MilliQ water. 150µl of 2X formamide-based hybridization buffer (Genisphere, PA, USA) were pre-heated at 65°C for 10 minutes and added to the sample.

The slides were mounted on a GeneMachines Hyb4 Microarray Station (Genomic Solutions, MI, USA) and after a pre-heating at 80°C for 10 minutes the sample was loaded by pipetting 150µl on each slide.

Hybridization was performed by the following protocol: 65°C for 2 hours, 55°C for 2 hours, 44°C for 12 hours. Slides were then washed 5 times with 2X SSC/0.2% SDS at 65°C, 5 times with 2X SSC at 55°C, and 5 times with 0.2 SSC at 42°C. Each single wash comprehended 10' of flowing solution, and 30' of holding temperature. The slides were centrifuged at 2500 x *g* for 10 minutes in the dark and then scanned with a GenePix Personal 4100A microarray scanner (Molecular Devices Corporation, CA, USA).

2.6 Microarray data analysis.

The pre-processing (reading of the slide, intra-array normalization and inter-array normalization) of the data was executed on every group independently. The loading, normalization and statistical analysis were performed by using the LIMMA package from the BioConductor collection of packages in the R programming environment for statistical computing. The normalization intra array has been performed by using the function "normalizeWithinArrays" applying the LOWESS algorithm: "normalizeWithinArrays(RG,method="loess",bc.method="normexp",offset=50)".

The inter array normalization by using the function "normalizeBetweenArrays" by the application of quantile method: "normalizeBetweenArrays (MA,method="quantile")".

All the statistical analyses have been performed by using the eBayes function from the LIMMA package. The filters used are the widely accepted: fold change $\leq \log2(-1)$ or fold change $\geq \log2(1)$ (which is a fold change of ± 2 on a linear scale) and corrected p-value ≤ 0.05.

Part 3: Whole mouse OE collection for NanoCAGE processing and NanoCAGE data validation.

3.1 Animals, tissue preparation, LCM and RNA quality control.

For the first OE collection, two C57BL/6J mice (a p20 male and a p21 female) were sacrificed by inhalation of carbon dioxide. After decapitation, the skin and the jaw were removed from the heads and the samples were left overnight in ZincFix fixative (BD Biosciences, CA, USA) diluted in DEPC-treated water. After a 4 hours cryoprotection step in a 30% sucrose/1X ZincFix solution the heads were included in Frozen section medium Neg-50 (Richard Allan scientific, MI, USA) and left on liquid nitrogen-iced isopentane for 2 minutes. The frozen blocks were brought into a cryostat (Microm International, Walldorf, Germany) and left at -21°C for 30-120 minutes. Serial coronal sections of mouse heads (16μm) were cut with a clean blade, transferred on PEN-coated P.A.L.M. MembraneSlides (P.A.L.M. Microlaser Tehnologies, Germany) and immediately stored at -80°C.

For the second OE collection, three C57BL/6J mice (two p12 males and a p13 female) were used; no major changes were applied confronting to the first collection. The total number of slices obtained in the two collections was 100, with 3/4 sections on each glass slide.

The olfactory epithelium was collected from mouse head sections by Laser Capture Microdissection technology (LCM). Before usage, the slides were brought at RT and air dried for 2 minutes. Olfactory epithelium contained in each coronal sections was morphologically identified, marked, microdissected and catapulted with a Zeiss P.A.L.M. LCM microscope (Carl Zeiss Inc., Germany) in P.A.L.M. tubes with adhesive caps (PALM Microlaser Technologies GmbH, Germany). After the harvest, 10μl of lysis buffer (Stratagene, CA, USA) were added in each cap; the samples were left capsized at RT for 10 minutes, centrifuged at 6000 x g for 10 minutes and stored at -80°C. RNA from the samples was extracted, DNase treated and purified with Absolutely RNA Microprep kit (Stratagene, CA, USA) following manufacturer's instruction. After the elution step in nuclease-free water (Ambion, TX, USA) the concentration of the samples was measured with measured with ND-1000 spectrophotometer; 500pg of each sample were run on a 2100 Bioanalyzer (Agilent, CA, USA); the samples with a resulting high total RNA quality were pooled together (26 out of 30 total samples) and stored at -80°C.

3.2 Animals, tissue preparation and RT-PCR.

5 adult C57Black/6J mice were killed by carbon dioxide inhalation and decapitated; the olfactory epithelium and the vomeronasal organ were dissected from the heads, immediately snap-frozen in liquid nitrogen and stored at -80°C. RNA extraction, DNase treatment and RNA quality test were carried out following the same procedures described in section 1.1 with no modifications. The oligonucleotide primer pairs designed to amplify the vomeronasal receptors, the Galpha subunits, the transient receptor potential channel-C2 and the olfactory marker protein are listed in the following table:

Gene name	Sequences (5'→3')	Expected PCR product size (bp)
V1rG7	Fw: CCTACTGAGTTGCTTCCAAGC Rev: GAGCACTATGGATATGCTTGACTT	381bp
Vmn2r29	Fw: CAGGAAGTAGAAAGATGCCATCCTC Rev: GAAACAGCCACAGTGAATACAATTCC	484bp
Vmn2r69	Fw: CAGAATTCCTGAGCTTTACTGTGGT Rev: AGGTATCTCAGGTTGCTGGTGT	508bp
Vmn2r95	Fw: CAAATGAAACAGATGTAGACCAGTG Rev: ATCTTGGTCAATGAATGGTGGA	539bp
Vmn2r99	Fw: TTCTTTCCATGGCAGCTTAACACC Rev: GGCAGTTAGTGCAGATAAGCACAA	507bp
Vmn2r118	Fw: TCAAATGCCACAGATCTAACAC Rev: GGAACAGATTGGAATGATGACTT	524bp
Gnao1	Fw: GCAACCTATTTGACTGCTTCATGG Rev: CACTGCCTGGTGGTATATGAGG	534bp
Gnai2	Fw: CTTACACTTCAAGATGTTTGATGTG Rev: GTCCTTCAGGTTGTTCTTGAT	472bp
Trpc2	Fw: CCAGAAGATCGAGGATGATGCTG Rev: CAATCCCAGGCATAGTCAGCT	569bp
Omp	Fw: AGCTAGCAACAGTGATGTCCCTG Rev: CGGATCCGAGTGAGGCAGAGTTG	655bp

To avoid unwanted amplification of residual genomic DNA the forward primer of each couple was exon-spanning.

First strand cDNA synthesis was performed as described in section (section) with no modifications; PCR were carried out by adding 1µl of first strand reaction to a mix containing 5u of Takara Taq DNA polymerase, 10X buffer, dNTPs mix 2.5mM each (all reagents from Takara, Japan), 50pmol forward and reverse primers and nuclease-free water (Ambion) to a final volume of 50µl; PCR products were analyzed on agarose gel.

3.3 Digoxygenin and biotin-labelled probes preparation.

PCR products were cloned in pGEM T-easy vector (Promega, WI, USA) and sequenced as described in section (section). 10µg of each plasmid containing the specific PCR product were linearized with SacII (NEB) or with SalI (Promega) restriction enzymes for transcription with SP6 and T7 promoter, respectively. After an ON incubation at 37°C, 0.5µg were loaded on agarose gel to check the complete linearization of the plasmids; the samples were then cleaned with the PCR purification kit (Qiagen), eluted in nuclease-free water (Ambion, TX, USA) and the DNA concentration was measured with a ND-1000 spectrophotometer.

For digoxygenin-labelled and biotin-labelled RNA probes transcription, 1µg of each digested plasmid was added to a mix containing 2µl of DIG or BIO labelling mixes (Roche Applied Science, Germany), 20 units of SP6 or T7 RNA polymerases, 5X transcription buffer (both reagents from Promega, WI, USA), 0.1M DTT, 20 units of SuperaseIn RNase inhibitor (Ambion) and nuclease-free water (Ambion) in a volume of 20µl. After 2 hours of incubation at 37°C, the transcription reaction was stopped by adding 2µl of 200mM EDTA pH 8.0. RNA probes were precipitated by adding 1.25µl of LiCl 4M and 37.5µl of absolute ethanol cooled at -20°C and placing the samples for 2 hours at -80°C. Samples were then centrifuged at 20.000 x *g* for 30 minutes at 4°C, the RNA pellets were washed once with 70% ethanol diluted in nuclease-free water (Ambion) and after a brief centrifugation at 10.000 x *g* they were air-dried and resuspended in 50µl of nuclease-free water with the addition of 20 units of RNase inhibitor. The presence of reaction products was verified by running 5µl of each sample on agarose gel, and the RNA concentration was measured with a ND-1000 spectrophotometer. Aliqouts of 5µl were prepared in silanized tubes and stored at -80°C.

3.4 Animals and tissue preparation for in situ hybridization.

18-25 days old C57Bl/6J mice were anesthetized with a 0.75g/kg urethane solution injection and perfused intracardially with a 4% parafomaldehyde/PBS1X solution pH7.4 prepared in DEPC-treated water. After the perfusion, mice were decapitated, the skin and the lower jaw were removed and the sample was put in the same PFA solution ON at 4°C. Samples were then ON decalcified in a 0.5M EDTA pH8.0/PBS1X solution prepared in DEPC-treated water. Cryoprotection was carried out in 10% sucrose/PBS1X for 2 hours, 20% sucrose/PBS1X for 2 hours and 30% sucrose/PBS1X 3 hours to ON at 4°C. The heads were included in Frozen section medium Neg-50 (Richard Allan scientific, MI, USA) and left on liquid nitrogen-iced isopentane for 2 minutes. The frozen blocks

were brought into a cryostat (Microm International, Walldorf, Germany) and left at -21°C for 30-120 minutes. Serial coronal sections of mouse heads (16µm) were cut with a clean blade, and transferred on Superfrost Plus glass slides (Menzel-Glaser, Menzel GmbH & co KG, Germany) with a maximum number of three slices per slide. Sections were air-dried for 30-120 minutes and immediately used for hybridization or either stored at -80°C.

3.5 In situ hybridization and washings.

All solutions used in hybridization protocol were prepared using DEPC-treated water. Slides were incubated in 4% PFA/PBS1X at RT for 10 minutes and washed in PBS1X two times for 5 minutes. For fluorescent ISH, The slides were incubated in a 1%-3% H_2O_2/PBS1X solution at RT for 30 minutes to block endogenous peroxidises. This step and the following two washes (5 minutes each in PBS1X) were omitted in NBT/BCIP revealed ISH. The slides were put at 37°C in a 0.1µg/ml Proteinase K solution prepared in TE buffer (1M Tris-Cl pH8.0 / 0.5M EDTA pH8.0) for 10 minutes. A second incubation on 4% PFA/PBS1X for 10 minutes at RT was followed by two PBS1X washes for 5 minutes each. The slides were then treated with 0.2M HCl at RT for 10 minutes, washed again in PBS1X and pre-incubated for 1 minute in 0.1M Triethanol amine-HCl pH8.0 (TEA buffer). After the pre-incubation, acetic anhydrate was slowly added to the TEA solution and incubated at RT for 5 minutes while gently stirring. The slides were washed in PBS1X for 5 minutes and air-dried for 30-180 minutes. An hybridization mix was prepared containing 1X salts solution (0.3M NaCl, 0.01M Tris-Cl pH8.0, 0.01M NaH_2PO_4, 0.005M NaEDTA pH8.0, 0.2% Ficoll, 0.2% Polyvinyl pyrrolidone), 0.05M DTT, 0.1mg/ml yeast tRNA (Sigma-Aldrich), 10% Dextrane sulphate, 50% Formamide and 0.5mg/ml Polyademilic acid (Sigma-Aldrich). 200-600ng of RNA probes were added to 150µl of hybridization mix pre-heated at 85°C for 5 minutes and left at the same temperature for additional 5 minutes. The appropriate mix was pipetted on the sections, the slides were covered with Parafilm (Alcan Packaging, WI, USA) and put at 58°C-60°C ON in humid chambers containing 50% formamide. The parafilm covers were gently removed from the slides and samples were washed following the listed steps:

1. 5X SSC for 5 minutes at 65°C
2. 2X SSC/50% formamide for 30 minutes at 65°C
3. TNE (10mMTris-Cl pH 7.5, 500mM NaCl, 1mM EDTA pH8.0) for 10 minutes at 37°C, two times
4. 2X SSC for 20 minutes at 65°C

5. 0.2X SSC for 20 minutes at 65°C
6. 0.1X SSC for 20 minutes at 65°C

Sections were then circled with Super PapPen and processed for detection.

3.6 Detection of digoxygenin- and biotin-labelled probes.

Slides hybridized with DIG-RNA probes were washed two times for 5 minutes in B1 solution (0.1M Tris-Cl pH7.5, 0.15M NaCl), blocked in heat-inactiveated foetal calf serum (HI-FCS, Sigma-Aldrich) in B1 buffer (blocking buffer) for 1 hour at RT and incubated ON with anti-digoxygenin-AP Fab fragments (Roche Applied Science, Germany) diluted 1:1000 in blocking buffer. After a brief pre-incubation in B2 solution (0.1M Tris-Cl pH9.5, 0.1M NaCl, 0.05M $MgCl_2$), the detection was carried out by adding a solution containing 4-Nitro blue tetrazolium chloride (NBT, Roche), 5-bromo-4-chloro-3-indolyl-phosphate, 4-toluidine salt (BCIP, Roche) and 1mM levamisol. Slides were mounted with a 70% glycerol solution. The staining was analyzed with a Leica DM6000B light microscope (Leica Microsystems GmbH, Germany).

Slides hybridized with BIO-RNA probes were incubated with TNB (0.1M Tris-Cl pH7.5, 0.15M NaCl, 0.5% Blocking Reagent from Roche) for 1 hour at RT, followed by incubation with Streptavidin-HRP (Perkin Elmer, MA, USA) diluted at 1:250 in TNB for 2 hours at RT. Slides were washed 3 times with TNT (0.1M Tris-Cl pH7.5, 0.15M NaCl, 0.05% Tween20 from Sigma-Aldrich) and probe detection was carried out with TSA Plus Cy3 system (Perkin Elmer) for 5-10 minutes. After additional three washes with TNT the slides were air-dried in the dark and mounted with Vectashield mounting medium (Vector Laboratories, CA, USA). The staining was analyzed with a Leica TCS LSI confocal microscope (Leica); the power of Argon laser was never raised over 30%.

Results

Part 1: The molecular identity of the Calcium-activated Chloride channel involved in olfactory transduction.

Experiments during the past two decades established the existence of several distinct families of chloride channels: the calcium-activated chloride channels (CLCAs, CLCs or CACCs), the cystic fibrosis transmembrane conductance regulator (CTFR), the family comprising γ-aminobutyric acid and glycine receptors; the more recently identified family is the one including Bestrophins.

1.1 Calcium-activated chloride channels expression in mouse olfactory epithelium.

In order to define the molecular identity of the chloride channel involved in the mechanism of cationic olfactory current amplification, the olfactory epithelium of adult C57Bl/6J mice was screened for the expression of known members of the CLCA family and members of Bestrophins family.

When this project was started the CLCAs family comprised 5 channels, but then a sixth member was identified in subsequent years and for this reason it was not included in the first screening phase. Exon-spanning oligonucleotide pairs were designed for CLCA1-5 and for mBest1, 2 and 4, along with primers for the olfactory-specific subunit A2 of the CNG channels as a control. Bestrophin-3 was not included in this experiment because reported as a non-transcribed pseudogene in mouse genome. The result of the RT-PCR on CLCAs revealed that the mRNA of CLCA1-4 was expressed in the MOE, while the PCR product for CLCA5 resulted to be aspecific; the amplification of the CNG-A2 confirmed the specificity of the starting total RNA sample (fig.1-a).

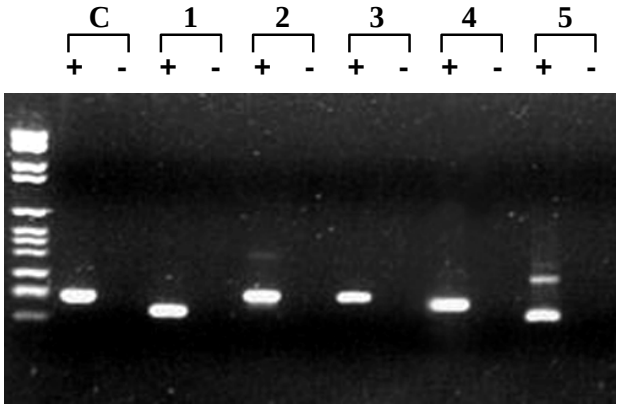

Figure 1-a: Expression of CLCA channels in MOE. Specific primers were used to verify the expression of known CLCAs isoforms starting from a sample of MOE total RNA. C: CNGA2 channel; 1-5: CLCA1-5. The identities of PCR products were verified by cloning and sequencing; CLCA5 revealed to be aspecific.

For Bestrophins family, a small fragment of mBest2 was amplified by RT-PCR from the starting sample of MOE total RNA, but not mBest1 nor mBest4. To understand whether this negative result could be due to poor efficacy in terms of primers design, primers for mBest1 and mBest4 were also tested by RT-PCR on commercial total RNA extracted from mouse testis and heart, two tissues in which mBest1 and mBest4 respectively are reported to be selectively expressed. While mBest2 mRNA resulted to be expressed also in mouse testis and heart, this experiment confirmed the selective expression of mBest2 in the main olfactory epithelium (fig. 1-b). The 240bp fragment amplified by mBest2 primers was cloned in TOPO vector and the sequencing confirmed the identity of the PCR product.

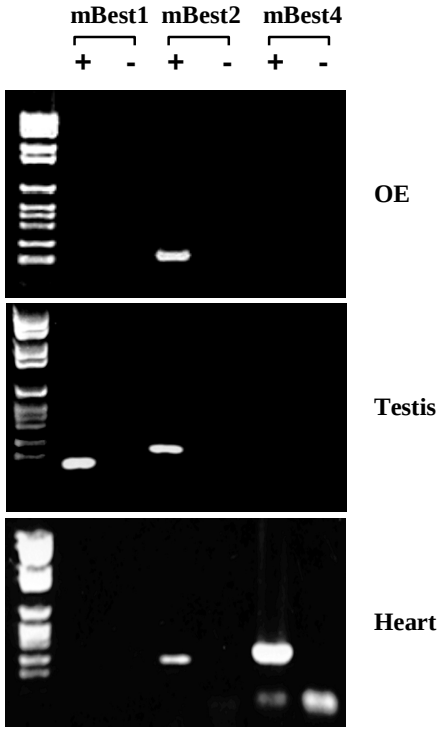

Figure 1-b: Expression of mBest2 in MOE and in OSNs. Primers specific for Bestrophin1, 2 and 4 were used to amplify cDNA made from RNA of OE, testis and heart. The identities of the PCR products were verified by cloning and sequencing.

Messenger RNA editing and alternative splicing are two molecular mechanisms largely exploited in the nervous system to create qualitative diversity in channels repertoires in terms of ligand specificity and elicited response. To assess the presence of sequence editing or splicing events in mBest2, a primer pair targeting the 5' and 3' boundaries of the vmd2l1 annotated mRNA (GenBank accession number # BC019528) was used to obtain the full-length mBest2 cDNA. After some trials, an RT-PCR product of the expected size was obtained using a DNA polymerase with a high proofreading activity and cloned in a pGFP vector. Once sequenced and analyzed, the full-length mBest2 showed no differences with the annotated sequence, proving that no MOE-specific post-transcriptional modifications occurred. A commercial clone of mBest2 was however purchased and used for subsequent heterologous transfection experiments in order to obtain the highest degree of reproducibility during electrophysiological recordings.

Although the screened CLCA1-4 were found to be expressed in the MOE, the electrophysiological properties of the chloride current measured following heterologous expression of mBest2 in HEK293 cells seemed to match better than others those well-documented of the native olfactory chloride channel; for this reason, all of the subsequent experiments were focused on mBest2.

1.2 mBest2 mRNA is specifically expressed in olfactory sensory neurons.

To assess whether mBest2 mRNA expression might be restricted to a particular cell-type in the MOE, a single cell RT-PCR protocol was set up to amplify the 240bp mBest2 fragment starting from small groups of olfactory sensory neurons and sustentacular cells. During the first steps of this experiment, the dissociation of MOE and the harvest of cells were completed by Dr. A. Mazzatenta of the laboratory of Prof.Menini at SISSA; the harvested cells were stored in TRIzol reagent at -80°C, a condition that is documented to preserve the integrity of the RNA for long periods.

The single cell RT-PCR protocol was set up from the scratch and it needed an accurate phase of trials during which a wide panel of DNA polymerases commercially available were tested for their ability to amplify a target gene starting from very low amounts of total RNA; the best amplification efficacy when starting from 0.01 nanograms of total RNA was reached by performing the RT reaction and a first round of PCR in the same reaction tube with a commercial kit (SuperScript One-step RT-PCR by Invitrogen), and using then a small amount of this first RT-PCR reaction in a second PCR exploiting a different DNA polymerase (fig. 1-c). Once optimized, this protocol was applied to samples containing groups of 2 and 10 harvested olfactory sensory neurons and 10 sustentacular cells, together with a sample containing only the medium in which the dissociated cells were maintained during the harvest session.

mBest2 was found to be selectively expressed in OSNs, and the titration observed in the PCR products obtained from 2 and 10 OSNs further confirmed the efficacy of the RT-PCR protocol and the specificity of this result (fig. 1-d).

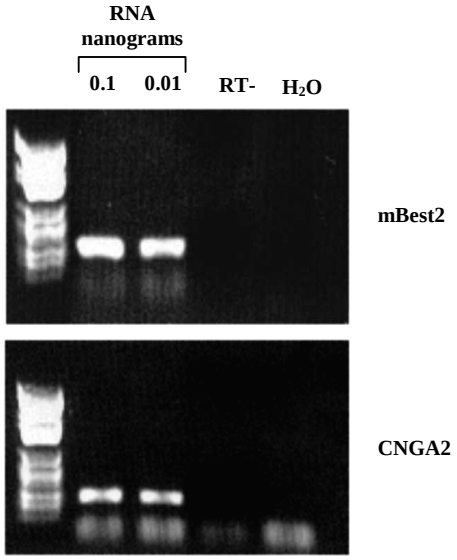

Figure 1-c: Custom single cell RT-PCR protocol efficacy. Specific primers were used to amplify mBest2 and CNGA2 from 0.1 nanograms and 0.01 nanograms of starting MOE total RNA with a custom two-step RT-PCR protocol.

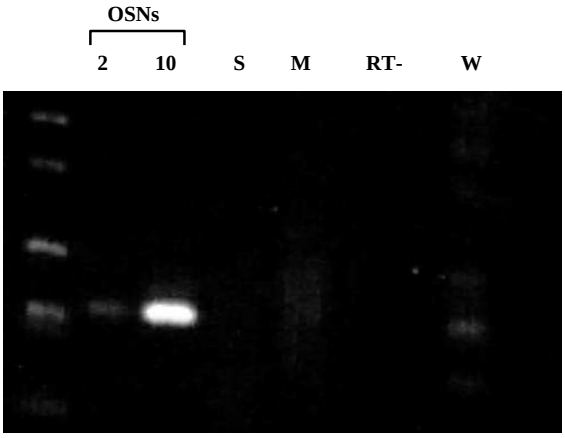

Figure 1-d: Expression of mBest2 in olfactory sensory neurons. Primers specific for mBest2 were used to amplifiy cDNA made from RNA of 2 OSNs, 10 OSNs and 10 supporting cells (S). Other negative controls are resuspension media for OSNs (M), retro-transcriptase free sample (RT-) and water only sample (W).

1.3 Production of rabbit polyclonal α-mouse Bestrophin-2 antibody and western blot.

Following the observation that primary sequence homology within the mouse Bestrophin family is lower in their C-terminal domains, the last 144 aminoacids of mouse bestrophin-2 were chosen as the antigenic region for the production of a polyclonal antibody raised in rabbits.

Mouse Bestrophin-2 antibody was purified from the last bleeding of the immunized rabbits, and its specificity was tested. In western blot experiments in which HEK293 cells were transfected with a commercial full-length clone of mBest2, the antibody recognized a band with the expected size of 57kDa, and the signal was demonstrated to be specific by a pre-incubation of the antibody with the purified GST-mBest2 protein that selectively abolished the 57kDa band (fig. 1-e). An in vitro transcription/translation experiment performed with commercial mBest2 clone demonstrated that the band recognized in western blot by α-mBest2 was comparable to the band recognized in a protein extract of HEK293 cells transfected with the same clone (fig. 1-f).

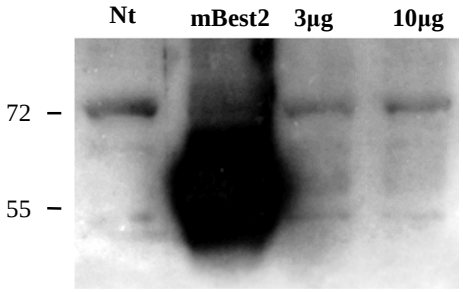

Figure 1-e: Specificity of polyclonal α-mBest2. mBest2 (RZPD clone) was transfected in HEK293 cells and the specificity of α-mBest2 was assessed in a competition assay with 3µg and 10µg of purified GST-mBest2 protein.

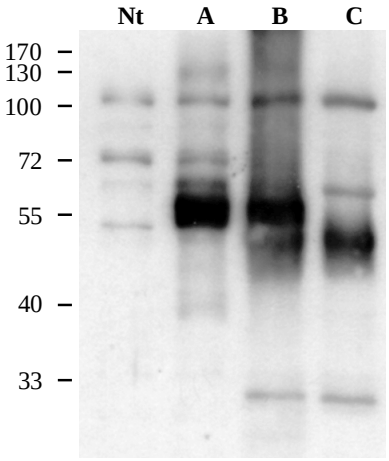

Figure 1-f: IVTT of mBest2 (RZPD clone). A commercial clone of mBest2 was used for an IVTT assay and the reaction product was compared with a lisate of HEK293 cells transfected with the same clone in a western blot revealed by α-mBest2.A: HEK293 lisate; B: IVTT product; C: IVTT reaction control (RNA pol-).

The specificity of mBest2 antibody was also tested in immunofluorescence on HEK293 cells transfected with the commercial mBest2 clone. Again, the pre-incubation of the antibody with GST-mBest2 protein fully competed the membrane staining observed with α-mBest2 (fig. 1-g).

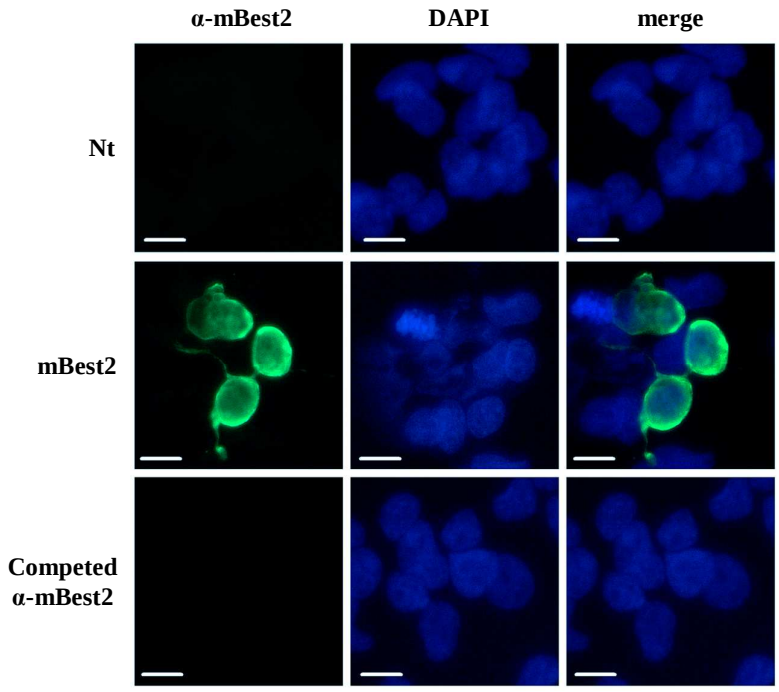

Figure 1-g: Specificity of α-mBest2 antibody tested in immunofluorescence. HEK293 cells were transfected with mBest2 (RZPD) and the specificity of α-mBest2 was verified in a competition assay with 30µg of purified GST-mBest2. Scale bar: 10µm.

The very first steps of olfactory transduction occur is the membrane of cilia belonging to OSNs, which lye on the surface of the MOE. The investigation on the electrophysiological properties of olfactory cilia has taken advantage of major improvements in protocols for the isolation and purification of intact cilia from samples of whole dissected MOE. Exploiting this knowledge a sample enriched in ciliary membrane was prepared by Dr. L. Masten and used for a western blot. Despite the low proteic concentration of the ciliary membrane-enriched sample, mBest2 antibody recognized a band in western blot whose size was comparable to the one observed in heterologous expression of commercial mBest2 clone in HEK293 cells (fig. 1-h). Importantly, the band identified in the cilia-enriched sample was competed after incubation of mBest2 antibody with GST-mBest2 purified protein (data not shown).

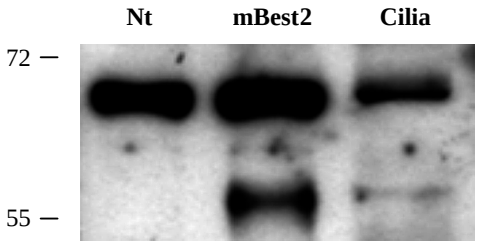

Figure 1-h: Expression of mBest2 in olfactory cilia. The expression of mBest2 in olfactory cilia was detected by Western blot analysis in a cilia-enriched preparation and compared with the band recognized by α-mBest2 after transfection of mBest2 commercial clone in HEK293 cells.

In immunofluorescence experiments on cryosections of MOE mBest2 antibody evenly stained the surface of the epithelium; the signal given by mBest2 antibody co-localized with signals given by antibodies specific for the olfactory subunit A2 of the CNG channel and for the olfactory marker protein (immunofluorescence experiments performed by Dr. S. Pifferi of the laboratory directed by Prof. Menini at SISSA shown in Appendix A).

These results confirmed that in MOE the expression of mouse Bestrophin-2 is restricted to OSNs, and the co-localization between mBest2 and CNGA2 supported the presence of this newly identified chloride channel in the main site of olfactory signal transduction.

A characterization of mBest2 electrophysiological properties in heterologous expression has been carried out by Dr. S. Pifferi and Dr. A. Boccaccio and confronted in a side-by-side comparison with those of the olfactory native chloride channel recorded in inside-out membrane patches of OSNs

dendritic knob and cilia. As reported in the published paper enclosed in the final section of this Ph.D. thesis, the electrophysiological behaviour of the two systems in terms of intracellular calcium sensitivity, single channel conductance, anion selectivity, rectification properties and sensitivity to known intracellular and extracellular blockers specific for chloride channels was similar though not perfectly overlapping.

1.4 Discussion.

The last 20 years of research on signal transduction events occurring in OSNs have actually produced almost the entire knowledge of this fascinating subject available at present. While at first the only data available on the electrical activity of the olfactory epithelium were not supported by evidences about the nature of cellular mechanisms producing the recorded responses, molecular biology has then rapidly gained an important role in this research field because of its essential role in defining the identity of the genes and hence proteins involved in the plethora of small-scale events that stand behind a single electrical recording.

The existence of an amplifying chloride current activated by calcium ions in the olfactory signal transduction cascade has been for a long time a phenomenon for which the existence of a dedicated channel had been postulated, but its identification has been slowed down by the scarce knowledge of gene families encoding for chloride channels displaying electrophysiological properties compatible with those well-documented in OSNs.

The data presented in this thesis have demonstrated that, in the mouse, a member of a newly identified family of calcium-activated chloride channels highly conserved across species displays a series of convincing molecular, immunological and electrophysiological properties according to which it has been proposed to contribute in the formation of the native olfactory chloride channel. As a matter of fact, mouse bestrophin-2 gene is expressed in the MOE, its expression is restricted to OSNs and the chloride channel encoded by this gene is located in proximity of OSNs cilia, where the entire olfactory transduction machinery converts the odorous stimuli into action potentials. The recorded electrophysiological properties of bestrophin-2 were found to be similar, but not perfectly adherent to those of the native channel. The reasons for the detected discrepancies can be various.

First of all, the electrophysiological recordings were made from the two channels in different systems. Recordings for bestrophin-2 were carried out in HEK293 cells transfected with a commercial clone encoding for the chloride channel, while recordings of the native channel were performed on dissociated OSNs. It is well known that channels expressed in heterologous systems

could lack post-transcriptional and/or post-translational modifications, and the hybrid form of the membrane-expressed channel will hardly have the same properties displayed in native conditions.

The second reason that could be at basis of the observed differences is the fact that technical difficulties have initially impeded the adoption of the same recording configuration for the two systems; while recordings of the calcium-induced current for the native olfactory chloride channel were successfully carried out by patch-clamping excised membrane patches of dendritic knobs and cilia in an inside-out configuration, this resulted to be a too difficult task for mBest2 in heterologous expression. This inside-out recording configuration has been used in a heterologous expression system involving human Bestrophin-4 (152) and it has produced positive results probably because of the large chloride current induced by this particular isoform. In the case of mBest2 the induced-currents were likely to be far smaller. Recordings of calcium-activated currents in HEK293 cells over-expressing mBest2 were thus performed by whole-cell patch-clamping.

As a final consideration, the native channel could be constituted by multiple homogeneous or heterogeneous subunits, as for example the CNG channel, and it could be regulated in native conditions by an array of cell-specific proteins of which the heterologous expression system is may be devoid.

It has been recently reported that knockout mice lacking Bestrophin-2 exhibit no obvious phenotypic abnormalities and are able to locate a source of food after starvation in a time lapse comparable to that recorded for wild type mice (153). However, the complete absence of any chloride current in OSNs of knockout mice was not demonstrated, and furthermore it has never been established to what extent the chloride current in wild type mice contribute to the main olfactory response.

It is clear that future studies will have to focus on the exact nature of the native olfactory chloride channel, on the identification of its modulators and on the understanding of its functional correlation with the other components of the olfactory transduction machinery. In this context the detailed examination of bestrophin-2 that has been presented in this thesis adds important information for a better interpretation of the formal olfactory sensitivity.

Part 2: A genomic investigation of the identity of olfactory microvillar cells.

The co-existence of multiple sensory cell-types within the same olfactory epithelium regions is a well-documented phenomenon in vertebrates lacking the VNO. Although little is known about a differential expression of receptors repertoire, there are some evidences about the fact these different cell-types have tuned during evolution towards specific perceptual ranges and therefore they can be considered as discrete olfactory subsytems.

In rodents, olfactory sensory neurons have always been considered as the only sensory cell type of the MOE capable of receiving signals from the outer world, but this acceptance has been recently challenged by speculations pointing at olfactory microvillar cells as a new sensory cell type in MOE. However, the evidences produced so far about a sensory role for MCs are questionable, and they are mainly based on the expression of some molecular players of the PLC transduction pathway that is responsible for signal transduction triggered by pheromonal cues in VSNs. The aim of this project was to create a molecular fingerprinting of MCs through a genomic approach, and to reveal more details about their neuronal or non-neuronal nature.

2.1 Olfactory microvillar cells identification and harvesting.

The isolation and purification of a discrete cell-type from complex tissues can be achieved in different ways, the choice of which may vary according to a series of parameters. For example, suction electrode techniques are still widely used in those cases in which the target cell-type is easily identifiable either by morphology or fluorescence following tissue dissociation.

However, when a higher number of cells is needed the choice usually falls on Laser Microdissection or Fluorescence-Activated Cell Sorting (FACS). While FACS needs a fluorescent marker, LCM allows the purification of a large number of cells or entire pieces of tissues for both morphological criteria and/or the presence of a fluorescent target. Furthermore, transgenic mouse models in which the expression of fluorescent proteins is driven by the expression of a given gene identified only in target cell-types has become a fundamental resource. When cells are purified to perform gene expression profiling experiments, the key factor influencing the entire outcome of the experiment is the quality of the RNA extracted from the isolated cell-type. During the planning of this project, we decided to take advantage of LCM technology to isolate MCs from cryosections of MOE, but no transgenic models involving MCs were available. The main technical goal was therefore to set up a short-timed immunofluorescence protocol capable to give an optimal balance in terms of observable fluorescent signal and preservation of RNA quality. To our knowledge there are very few markers

for MCs. We therefore chose a commercial antibody against the inositol triphosphate receptor-type 3 (IP3R3), used also by Rebecca Elsaesser and colleagues in their publications on MCs. The α-IP3R3 was tested with several fixatives and immunofluorescence (IF) protocols. A nice staining of the entire MCs body, from the apical region to the basal process, was obtained only with a Zinc salts-based commercial solution ("ZincFix") and with a mix of absolute ethanol/acetone. The two protocols resulted in slightly uneven outcomes affecting the quality of tissue morphology (fig. 2-a). According to these observations, ethanol/acetone fixation was initially discarded in favour of ZincFix fixation. Examples of MCs stained for IP3R3 by using ZincFix as fixative are shown in also figure 2-b.

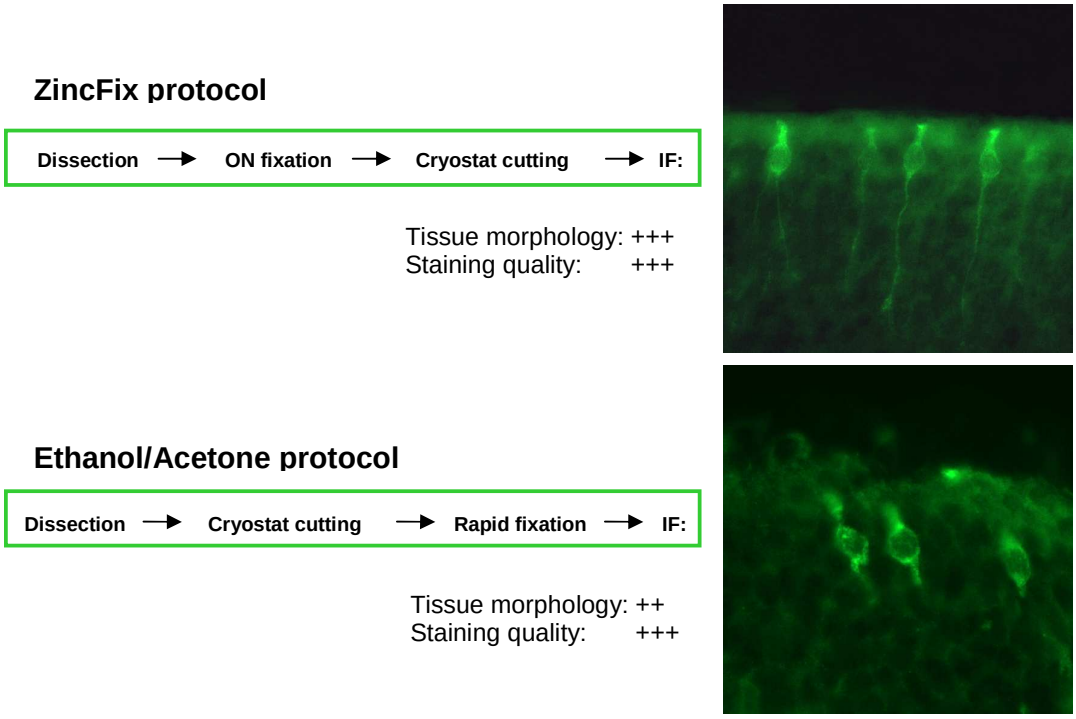

Figure 2-a: Comparison of ZincFix and ethanol/acetone fixation protocols.

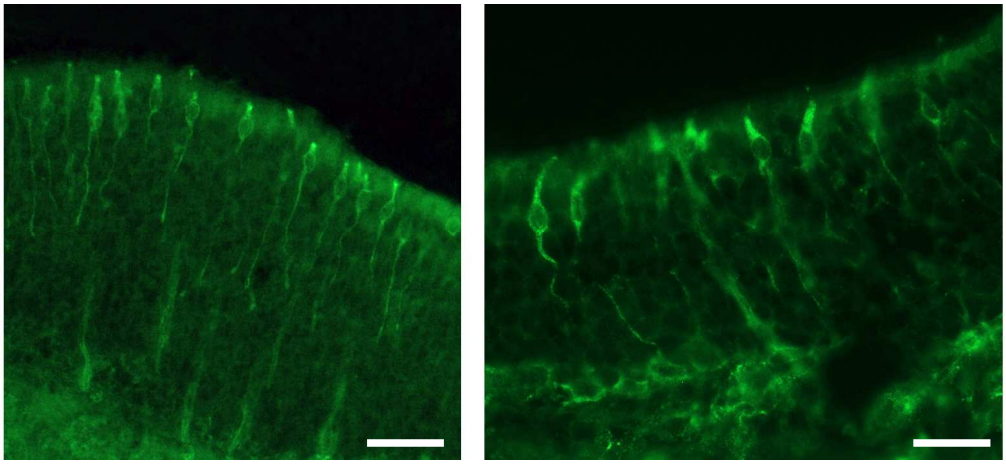

Figure 2-b: Olfactory microvillar cells stained with α-IP3R3. The olfactory epithelium was fixed before cryosectioning with ZincFix; the thickness of the shown sections is 16μm. Scale bars: 30μm (left picture) and 20μm (right picture).

This choice was partially supported by the fact that Zinc-based fixatives have been reported in literature to have a moderate RNA-protecting behaviour (154) and this was confirmed by some experiments of RNA extraction from MOE after different fixation times in ZincFix. The classic paraformaldehyde fixation was not successful.

The ZincFix IF protocol included the standard steps of a common IF (30 minutes of blocking, 90 minutes of incubation with primary antibody buffer, washings, 60 minutes of incubation with secondary antibody buffer, washings) with all of the reagents commonly used to obtain an optimal staining (foetal bovine serum, bovine serum albumine, triton X-100, PBS1X). To maximize RNA integrity, each step was tested in buffer compostions and time lengths.

An exclusion of the blocking step and a reduction of the primary and secondary antibody incubation steps to 30 minutes each were found not to negatively affect the quality of the α-IP3R3 staining. However, although the usage of nuclease-free water and PBS, the RNA extracted from the tissue slices processed with this IF protocol was completely degraded. This issue was not solved by a particular care that was taken in all the processing steps, including decontamination of glass slides from RNases prior cryostat cutting and elimination of BSA and Triton from all the buffers.

After many trials, the reason for RNA degradation was finally identified in the washing steps adopted to get rid of residual primary and secondary antibodies solutions. Therefore we used a protocol with a single buffer exchange between the primary and secondary antibody thus increasing RNA quality. Unfortunately, in these conditions the MOE resulted covered by precipitates that

made impossible the identification of MCs; these precipitates were originated by the interaction between ZincFix and PBS, and this phenomenon was present also when substituting PBS with other saline buffers, and a series of trials involving chemical organic solvents to dissolve the precipitates proved to be ineffective, or resulted in a loss of signal, or in a degradation of the RNA.

It was then decided to abandon the fixation with ZincFix and to repeat all the trials with ethanol/acetone fixation protocol. It was possible to exclude the blocking step, to reduce to 30 minutes each incubation steps with primary and secondary antibodies, to eliminate the use of BSA and Triton X-100 without affecting the quality of MCs staining given by α-IP3R3. Moreover, avoidance of washing steps revealed to be feasible with this IF protocol. Unluckily, the quality of RNA extracted from IF-processed slices was still not sufficient, and this result was not altered by adding high amounts of two different commercial RNase inhibitors (from Ambion and Sigma) directly in the buffers for primary and secondary antibodies, now containing only nuclease-free water and PBS1X (fig.2-c). All the efforts to couple the incubation with primary and secondary antibody in a single step were not successful.

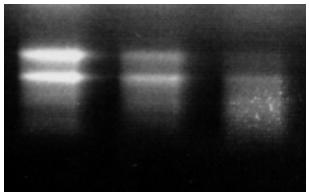

Figure 2-c: Effect of ethanol/acetone IF protocol on RNA quality. RNA was extracted from fresh MOE sections prior IF protocol (A), after 1 hour of incubation with all the components of primary and secondary antibody buffers without any buffer exchange (B) and after a complete ethanol/acetone IF protocol with only one buffer exchange between primary and secondary antibody incubation (C). 1000u/ml of RNase inhibitor from Ambion were added to all buffers used in (B) and (C).

Following some initial trials in which different amounts of the RNA preserving and stabilizing commercial reagent RNAlater were added to the buffers, the quality of recovered RNA had a major improvement, but too high concentrations of the reagent severely affected the staining of α-IP3R3. However, by limiting the dilution rate of RNAlater in the buffers it was possible finding a balance

between these two factors. In the final protocol there was a ratio with PBS1X of 1:5 in the first antibody buffer and 1:7.5 in the secondary antibody buffer (fig. 2-d).

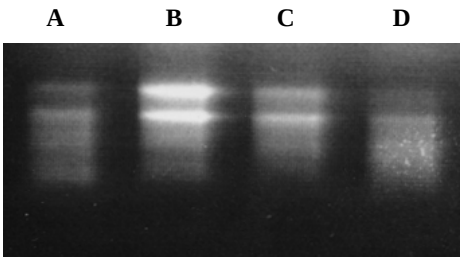

Figure 2-d: Effect of *RNAlater* on RNA quality of IF-processed MOE sections. RNA was extracted from fresh MOE sections prior IF protocol (A), after a complete ethanol/acetone IF protocol including buffer exchange with a 1:3 (B), 1:5 (C), 1:10 (D) ratio of RNAlater/PBS in primary and secondary antibody buffers.

In order to be processed by LCM, the tissue slices have to be perfectly dried; unfortunately, even if removed from samples in the drying process the residual RNAlater tended to form crystals on the slices, and this event blocked any possibility to identify and/or harvest MCs; a final wash step with ZincFix after antibodies incubation was effective only in avoiding crystals formation and slightly improved the quality of recovered RNA (fig. 2-e)

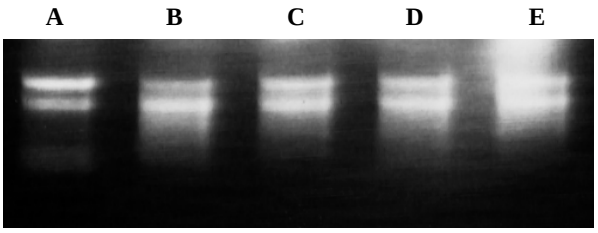

Figure 2-e: Effect of ZincFix wash on RNA quality after IF protocol. RNA was extracted from fresh MOE sections prior IF protocol (A), after a complete IF protocol including RNAlater in the buffers (B), and after an additional wash step with ZincFix of 30 seconds (C), 1 minute (D) and 5 minutes (E).

However, due to vanishing of α-IP3R3 signal after drying of the slices it was necessary to adopt a strategy in which, immediately after the end of incubation step with secondary antibody buffer, the slides were brought at the LCM microscope and the "still well-visible position" of MCs was marked and recorded with the instrument software. In this final protocol the ZincFix wash was made after the identification of MCs, and the harvest of the cells was started when the slides were air-dried (fig. 2-f).

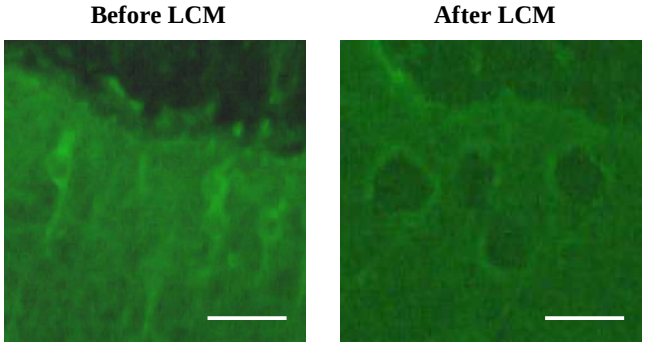

Figure 2-f: Laser catapulting microdissection of MCs after IF protocol. Two pictures were taken with a CCD camera connected with LCM microscope before and after MCs harvesting; the pictures are from different fields of the same MOE section. Scale bar: 20μm.

When using this protocol, before starting to collect the target cells it was absolutely necessary to make sure that the slides did not accidentally move after marking the position of fluorescent MCs, for example during the ZincFix washing procedure. This was obtained by setting specific parameters on LCM software, or by marking each slide with the laser before each harvest session and verifying that the slide did not moved from that mark after the procedure.
For three microarray hybridizations a total amount of 1000 OMCs were independently harvested and immediately post-processed for mRNA extraction, purification and amplification.

2.2 Microarray hybridization and data analysis.

The core of the custom microarray approach used to scan the identity of MCs has been the availability of the release of RIKEN FANTOM2 full-length cDNA clone collection which has derived from a collaboration between our Institute and RIKEN Institute in Japan. The original FANTOM clone collection in its first version consisted of 21.076 full-length cDNAs cloned from 160 libraries derived from various mouse tissues and developmental stages (155). At SISSA the

FANTOM2 collection of 60.700 clones was available. 14.658 unique clones representative for protein-encoding genes were chosen for our dual-channel cDNA microarray platform. All the clones were PCR-amplified, gel purified and spotted in triplicates along with a series of control spots on two microarray slides named “SISSA1” and “SISSA2”.

The common hybridization strategy adopted in our Institute for this microarray platform uses a commercial reference mouse RNA, that includes RNA extracted from 11 different tissues, against which every target cells/tissues sample is hybridized in order to provide a uniform and reproducible source of data normalization.

Therefore, in this experiment, we performed three different harvests of 1000 MCs each with LCM. MCs were identified by using our IF protocol with α-IP3R3 antibody under conditions compatible with high RNA integrity as described above. RNA was purified and amplified with the μMACS SuperAmp kit by Mylteni Biotech, a system that enables the combination of mRNA isolation with in-column cDNA synthesis, tailing and global cDNA amplification and allows reducing the number of purification steps.

Global cDNA amplification products and standard RNAs were labelled and mixed and described in Materials and Methods section.

Labelled probes were purified and hybridized to SISSA1 and SISSA2 cDNA microarray slides. After a phase of washes, they were then scanned with a GenePix Personal 4100A microarray scanner. Data were analysed with GenePix Pro 4.1 microarray analysis software.

The following two tables display a list of the first more expressed 30 genes in the sample enriched in MCs, extracted from SISSA1/SISSA2 after data normalization with the standard universal RNA hybridizations; the genes included in the list have an MCs/Standard RNAexpression level ratio at least ≥ 2.

SISSA1

1.	RIKEN cDNA 9030603L14 hypothetical protein
2.	NEURON SPECIFIC PROTEIN FAMILY MEMBER 1 (BRAIN NEURON CYTOPLASMIC PROTEIN 1) (P21) (M234)
3.	ANTIOXIDANT PROTEIN 2 (1-CYS PEROXIREDOXIN) (1-CYS PRX) (ACIDIC CALCIUM-INDEPENDENT PHOSPHOLIPASE A2) (EC 3.1.1.-) (AIPLA2) (NON- SELENIUM GLUTATHIONE PEROXIDASE) (EC 1.11.1.7) (NSGPX)
4.	G protein-coupled P2Y receptor 14
5.	RIKEN cDNA A230050P20 hypothetical protein
6.	weakly similar to SHC TRANSFORMING PROTEIN [Homo sapiens]
7.	similar to DOLICHYL-P-MAN:MAN(5)GLCNAC(2)-PP-DOLICHYL MANNOSYLTRANSFERASE (EC 2.4.1.-) (DOL-P-MAN DEPENDENT ALPHA(1-3)-MANNOSYLTRANSFERASE) (NOT56-LIKE PROTEIN) [Homo sapiens]
8.	hypothetical ATP/GTP-binding site motif A (P-loop) containing protein
9.	RIKEN cDNA 0710008A13 (WD-repeat domain 23)
10.	GUANINE NUCLEOTIDE EXCHANGE FACTOR DBS (DBL'S BIG SISTER) (MCF2 TRANSFORMING SEQUENCE-LIKE PROTEIN)
11.	RIKEN cDNA A030005L19 hypotetical protein
12.	PUTATIVE PHEROMONE RECEPTOR (FRAGMENT) homolog [Mus musculus]
13.	transmembrane protein 4 (hypothetical Saposin type B containing protein)
14.	acidic nuclear phosphoprotein 32
15.	RIKEN cDNA A130019H11 hypothetical protein

SISSA2

1.	vertebrate homolog of C. elegans Lin-7 type 2
2.	TAF15 RNA polymerase II. TATA box binding protein (TBP)-associated factor. 68 kDa
3.	LUNG CARBONYL REDUCTASE [NADPH] (EC 1.1.1.184) (NADPH-DEPENDENT CARBONYL REDUCTASE) (LCR) (ADIPOCYTE P27 PROTEIN) (AP27)
4.	RIKEN cDNA 1810055G02 (hypothetical Threonine-rich region containing protein)
5.	G21 protein
6.	Calmodulin 1
7.	HOMOCYSTEINE-RESPONSIVE ENDOPLASMIC RETICULUM-RESIDENT UBIQUITIN-LIKE DOMAIN MEMBER 1 PROTEIN
8.	Neuron specific protein BM88 antigen
9.	DiGeorge syndrome chromosome region 6
10.	Citrate lyase beta like
11.	similar to PUTATIVE LAG1-INTERACTING PROTEIN (FRAGMENT) [Homo sapiens]
12.	RIKEN cDNA 1110004F10 (small acidic protein)
13.	THIOSULFATE SULFURTRANSFERASE (EC 2.8.1.1) (RHODANESE)
14.	UBIQUITIN FUSION DEGRADATION PROTEIN 1 HOMOLOG (UB FUSION PROTEIN 1)
15.	FRUCTOSE-BISPHOSPHATE ALDOLASE C (EC 4.1.2.13) (BRAIN-TYPE ALDOLASE) (FRAGMENT)

Table 1: First 15 genes in SISSA1 and SISSA2 slides with an expression level in MCs at least 2-fold higher than RNA commercial reference. Hybridazion of 1000 MCs and reference RNA were done in triplicate.

For some of these genes a validation phase was undertaken based on in situ hybridization (ISH) followed by immunohistochemistry (IHC) to stain the MCs with α-IP3R3; since the electing fixative for ISH is paraformaldehyde, to start the validation it was at first necessary to overcome the issue of lack of signal from α-IP3R3 after PFA treatment. While the majority of antigen retrieval protocols failed to free the antigen from PFA-induced cross-linking, a good staining of MCs was observed after microwave treatment in a citrate buffer. Unluckily, when an experimental coupling between the ISH and IHC was carried out, the staining on tissue slices obtained with a given RNA probe and revealed with NBT/BCIP was almost completely compromised by the microwave treatment necessary to visualize the MCs.

Fluorescent double in situ hybridization experiments are currently undergoing for validation of MCs-enriched genes. As a marker of MCs, a cDNA clone for IP3R3 is used.

2.3 Discussion.

After more than 30 years from their initial discovery by François Jourdan, olfactory microvillar cells can still be considered a mystery.

Since their role in the MOE is far from being understood, they represent an optimal target for a genomic analysis in an era in which expression profilings of single cell populations isolated from their tissues have become an affordable and technically feasible approach.

The few published works that have so far targeted the identity of MCs have revealed some interesting details of this peculiar cell-type: given the expression of PLC-β2 and the IP3R3 their molecular phenotype partially matches the one of vomeronasal sensory neurons, although while MCs have been found to express the TRP channel C6, in most of the VSNs the signal transduction is committed to TRPC2. Interestingly, the olfactory epithelium of a transgenic mouse model expressing the GFP under the control of TRPM5 promoter was shown to contain some apical, flask shaped fluorescent cells scattered in all the regions of the MOE, but it is still unknown whether they represent a particular subtype of MCs, or rather a new and still undefined category of olfactory cells (70). While some interesting data about the responsiveness of dissociated MCs to discrete odour mixes were observed in calcium-imaging experiments, these have remained solitary evidences and are still waiting for confirmation (145).

MCs have been proposed to be the functional link between OSNs that are undergoing apoptosis and the staminal cells contained in the germinative basal layer, hence regulating the regeneration of the olfactory epithelium. This theory is supported by the evidence that MCs selectively contain the neuropeptide Y (146), a neurotransmitter that is widely expressed in central and peripheral nervous

system and that had already been identified as a strong promoter of neurogenesis in the olfactory epithelium. However, at present it is not clear what is the trigger of NPY release, the expression and/or cellular distribution of NPY receptors in the germinative region is missing, and it is has to be still demonstrated that NPY is expressed by all the MCs present in the olfactory epithelium, or by a subpopulation specialized for the proposed regenerative function.

Our project aimed to gain an insight on the biology of MCs by gene expression profiling. Although the list of genes enriched in MCs is short, some interesting data are present. The RIKEN 6430701C03 clone contains the sequence of a transcript annotated as "PUTATIVE PHEROMONE RECEPTOR (FRAGMENT) homolog". This clone does not contain a full-length cDNA since the 5'-end is unknown and the 3'-end is truncated.
However, in its 1500bp DNA sequence it has a striking 99% homology with a member of V2Rs, the Vmn2r29. The longest identifiable ORF includes 101 aminoacids, and 94 out of 101 present a 100% match with Vmn2r29 and with other 3 isoforms of a predicted gene located in the same V2Rs cluster on chromosome 7, defined as "similar to vomeronasal 2, receptor 15".
It is clear that, regardless of the cell-type expressing the gene in question, this is an intriguing discovery since genes encoding for V2Rs, or genes coding for homologs of V2Rs, have never been identified in the MOE. Importantly, a contamination of the sample with any material coming from the VNO has to be excluded because of the high harvesting selectivity of LCM.
We are currently validating this expression by double fluorescent in situ hybridizations on MOE sections.

LCM technology has an intrinsic and physiological risk of collecting small amounts of aspecific material together with the target cell-type/tissue. The weight of these undesired contaminations in the final sample depends on a series of parameters including the ability of the operator, the complexity of the processed tissue in terms of morphology and cell composition, and the quality of the histological preparation. In the case of MCs harvesting, this risk was significantly high considering the high degree of cells packing in the MOE and the fact that MCs are completely surrounded by axons of the OSNs heading to the surface of the epithelium, and by cell bodies of sustentacular cells. In order to get rid of these possible sources of contamination, we are carrying out by LCM three harvests of random pieces of MOE to be then processed for microarray hybridization like the 1000 MCs samples. This triplicate of hybridizations will be used as a background for aspecific signal subtraction during the data analysis, a procedure that may improve the specificity of signals observed with MCs hybridizations. Until now we have completed two of

such hybridizations but it was impossible to complete the three MOE background hybridizations because of technical issues occurred with a bad batch of SISSA1 slides.
The lack of background MOE hybridizations has covered with a shade of uncertainty the result of the gene expression profiling carried out on harvested MCs. To cover this gap, it would have been helpful to check out in the completed MCs hybridizations the expression levels of genes specific only for MCs or OSNs such as PLC-β2, NPY, IP3R3, TRPC6 or OMP but they were not present in the selection of cDNAs spotted on SISSA1/SISSA2 slides.

Together with the list of genes, this work has produced a new IF protocol that preserves RNA integrity after LCM, and we believe this technique may be useful in the scientific community. Commercial reagents available at present to perform fast IFs in combination with RNA isolation do not allow such long times of incubation., therefore the spectrum of usable antibodies is currently very limited. The use of our protocol may thus extend the potential applications of antibodies staining.

Part 3: NanoCAGE of mouse MOE.

The olfactory epithelium represents a peripheral component of the central nervous system that in a very large number of species is easy to be approached and analysed as an independent functional unit. This is the main reason why for years most the research conducted on the MOE has involved electrophysiology and behavioural studies, with very minor advancements in molecular biology. This landscape was completely capsized with the discovery of odorant receptors in 1991.

Even though the following years of research have provided answers for some key topics, as for example the guidance mechanism of axons belonging to discrete OSNs population towards the MOB and the consequent deciphering of topographic odour maps, the identity of vomeronasal receptors, the description of signal transduction pathway in ONSs and so on, the number of new questions that have arisen from the emerging scenery of a multi-functional olfactory system is still large.

Among the most provocative evidences, the sensory interplay between the VNO and the MOE has recently altered the longly held perspective of these two subsystems as functionally unrelated olfactory units. The data available in literature clearly suggest that social behaviours like mating and aggressiveness cannot be ascribed to the effect of a single chemical cue elicited on a single olfactory subsystem, but most likely they are the result of a complex processing of external inputs collected from different sensory sources. However, in order to head towards a rational point of view of these innate responses, it is necessary to identify and functionally dissect all of the sources contributing to discrete behaviours.

Some evidences attest to an involvement of the MOE in well-documented pheromonal responses previously ascribed to the VNO, but at present the molecular mechanism or even the receptorial systems that mediate these responses are unknown. Taking advantage of a newly developed high-throughput tagging methodology, this project has targeted the entire transcriptome of mouse MOE in search for an answer to these intriguing issues.

3.1 Whole sensory olfactory epithelium microdissection and harvesting.

The structural anatomy of the MOE presents peculiar characteristics, with the sensory epithelium spread over several small curved bones (turbinates) that extends horizontally along the nasal cavities and flanked by pseudo-stratified non-sensory epithelium without any evident anatomical separation. It is therefore likely that in the common rough dissection procedures used to collect the MOE usually result in a contamination of the sample with non-sensory end even non-olfactory tissues but, according to the nature of tissue post-processing, this may not represent a major issue.

Considering the aim and the nature of NanoCAGE post-processing, it was essential to adopt a collection strategy able to guarantee for the maximum specificity of MOE sample; the choice of the harvesting method fell on LCM on the basis of its ability to precisely isolate and gather large pieces of the target tissue (fig. 3-a).

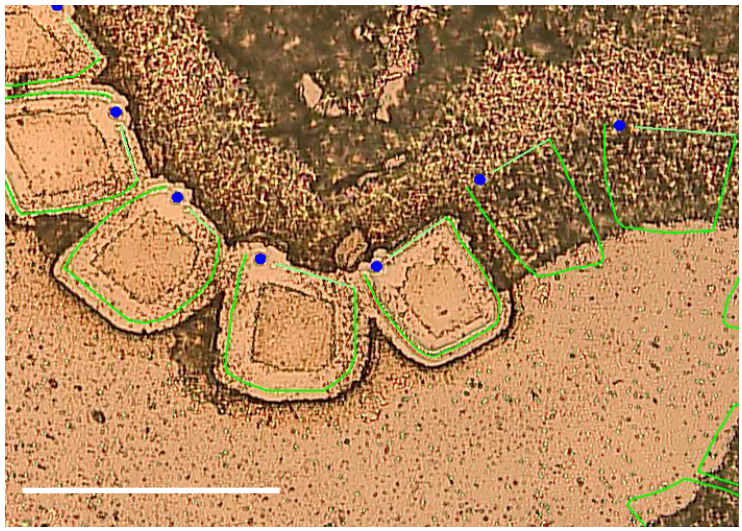

Figure 3-a: LCM of sensory epithelium from whole MOE sections. This picture was taken with a CCD camera connected with LCM microscope during the harvesting of discrete pieces of olfactory sensory epithelium. Scale bar: 150µm.

Moreover, in order to ensure a precise representation of the entire MOE, the tissue was microdissected from a collection of slices obtained by cryostat cutting from the whole MOE of both a male and a female mouse. Considering the high number of tissue slices, it was not possible to process all of them in a single LCM session, and therefore the glass slides were kept in a -80°C fridge and thawed immediately before the microdissection. The freeze-defrost procedure negatively affected the RNA quality of a small number of microdissected samples as detected by a Bioanalyzer run, and they were therefore excluded. The overall quality and quantity of the final RNA sample was higher than expected with an average RNA integrity number (RIN) value of 6.8, and confirmed the efficacy and robustness of LCM harvesting.

The whole MOE total RNA sample was splitted in two parts; one was sent to Japan for NanoCAGE library synthesis, whereas the remaining half was stored in appropriate conditions for NanoCAGE data validation.

3.2 NanoCAGE data analysis.

The NanoCAGE protocol on the whole MOE total RNA sample was applied at RIKEN Institute in Japan by Roberto Simone and Charles Plessy in a collaborative effort between the laboratories of Dr. Piero Carninci and Stefano Gustincich, while the analysis of the data including tag clustering and TCs genome mapping has been carried out by Charles Plessy and Nicolas Bertin.

The NanoCAGE-processed MOE sample was used for two consecutive rounds of sequencing with a high-thoughput Solexa sequencer; the total number of reads was 21.353.318, out of which 18.229.100 resulted to be real tags and 232.814 were categorized as ribosomal tags. Of the total 18.229.100 tags, 16.568.480 were mapped on the genome and processed for clustering.

The clustering approach was initially carried out with the same "proximity tag clustering" (PTC) methodology used for CAGE, in which every TC was defined by a group of tags that overlapped for at least one base; this calculation returned a total number of 2.068.275 TCs. However, the PTC is limited by the fact that it does not consider the existence of TCs within larger TCs, and the switching to a parametric clustering (PC, ref.156) to take into account this diffused phenomenon counted a total number of 4.736.538 TC, out of which 526.461 TC had a "tag per million" (TPM) score above 1. As for CAGE tags, the normalized TPM score of each TCs is a direct indicator of the genes expression level, and it depends on two main parameters: the abundance of a transcript encoded by a given gene, and the rate of sequencing in terms of number of sequenced tags.

When the target of the genomic analysis is a discrete cell-type, the abundance of a particular transcript can be influenced, for example, by external factors affecting the transcriptional activity of that cell system. However, when the target is a complex tissue, e.g. the MOE, the outlook can be far more complex since the abundance of the transcript will also depend on the relative abudance of the cell-type expressing that particular transcript in the cellular context of the tissue.

Since it is quite straightforward that the likelihood of detecting a rare transcript increases with the rate of sequencing, the absence of a given transcripts from a CAGE or NanoCAGE library do not exclude its expression in a very small number of cells. On the other hand, the presence of TCs in a given genomic region, apart from their overlapping with annotated genes, is considered as a reliable marker of a real TSS if the TPM score of the most represented TC in that region is ≥ 1.

A major problem of NanoCAGE tag mapping, already manifested with CAGE libraries, is that only a given fraction of all the sequenced tags could be mapped unequivocally to a single genomic location; the remaining tags either did not map or mapped to multiple genomic locations ("multimappers"). The reason for the presence of multimappers is that short sequence tags extracted from the transcriptome are inherently far more redundant than random expectation would suggest.

This may be a consequence of gene duplication events. Initially, multimappers were excluded from data analysis because of their intrinsic noise and ambiguity, but since it has been demonstrated that a significant proportion of the transcriptome can be detected only by multimap tags (157), some algorithms have been developed in recent years to reintroduce them in mapping procedures; however, these methods need to be improved.

To give a precise initial description of the correlation between TCs and annotated transcripts, the genomic coordinates of 20.649 Refseq genes were retrieved from mouse genome release UCSC mm9, and they were crossed with the genomic mapping of NanoCAGE TCs. The clustered and mapped data along with the TPM score of each TC were then made available as a single track uploadable in the user interface of the online Genome Browser.
The first information that emerged from a superficial analysis of the MOE track was the presence of a bias of TCs towards the 3'-end of annotated transcripts (fig. 3-b). While some control experiments confirmed that the over-representation of this phenomenon in NanoCAGE data could have derived from an unbalanced efficacy of oligo-dT priming and random priming in the initial phases of NanoCAGE protocol, on the other hand increasing amount of data is unexpectedly consolidating the existence of multiple promoters in proximity of the 3'-end of genes, even though many of these promoters are probably incapable of driving the synthesis of a meaningful protein-encoding transcript.

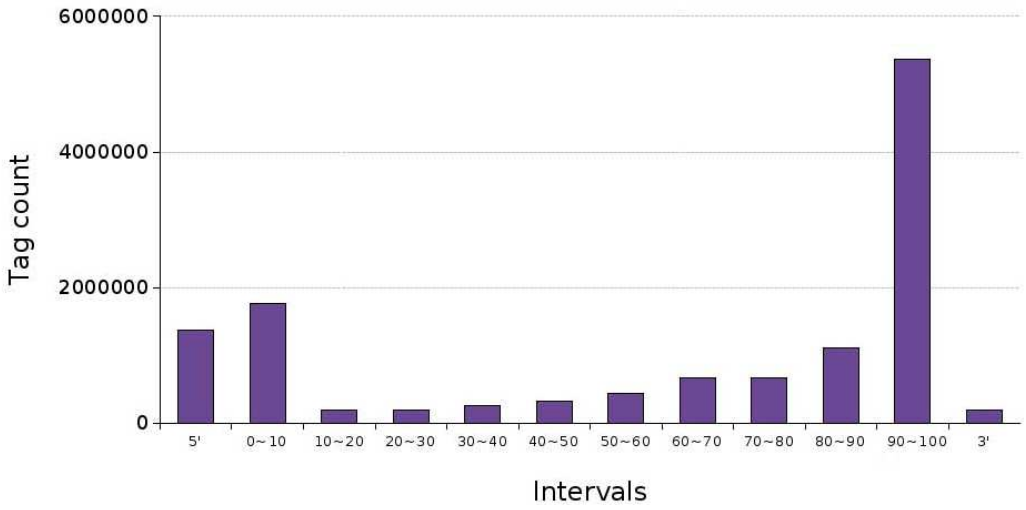

Figure 3-b: Distribution of MOE NanoCAGE tags on Refseq annotated genes. Y axis: relative numbers of mapped NanoCAGE tags; X axis: representation of NanoCAGE tags distribution on whole Refseq genes library subdivided in arbitrary intervals.

A clear example of this 3'-bias in MOE track is given by the TCs mapping on the monoexonic gene encoding for the olfactory marker protein, with the largest part of the TCs falling in the 3'-untranslated region of OMP gene. Although the biased TCs mapping is very unlikely to represent the real transcriptional dynamic of OMP, this technical issue does not affect the TPM information linked with its expression: as a matter of fact, in MOE NanoCAGE data OMP results to be the first gene in the list of top 10 more represented clusters, which is somehow expected considering the cell-type composition of the olfactory epithelium (fig. 3-c).

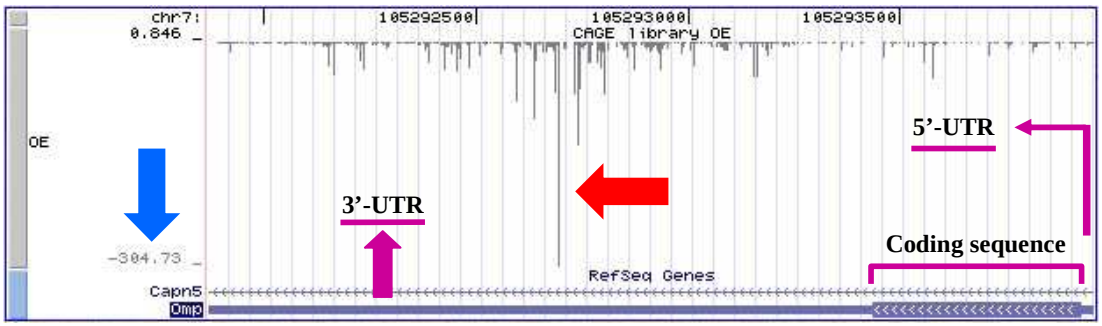

Figure 3-c: MOE NanoCAGE TCs distribution on Refseq OMP. This picture has been taken from Genome Browser website after uploading of the MOE NanoCAGE track; red arrow: most represented TC; blue arrow: TPM score associated with the most respresented TC. The TPM score has a negative value because Omp gene is located on (-) strand; genes on (+) strand have TC with positive associated TPM scores.

During this phase of the analysis it was also observed that, among the most represented clusters, the TCs mapping in correspondence of the Refseq annotated for alpha-synuclein (Snca) were displaying high TPM scores. The MOE track uploaded in the Genome Browser confirmed a nice distribution of the TCs in proximity of Snca genomic 5'-end strongly suggesting the presence of a TSS. Since in our laboratory a monoclonal α-Snca was available, we performed a preliminary validation through an IF experiment. The result highlighted the expression of Snca protein in all OSNs, a data that was not present in literature (fig. 3-d). Mutations in alpha-synuclein gene are known to cause familial autosomal dominant Parkinson's disease. The aberrant form of alpha-synuclein protein accumulates in small, dense deposits termed Lewy bodies, a cellular hallmark of Parkinson's disease found in the brain of all the affected patients. One of the early symptoms of the onset of this disease is a decrease in olfactory performances, but the cause for this defect has not been precisely identified yet. Interestingly, it has been recently reported that in mice the simple overexpression of the human

wildtype form of alpha-synuclein is able to trigger olfactory deficits (158) but it remains to be demonstrated whether they are due to central or peripheral neurodegeneration.

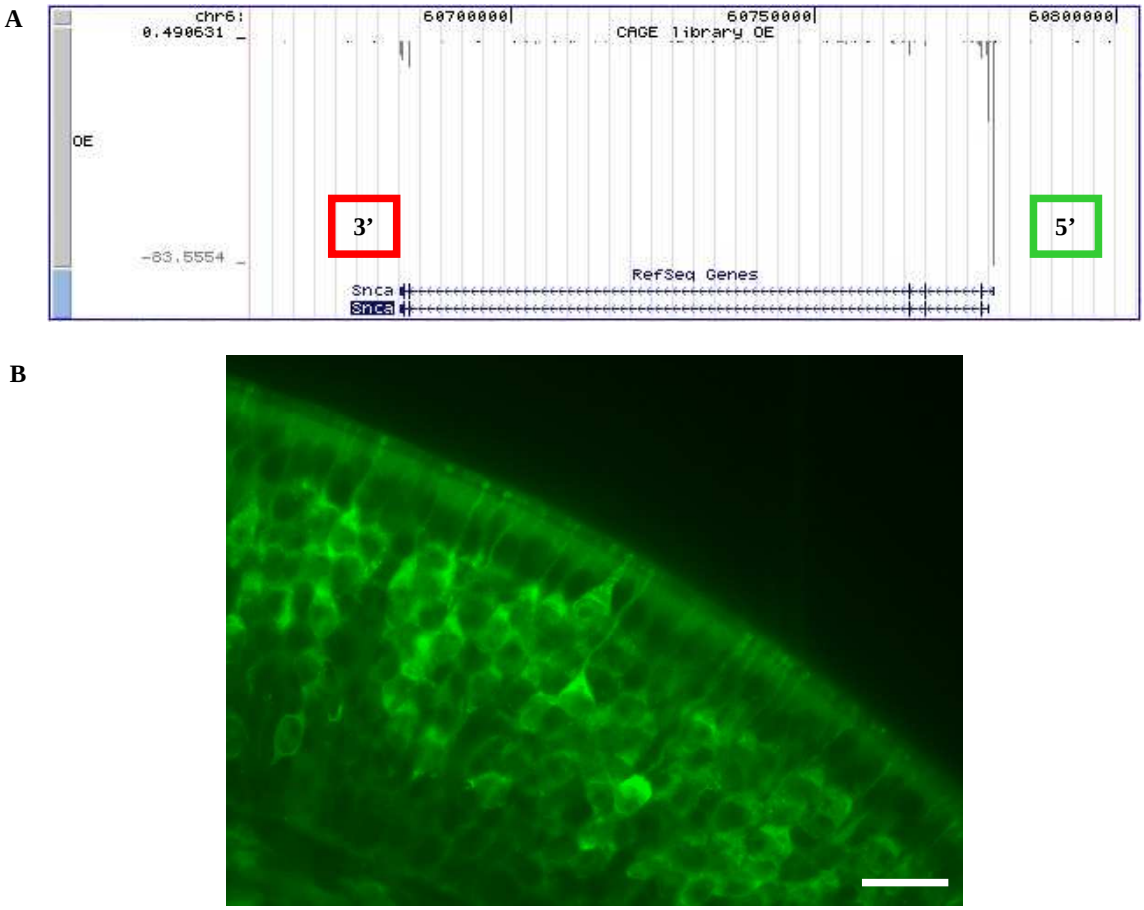

Figure 3-d: Expression of alpha-synuclein in MOE indicated by NanoCAGE TCs and revealed by IF. A: TCs in MOE NanoCAGE library mapping in correspondance of 5'-end of Refseq Snca gene; B: ZincFix IF protocol on MOE sections with α-Snca revealed the selective expression of alpha-synuclein in OSNs. Scale bar: 20μm.

Another significant finding was the frequent lack of correspondence between the TSSs identified by NanoCAGE TCs and the annotated 5' genomic position of Refseq transcripts, but it has to be noted that the deposited Refseq is often a sequence chosen as representative from a group of related sequences only on the basis of its length, without considering the datum of relative abundance. The inadequacy of this procedure is likely to be the heritage of a long period in which the isolation of the true 5' of a gene was a difficult task. Furthermore, when the full-length cDNA was not available

it was substituted during annotation by the longest known sequence of the transcript encoded by that gene.

3.3 Detection of transcripts encoding for housekeeping and marker genes in MOE NanoCAGE library.

The second phase of NanoCAGE data analysis consisted in a manual scanning of the MOE track in order to confirm the reliability and robustness of the library. Considering the massive availability of information contained in this library, it has been necessary to focus on discrete categories of genes including house keeping genes, neuronal markers reported in literature to be expressed in the MOE, markers of sustentacular cells, markers of microvillar cells, markers of olfactory stem cells, genes encoding for proteins involved in olfactory transduction. The analysis confirmed the presence of TCs for all of the observed Refseq genes.

3.4 Detection of transcripts encoding for OR.

The massive amount of data contained in MOE NanoCAGE library is currently under analysis to create a database of all the TCs mapping in correspondence to annotated genes encoding for ORs. While providing a detailed description of the entire repertoire of expressed ORs, this analysis will precisely allow identifying the TSSs of the expressed OR-genes and will expand the knowledge of their genomic structure that, in all the annotations available at present, is only partial and mostly includes only the coding sequences. As an example of the clusters included in this analysis, figure 3-e shows the TCs in the MOE NanoCAGE library identifing the TSSs of Olfr434 and Olfr435 genes.

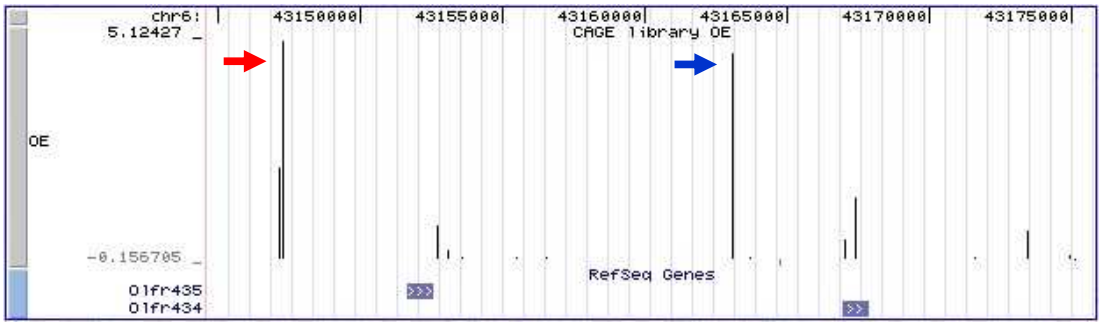

Figure 3-e: Example of NanoCAGE TCs mapping in correspondence of the TSSs of Olfr434 (blue arrow) and Olfr435 (red arrow), two genes encoding for ORs.

3.5 Detection of transcripts encoding for known components of vomeronasal sensory transduction pathway in MOE NanoCAGE library.

Since in the previous section of the thesis I have found that a V2R gene was potentially expressed in the MOE, NanoCAGE library tracks were then scanned for the presence of TCs mapping in genomic regions that include the genes encoding for the proteins associated with signal transduction in the VNO.

As shown in figure 3-f, it was possible to detect the presence of TCs with a significant TPM score mapping on the 3' of a specific Gnao1 gene which encodes for Gαo, the guanine nucleotide binding protein selectively associated with V2Rs in basal VSNs.

Other TCs were found to specifically map the 3' region of Gnai2 gene, encoding for the V1R-associated Gαi2, although with a lower TPM score; a similar TCs display was observed for the gene encoding the transient receptor potential C2, TRPC2, but in this case the additional presence of TCs located next to the 5'-end of a specific isoform suggested its expression in the MOE.

For genes known to be expressed in MCs, TCs with a low TPM score were detected also in correspondence of the genes encoding for phospholipase C-β2 (PLCB2) and type-3 receptor for inositol triphosphate (ITPR3, data not shown) proving that our approach was sensitive to detect expression in MCs.

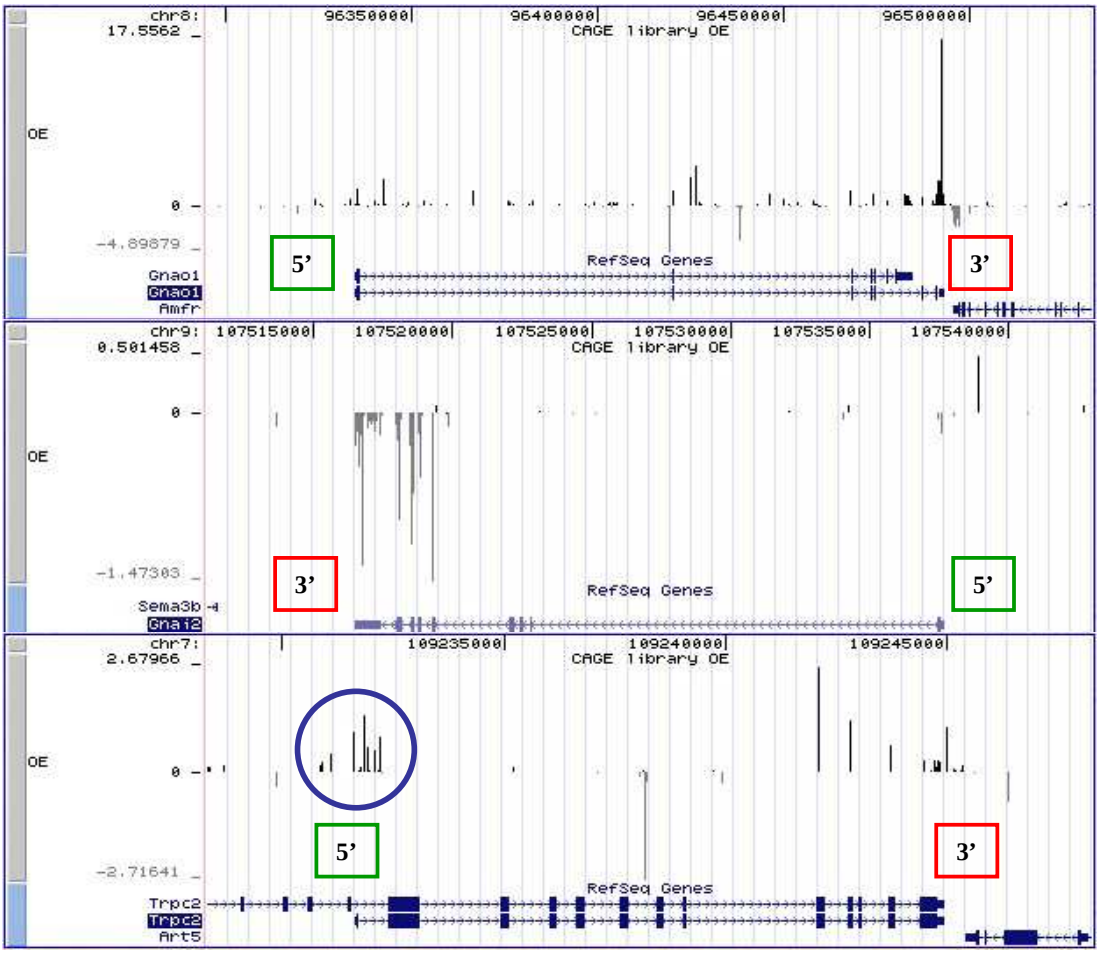

Figure 3-f: MOE NanoCAGE TCs distribution on Refseq genes involved in VSNs signal transduction. TCs in the blue circle indicate the presence of a TSS in correspondance of a specific isoform of Trpc2 (no TCs were detected in correspondance of the 5'-end of the longer isoform, not visible in the same picture).

3.6 Detection of transcripts encoding for vomeronasal receptors-type 2 in MOE NanoCAGE library.

The analysis of the genomic regions comprising the known annotated genes encoding for vomeronasal receptors highlighted the presence of several TCs with TPM ≥ 1 on different V2R-genes clusters. The most interesting signals were observed on chromosome 7 in correspondence of the V2R cluster comprising Refseq genes annotated as Vmn2r29-51, Vmn2r53-56 and Vmn2r65-76, and on chromosome 17 for the V2R cluster including Vmn2r91-110 and for Vmn2r118.

Interestingly, a RIKEN clone containing a 100% homolog portion of Vmn2r29 was found expressed in MCs in the previous section of the thesis.

Inside these clusters, the TCs mapped in exonic, intronic and intergenic, but a closer observation of these signals revealed that in some cases the TPM scores were perfectly matched along different genomic positions thereby indicating the presence of multimapper TCs that had been erroneously re-introduced in the library in multiple copies by the multimapping rescue strategy. Only some of these TCs were therefore likely to represent real TSSs, but it was impossible to determine which ones on the sole basis of NanoCAGE data analysis (fig. 3-g). Figure 3-h shows the TCs detected in correspondence of the V2Rs chosen for experimental validation.

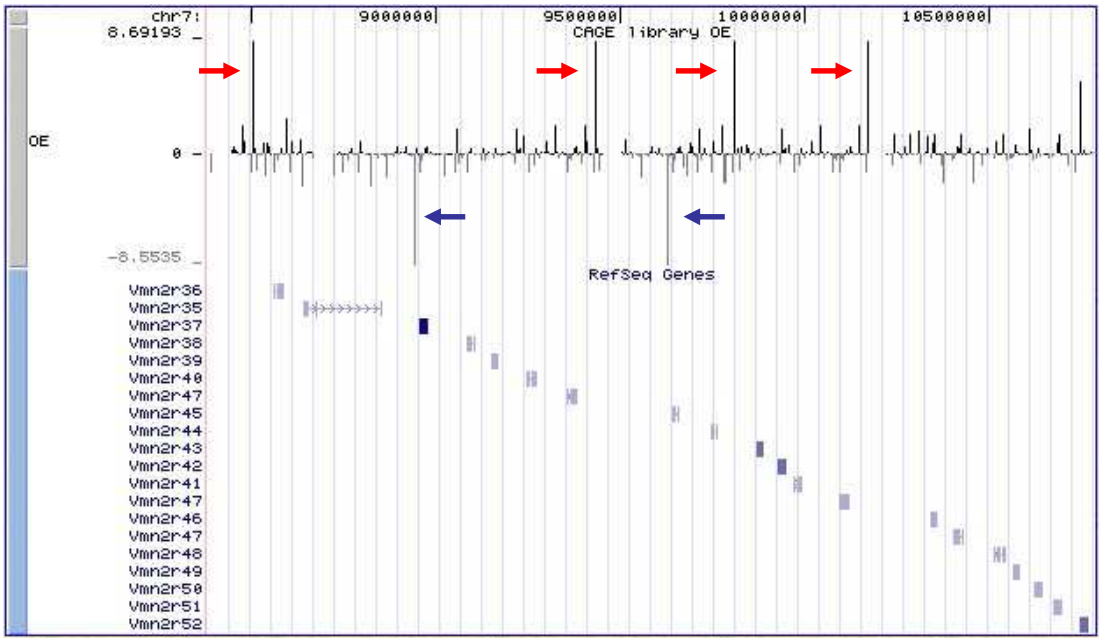

Figure 3-g: Example of NanoCAGE TCs distribution in a V2Rs clustrer on chromosome7. Arrows indicate the more evident TCs displaying the same TPM score on (+) strand (red arrows) and (-) strand (blue arrows). Other minor TCs were found to be affected by the same issue.

Vmn2r29

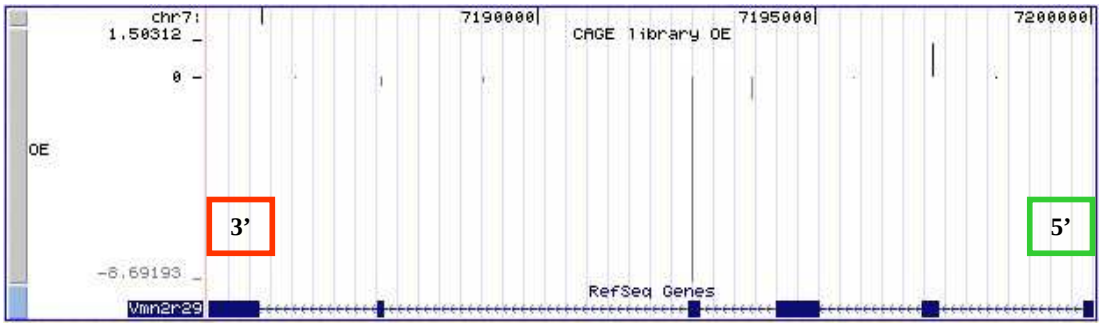

Vmn2r69

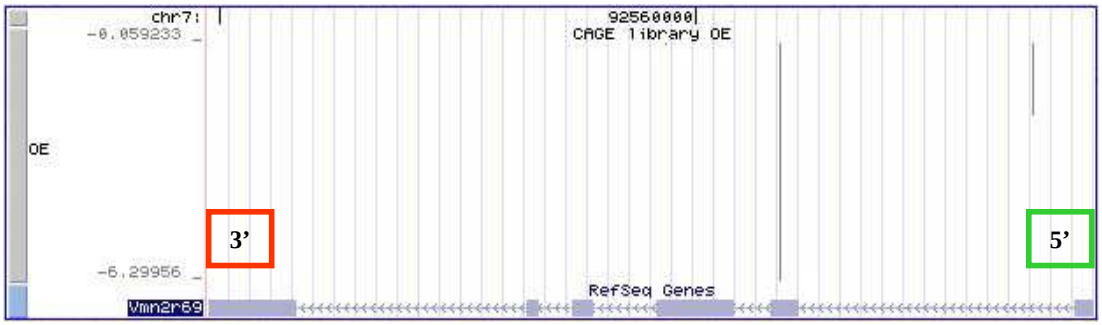

Vmn2r95

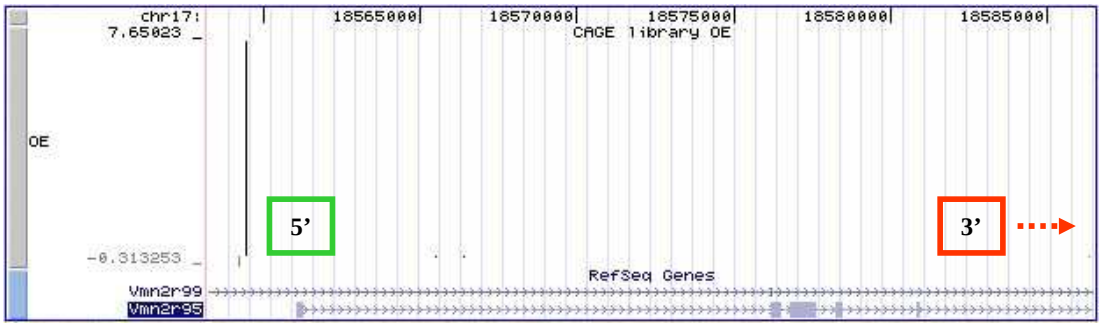

Figure 3-h: MOE NanoCAGE TCs in correspondance of the V2Rs selected for experimental validation.

Vmn2r99

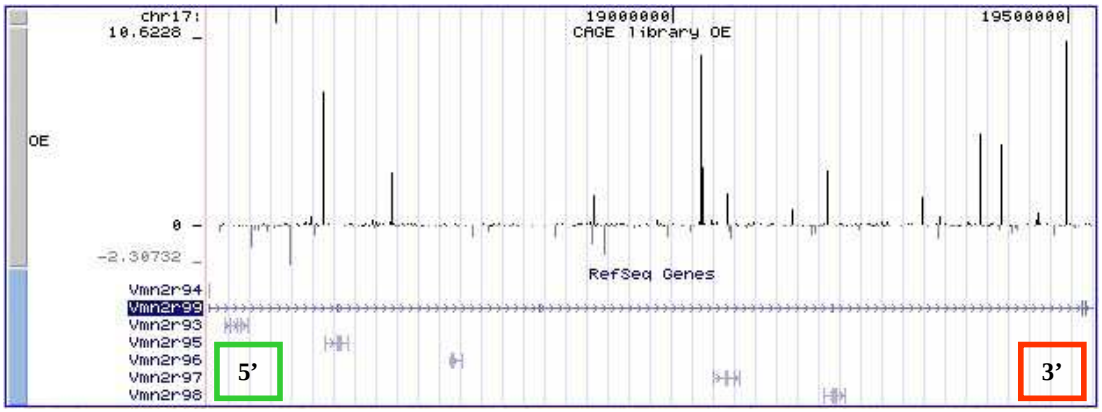

Vmn2r118

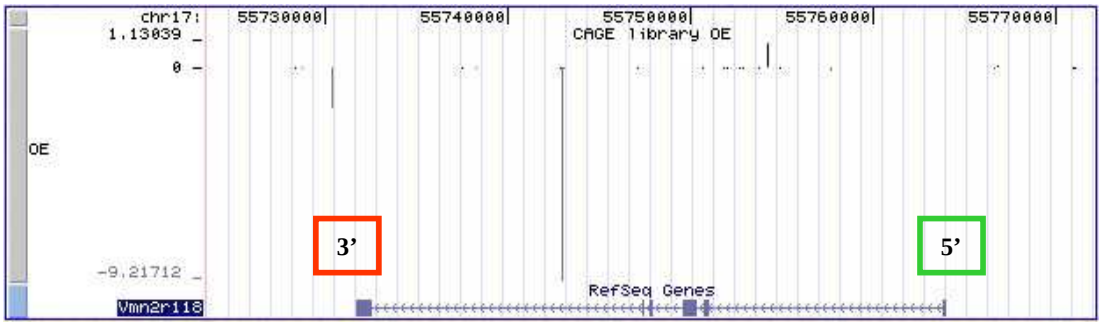

Figure 3-h (continued): MOE NanoCAGE TCs in correspondance of the V2Rs selected for experimental validation.

3.7 Validation of MOE NanoCAGE data by RT-PCR.

During the first validation phase of the data extracted from MOE NanoCAGE library, several sets of exon-spanning primers were designed proximal to the Refseq positions mapped by TCs to verify by RT-PCR the expression of selected genes showing corresponding TCs in the library. The target genes were those encoding for $G_{\alpha o}$, TRPC2, Vmn2r29, Vmn2r69, Vmn2r95, Vmn2r99, Vmn2r118 and OMP as a positive control. As a negative control, primers were designed also for a vomeronasal receptor-type 1, V1rG7, for which no TCs had been observed in the MOE library.

The first RT-PCR was performed starting from the second half of RNA extracted from the microdissected whole MOE ("OE-LCM"); the total amount of RNA contained in the sample was enough to carry out a single RT reaction. After 35 cycles of PCR, amplification products for Vmn2r29, Vmn2r69, Vmn2r95, $G_{\alpha o}$ and OMP were detected (fig. 3-i).

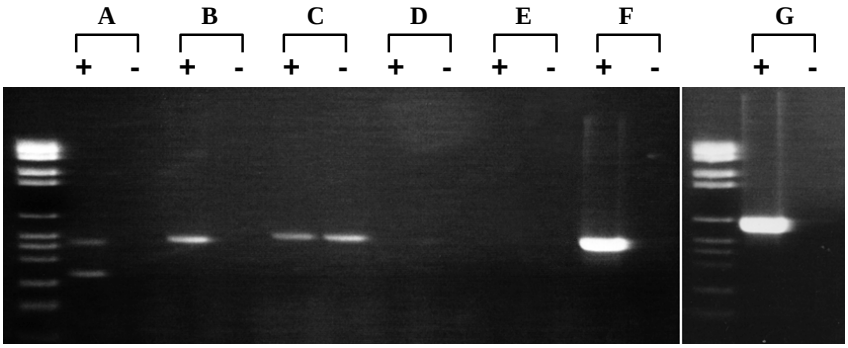

Figure 3-i: V2Rs and Gαo are expressed in the main olfactory epithelium. Specific primers have been used to amplify Vmn2r29 (A), Vmn2r69 (B), Vmn2r95 (C), Vmn2r99 (D), Vmn2r118 (E), Gαo (F) and Omp (G) by RT-PCR using RNA exctracted from whole olfactory sensory epithelium harvested by LCM.

A second PCR reaction was performed with the same protocol using a small amount of the first reaction in order to understand whether the negative result for Vmn2r99 and Vmn2r118 could be due to a low abundance of the transcripts for these two receptors, but a second negative result for both of them supported the hypothesis that the TCs observed in the MOE library in correspondence of these two genes might have been false positive multimappers, or that the primers did not work because the two receptors might be expressed in the MOE with splice variants different than those detected in the VNO. When tested by RT-PCR on VNO total RNA extracted after dissection the primers for Vmn2r99 and Vmn2r118 amplified fragments of the expected size (data not shown).
A PCR product was obtained starting from the same OE-LCM cDNA also for TRPC2; as a positive control, TRPC2 was amplified with the same RT-PCR protocol using as starting material total RNA extracted from dissected VNO (fig. 3-l).

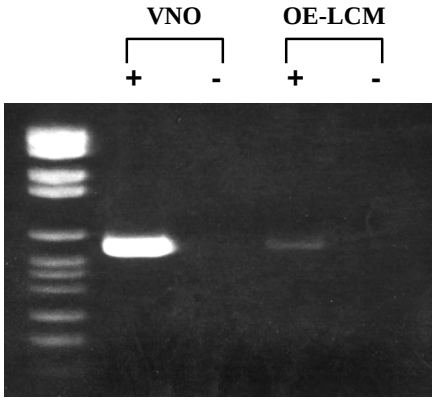

Figure 3-l: TRPC2 is expressed in the main olfactory epithelium. Specific primers were used to amplify by RT-PCR TRPC2 using total RNA etxracted from dissected VNO or from whole olfactory sensoryepithelium harvested by LCM.

To confirm the specificity of the RNA extracted from the microdissected MOE, V1RG7 was amplified by RT-PCR using a sample of RNA extracted from the VNO, but no amplification products were obtained using the same reaction conditions from the OE-LCM cDNA sample (fig. 3-m).

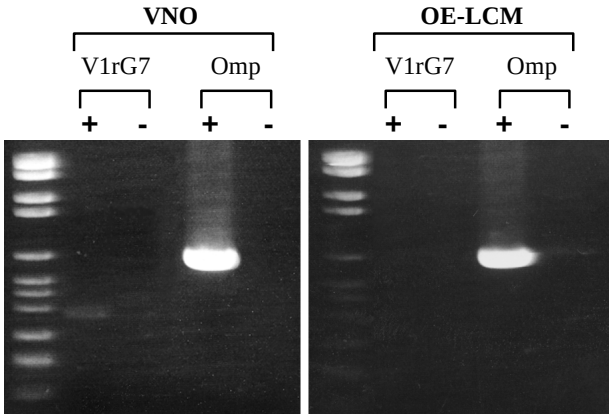

Figure 3-m: Amplification of V1rG7 from VNO and microdissected OE. Specific primers were used to amplify V1rG7 by RT-PCT using RNA extracted from dissected VNO and RNA exctracted from whole olfactory sensory epithelium harvested by LCM.

Due to its very limited availability, the OE-LCM cDNA sample was entirely used up for this preliminary validation phase. RNA was then extracted from MOE according to the published protocols.

Vmn2r29, Vmn2r69, Vmn2r95, $G_{\alpha o}$, TRPC2 and OMP were again amplified by RT-PCR from this RNA and cloned in pGEM T-easy vector for sequencing and RNA probes transcription; the two

PCR products obtained with Vmn2r29 primers were separately cloned and referred to as Vmn2r29L (for “Low”) and Vmn2r29H (for “High”).

3.8 Validation of MOE NanoCAGE data by in situ hybridization.

A first set of in situ hybridizations was carried out on a limited number of slices of MOE to assess the validity of the RNA probes and ISH reagents with NBT/BCIP revelation before proceeding with FISH. The first set of genes chosen for ISH validation included $G_{\alpha o}$, Vmn2r29H and OMP as a positive control; for all of them a set of sense/antisense RNA probes labelled with digoxygenin were transcribed from the fragments previously amplified and cloned.

In these initial trials the signal observed with OMP probes resulted to be highly specific and neat; the staining observed after incubation with the antisense probe was evenly restricted to the middle layer of MOE, as expected. $G_{\alpha o}$ antisense probes hybridized with a high number of cell bodies mainly localized in the basal layer in all of the MOE sections examined, a staining pattern similar to that observed in the sensory basal epithelium of the VNO; slices of MOE incubated with $G_{\alpha o}$ sense probe were devoid of any signal (fig. 3-n).

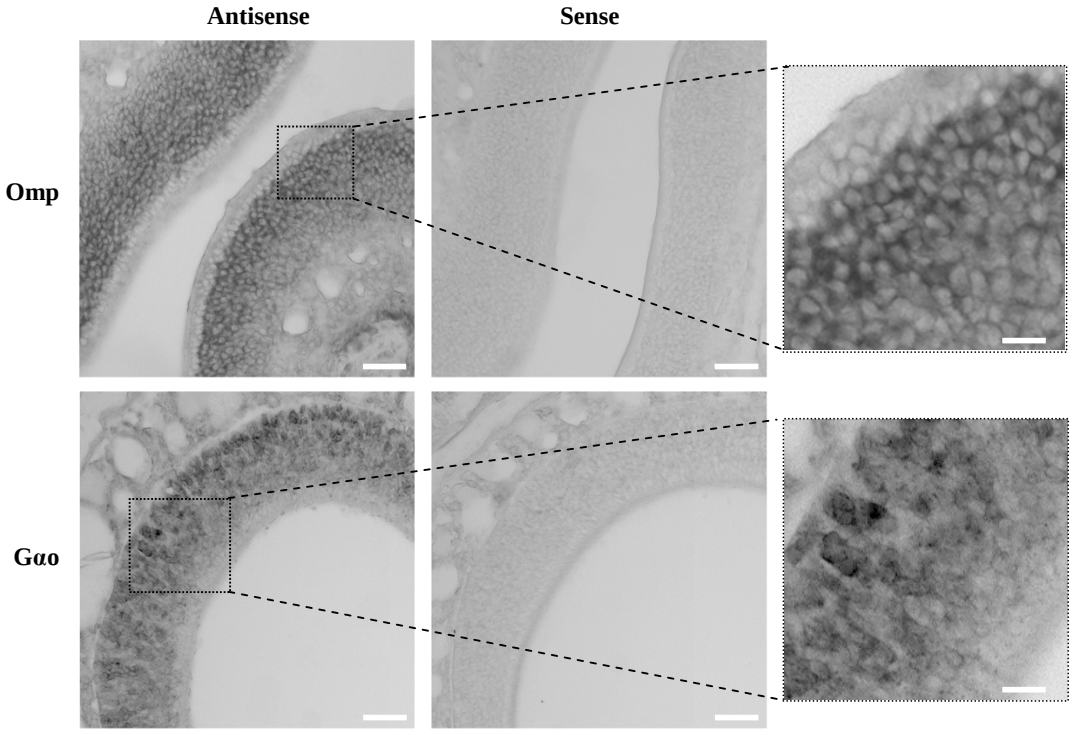

Figure 3-n: ISH of Omp and Gαo on main olfactory epithelium sections with respective magnifications. Scale bars: 75µm; magnifications: 30µm.

The amplified Vmn2r29H PCR fragment showed in its sequence an homology rate ≥ 80% with other V2Rs belonging to the same receptorial cluster, and the probes transcribed from this cloned PCR product were then predicted to have a low-selectivity when used for ISH; as a matter of fact, the Vmn2r29H antisense probe gave a nice staining of multiple cell bodies belonging to neurons located in the basal layer of the VNO. Considering the high number of positive cells observed, it was evident that the probe hybridized not only with the target mRNA but with also other homologous transcripts coding for V2Rs originated from the same cluster; the VNO slices hybridized with the control sense probe resulted to be clean (fig. 3-o).

Figure 3-p shows a rooted phylogenic tree built using the mRNA Refeseq sequences of all the V2Rs genes sharing with Vmn2r29 a homology rate ≥ 80%.

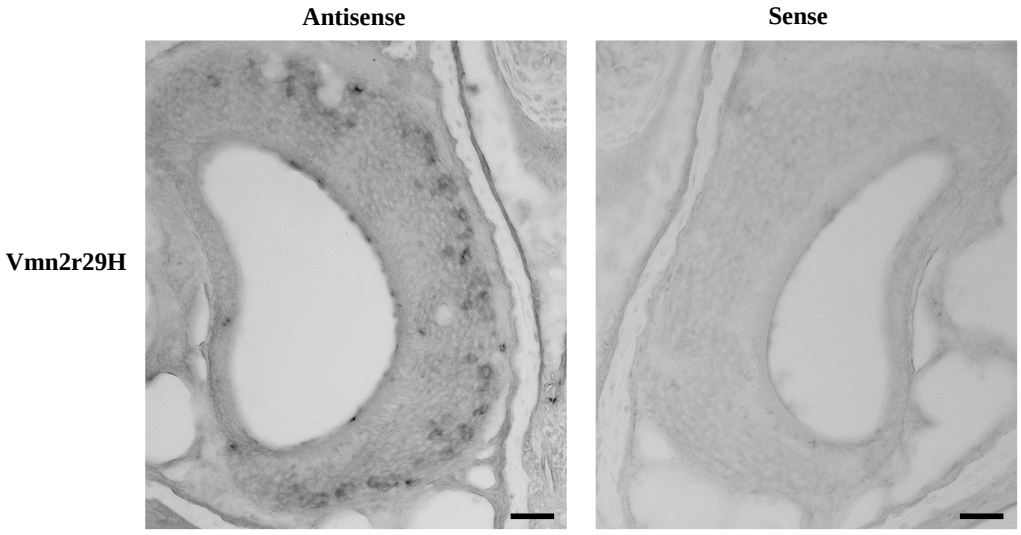

Figure 3-o: ISH of Vmn2r29H on VNO sections. Scale bars: 75μm

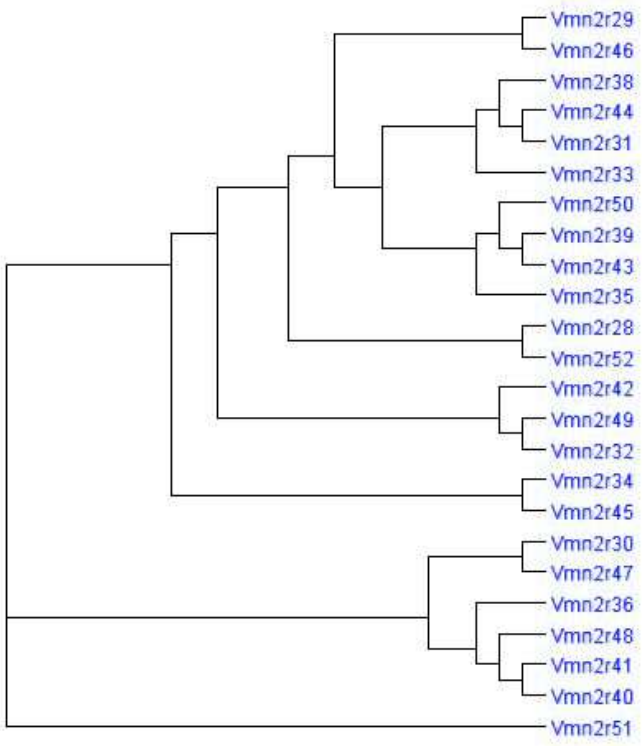

Figure 3-p: a rooted phylogenic tree built using the mRNA Refseq sequences of all the genes coding for V2Rs sharing with Vmn2r29 a homology rate ≥ 80%.

The Vmn2r29H DIG-probes were tested on MOE slices randomly collected and not representative of all the zones of the epithelium (data not shown). Since it was not possible to observe any positive result, it was then decided to proceed with a more rational approach in which serial cryo-sections of the VNO and the MOE were collected from mice at same stage of the animals used for LCM of the whole sensory OE, without skipping any region, and hybridized with Vmn2r29H probes. Adoption of this strategy was essential because of the fact that cells expressing the V2R might have been located anywhere in the MOE, with an unpredictable abundance.

Moreover, it was decided to carry out this series of experiments with a set of Vmn2r29H probes labelled with biotin, recognized with a streptavidin-HRP reagent and revealed by a tyramide high-sensitivity system based on the in loco deposition of tyramide-cy3 precipitates catalysed by HRP.

The efficacy of this system was clearly visible on the VNO slices where the signal given by Vmn2r29H antisense probe was clear and strong whereas no significant staining was observed with sense probe (fig. 3-q).

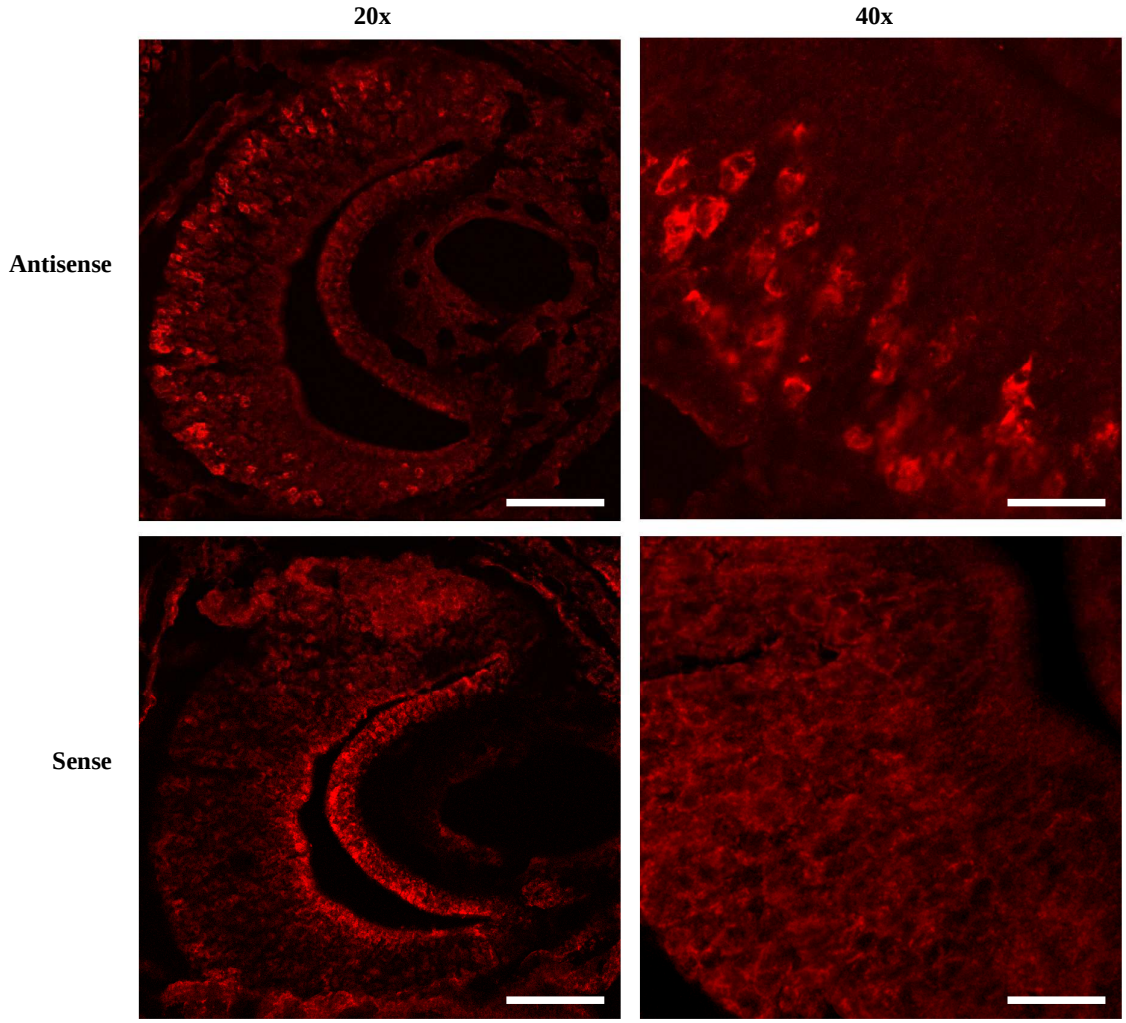

Figure 3-q: FISH of Vmn2r29H on VNO sections. Scale bar 20x: 180µm; Scale bar 40x: 30µm.

In the MOE, Vmn2r29H antisense probe surprisingly hybridized with a relevant number of cells scattered on different slices of the sensory epithelium, but mostly located only within a small number of dorsal endoturbinates; exceptions were found for some positive cells observed in the MOE lining the nasal septum and others in medial endoturbinates. The bodies of positive cells were found to reside in the basal layer, the middle layer and the apical layer of the epithelium, and the observed cellular morphology varied according to the occupied position, with the one presented by cells in the basal and middle layer directly resembling the morphology of OSNs. In some cases it was possible to dinguish also some processes departing from positive cells towards the surface or the basal layer of MOE; positive flask-shaped apical cells were slightly more abundant than OSN-

like positive cells, but a count for each cell-type was not carried out. Apical positive cells are shown in figure 3-r, OSNs-like positive cells in figure 3-s and an example of basal positive cells is shown in figure 3-t.

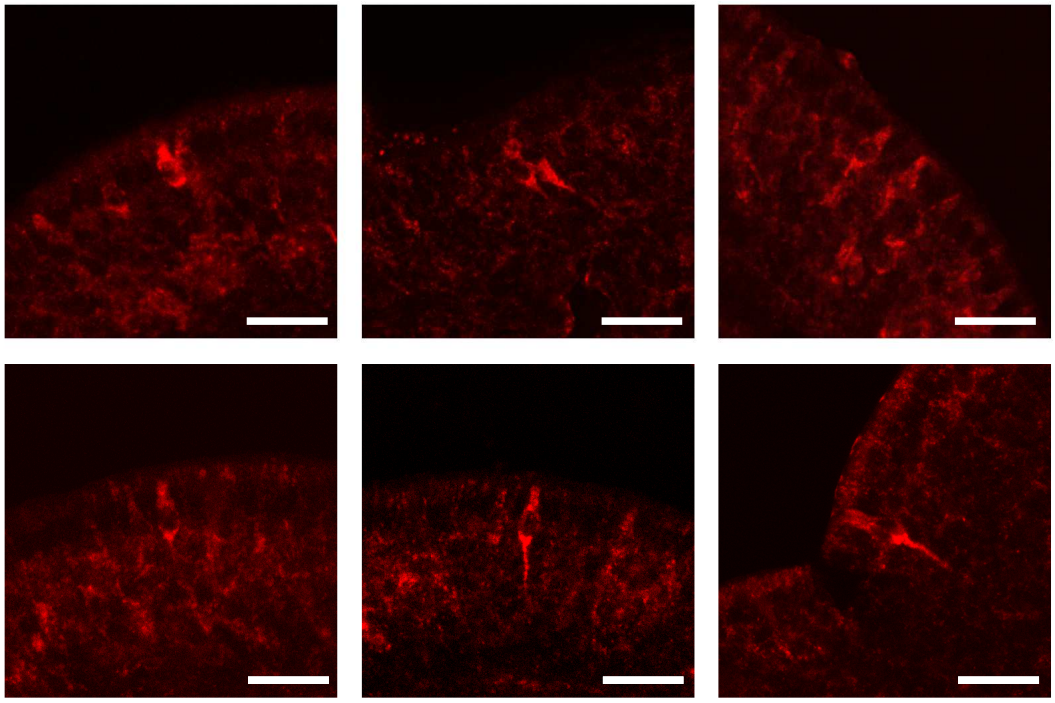

Figure 3-r: Examples of apical cells recognized in FISH by Vmn2r29H antisense probe. These flask-shaped cells were found in several sections of MOE; pictures acquired with a confocal microscope. Scale bars: 20μm.

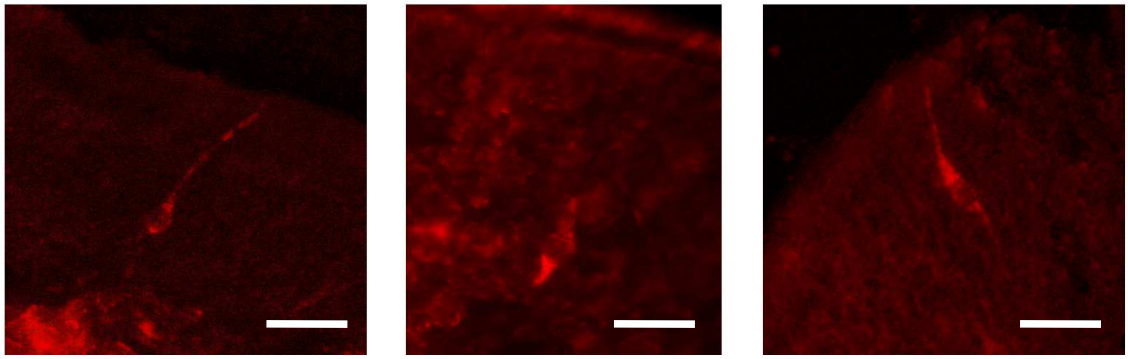

Figure 3-s: Positive cells in the middle layer of sensory OE recognized in FISH by Vmn2r29H antisense probe. Like apical positive cells, this cell type was found in several sections of MOE; pictures acquired with a confocal microscope. Scale bars: 20µm.

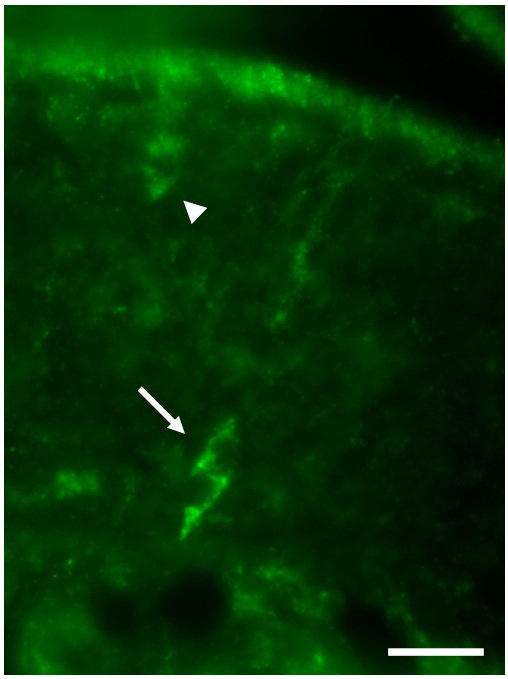

Figure 3-t: Example of basal cells recognized in FISH by Vmn2r29H antisense probe (white arrow). In this same picture is possible to identify the body of an apical positive cell (white arrowhead). Picture acquired with a UV microscope. Scale bar: 20µm.

While sections of the VNO hybridized with Vmn2r29H sense probe were free of any specific signal, in the MOE the control hybridization with Vmn2r29H sense probe highlighted the presence of a small number of flask-shaped positive cells, whose position was restricted to a couple of dorsal endoturbinates; it was not possible to find any OSN-like positive cells in these sections (fig. 3-u).

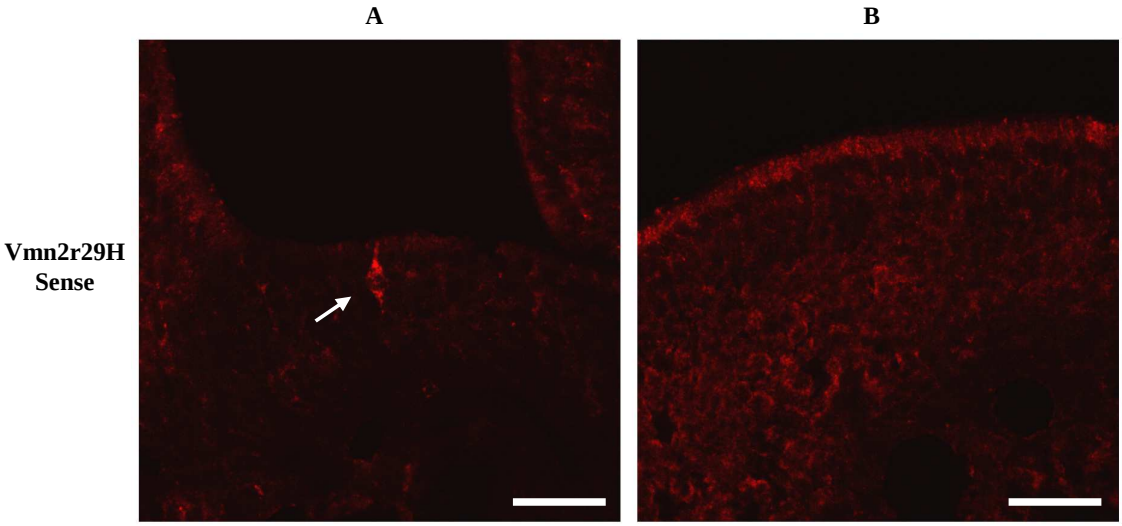

Figure 3-u: FISH of Vmn2r29H sense probe on MOE sections.Vmn2r29H sense probe recognized a small number of apical cells in some sections of MOE (A). In the largest part of sections it was not possible to observe any kind of relevant staining (B). Scale bar: 50μm.

The reason for this unexpected result is likely to be due to a sense/antisense transcripts interaction. Vmn2r29H sense probe presents a very high homology with a multitude of genomic spots and, at least in two different cases, the analysis of MOE NanoCAGE library revealed the presence of TCs with significant TPM scores in correspondence of these genomic positions. The features recognized by NCBI in these two examined homology spots are defined as “similar to vomeronasal 2, receptor 15 isoform 1” and “putative pheromone receptor”, and are located on chromosome 7 and chromosome 17, respectively. Although no known transcripts are annotated in these regions (apart from two mouse ESTs in the first case), they both interestingly show a high degree of conservation in several other species (fig. 3-v).

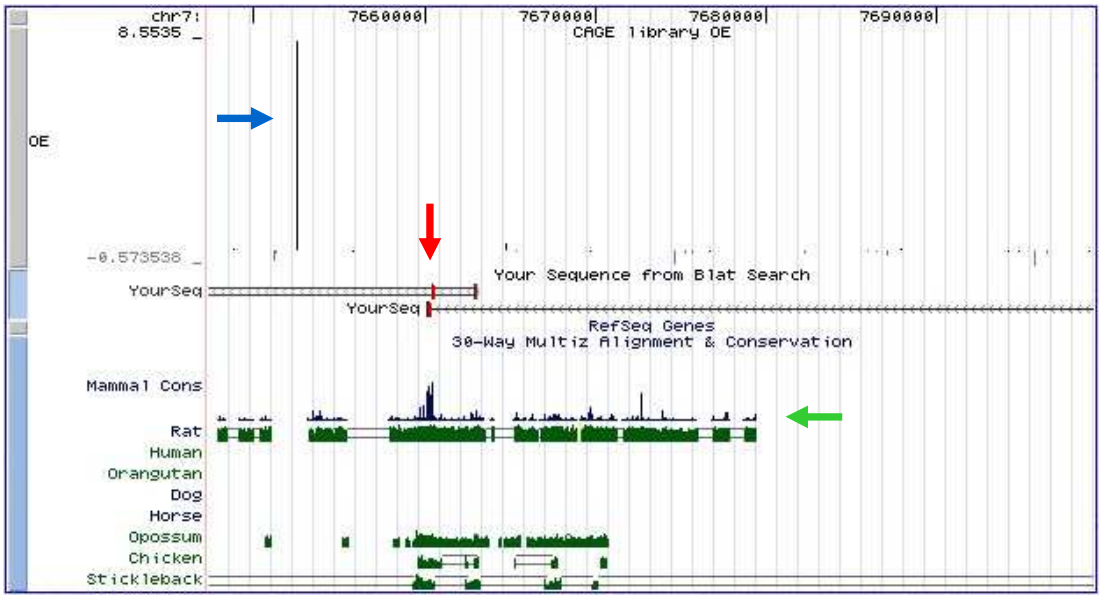

Figure 3-v: TCs mapping on chromosome 7 (blue arrow) indicate the TSSs of an hypothetical transcript predicted that do not correspond to any annotated Refseq but that may hybridize with Vmn2r29H (Vmn2r30) sense probe (red arrow). Green arrow indicates the rate of conservation of this genomic spot with rat, opossum and chicken.

3.9 Discussion.

The advent of post-genomic era has opened the doors to a new exciting period of scientific discoveries in neuroscience.

Long before the recent advancements of genomic tools, a first revolution in the research field concerning olfaction had been triggered by the discovery of genes coding for odour receptors expressed in the main olfactory epithelium, which provided the key for the interpretation of odours coding and representation in the brain, and which had been followed some years later by the identification of two discrete gene families coding for pheromone receptors expressed in the vomeronasal organ.

The selective expression of the two categories of receptors by the MOE and the VNO was found to be perfectly in line with the dual olfactory hypothesis, and accounted for the involvement of the two subsystems in separate and discrete behavioural and functional contexts. However, this schematic interpretation that has been adopted for years did not consider some important details that were

pointing at the existence of a more complex landscape, not necessarily ruled by the widely spread and accepted theories.

As an example, in 1996 Linda Buck and Richard Axel examined in a detailed work the expression in the olfactory system of genes coding for components of the pheromone signalling cascade (159). Their data highlighted for the first time the differential association of $G_{\alpha o}$ and $G_{\alpha i2}$ proteins with two neuronal populations of the VNO that hence resulted to be functionally and anatomically segregated. However, in the same work they also tested the expression of $G_{\alpha o}$ and $G_{\alpha i2}$ in the MOE, and by ISH they demonstrated that the two transcripts, in particular $G_{\alpha o}$, were widely and strongly expressed by a very large number of cells. Their ISH data were also confirmed by a northern blot analysis, and again the two genes were found to be expressed both in the VNO and in the MOE. Surprisingly, these data seem to have been forgotten by the scientific community, probably covered by what at that time were considered more important discoveries. In that period the attention was mainly focused on the VNO because for the first time details about the molecular biology of neurons involved in pheromones sensing were emerging. Nevertheless the expression of $G_{\alpha o}$ and $G_{\alpha i2}$ in the MOE was implying that some OSNs could have been endowed with signal transduction machineries alternative to the well-characterized one involving $G_{\alpha olf}$, ACIII and the CNG channel and, as a logical consequence of this observation, they could have expressed some receptors not related to the OR family. Subsequent works hardly mentioned these evidences.

Similarly, in a pivotal study published in 1999 in which Emily Liman and colleagues demonstrated the fundamental role of TRPC2 in VSNs transduction, it was showed by ISH that this channel is expressed not only in VSNs but also in some sparse cells located in the basal district of the MOE (90); however, it is very difficult, if not impossible, to find similar data in succeeding publications.

Moreover, the involvement of the MOE in some pheromone-based behaviours had been proposed several years before the work by Buck and Axel was published; as already cited it was demonstrated in 1986 that the surgical removal of VNO in newborn rabbits had no effect on nipple searching and lactation, two behaviours known to be elicited by the same pheromone. In 1994, a study on hormonal and behavioural responses of male hamsters to feminine cues had concluded that both the VNO and the MOE are important for androgen responses to female odours in sexually naïve males (160). More convincingly, some years later it was proved that the source of the neural inputs going from the peripheral olfactory system to hypothalamic neurons controlling reproduction and fertility are not originated from the VNO, but rather from a discrete subpopulation of OSNs residing in the MOE. Despite of the availability of these intriguing data, a comprehensive description of these mechanisms in terms of cellular characterization, identity of the receptors

involved, behavioural responsibility of each of the defined subsystems is missing mostly because of intrinsic difficulties arising from the complexity of the targeted system.

The project described in the third section of this thesis has taken advantage for the first time of the combination of LCM with a high-throughput tagging technique providing a first description of the complete landscape of MOE transcriptome.

The achievements of this approach are actually many. First of all, the olfactory epithelium has been collected in a selective way that has permitted to avoid contamination of surrounding tissues (respiratory epithelium, cartilage, bones etc.) thus guaranteeing the specificity of the starting sampe. This has represented a great advantage and has confirmed the efficacy of the LCM technology also for thorough harvesting of entire tissues with a complex morphology.

Second, the data made available by the application of the newly developed NanoCAGE protocol have revealed its power for gene discovery, and it represents a precious source of information about the quantity and quality of gene expression. MOE NanoCAGE library allows in fact gathering details about the abundance and the transcription starting site of any of the transcripts included in MOE transcriptome, whether they are already known and annotated genes, new splicing forms, non-coding RNAs, or unknown and still unidentified transcripts.

In this project the MOE library has been primarily used to assess the expression in the MOE of genes encoding for pheromones receptors, but other analysis concerning a description of the entire repertoire of expressed OR genes are currently next to completion.

The identification of TSS will allow a bioinformatic analysis of the distribution of DNA binding sites for transcription factors in OR promoters. In a collaborative effort with the laboratory of B. Lenhart, we have already identified a class of transcription factors that may be involved in OR control (C. Plessy, personal communication).

To date, the only genomic approach with a similar goal used custom oligonucleotide chips, and due to the unavailability of commercial array containing probes for the entire mouse repertoire of ORs, V1Rs and V2Rs the sequences were manually inserted one by one with a highly demanding and time-consuming procedure. Moreover, due to their intricate genomic structure, the V2Rs coding gene family was left aside and not tested.

The analysis of NanoCAGE data has revealed the presence of several tag clusters in the MOE library that have mapped on the genome in correspondence to different loci containing discrete V2Rs clusters. Only a small number of these TCs mapped in proximity of the annotated 5’-end of V2R-Refseq genes, while the majority was found to be both exonic and inronic. These data are

nicely supported by the presence of TCs located in correspondence of genes coding for $G_{\alpha o}$, $G_{\alpha i2}$, TRPC2, IP3R3 and PLC-β2. The evidences reported by Buck and Axel in the previously cited work about the different expression levels of $G_{\alpha o}$ and $G_{\alpha i2}$ in the MOE are precisely confirmed by the NanoCAGE library in which TCs for Gnao1 gene have a maximum score of 17.55 TPM, while the maximum score fro Gnai2 gene is 1.47.

The first experimental validation phase has confirmed by RT-PCR the expression in the MOE of $G_{\alpha o}$, $G_{\alpha i2}$, TRPC2 and some V2Rs (Vmn2r29, Vmn2r69 and Vmn2r95) chosen on the basis of the intensity of their TPM scores. Although displaying TCs with rather high TPM scores, it was not possible to verify the expression of Vmn2r99 and Vmn2r118; while it is likely that the observed TCs for these two genes have arisen from an inaccurate multimappers rescue strategy, on the other hand the two mRNAs could present in the MOE transcriptome a splicing form that the designed primers did not manage to amplify.

The ISH results highlighted in this thesis are to be considered as preliminary and need a very careful interpretation. The ISH data for $G_{\alpha o}$ are quite clear and actually match those already published by Buck and Axel in 1996. In all the MOE sections examined, the staining given by $G_{\alpha o}$ probe involves a large number of cells, located in the basal layer of the MOE and, to a minor extent, in the middle layer. This staining resembles the one observed with the same RNA probe in the VNO, but at present the identity of the cells expressing $G_{\alpha o}$ in the MOE is not further characterized, and it is therefore impossible to assess its association with functional ORs, VRs or other unidentified receptors. Given its localization, it may be that $G_{\alpha o}$ is expressed by immature sensory cells and that during the differentiation process its expression is substituted with that of $G_{\alpha olf}$. Another possibility is that $G_{\alpha o}$ is actually expressed by mature and sensory cells. In this case given the relevant frequency of positive cells it may signal the existence of a new class of sensory neurons. This would immediately raise important questions concerning the identity of the receptors that are co-expressed with $G_{\alpha o}$.

The results obtained from a FISH experiment in which sections representing an entire MOE have been hybridized with a probe transcribed from Vmn2r29H PCR product are intriguing. In the VNO this probe has recognized a high number of V2R-neurons located in the basal layer; this was somehow expected, considering the ≥ 80% homology of Vmn2r29H probe with at least other 15 V2Rs belonging to the same cluster. In the MOE, the number of positive cells is high.

It is possible that all the detected cells express the same receptor, but at the same time it can also be that the receptors recognized in the MOE are multiple. As a matter of fact, the analysis of the MOE track has revealed tens of other TCs, even though with low TPM scores, in the same V2R cluster

including Vmn2r29. The low TPM scores could be due to the fact that a given receptor is expressed only by a restricted number of cells.
Interestingly, the Vmn2r29H-positive cells display different morphology and different localizations in the context of the MOE; a small number of cells have been identified on the basal layer, and curiously it was not rare to observe groups of two positive cells vertically coupled head-to-tail. Some other cells have been found in the middle layer, showing a process headed towards the surface of the epithelium and another thin process directed to the basal layer. 3D-stacks of these cells obtained by confocal microscopy have in some cases confirmed the presence of both processes. The third and maybe more represented cell-type is located in the apical layer and has a flask-shaped morphology, with a typical apical short process and a second, thin process running to the base of the epithelium.

The next experiments will be aimed at creating a detailed description of the data, including a screening of all the V2Rs expressed in the MOE which will be supported also by the second MOE NanoCAGE library, a series of double and triple FISH to understand whether the identified V2Rs associate with known players of vomeronasal or olfactory signal transduction, thus determining the identity of the different cell-types involved in V2Rs expression. Double FISH with either $G_{\alpha o}$ or $G_{\alpha i2}$ will clarify the possibility of a differential association of these two proteins with the screened V2Rs. Additional ISH experiments will try to establish the location in MOE of the cells expressing TRPC2; moreover, 5'-RACE experiments will be carried out to define the genomic structure of the vomeronasal receptors found in the MOE.

It is clear that further studies will be required to demonstrate that the V2Rs expressed in the MOE are functional, and to define the chemical nature of their ligands.
The list of biological mechanisms in which the so far detected V2Rs could be involved is quite long and exciting, not considering those which are still unknown or considered as unrelated from already described pheromone-induced behaviours. Just to mention two of the most fascinating ones, MHC peptides have been demonstrated to elicit specific electrical responses in the MOE but the receptors or even the cell-types involved in this mechanism are still unidentified. Although the electrophysiological dynamics of MHC peptides in MOE are slightly different from those recorded in the VNO, at present it is impossible to ascribe these discrepancies to the expression of a differential set of receptors or to a differential regulation of the same set of receptors in the VNO and MOE. Moreover, it is now clear that discrete populations of OSNs contribute via a direct link with the hypothalamus to processes of sexual arousal and mating, two behaviours that for long time

have been considered to be triggered by pheromonal activation of VSNs. In this case, the molecular identity of receptors expressed by OSNs projecting towards the hypothalamus is unclear, thus leaving enough space to speculate about the involvement of vomeronasal receptors.

References

1. Butler AB, Hodos, W in: Comparative Vertebrate Neuroanatomy: Evolution and Adaptation, Wiley-Liss, New York, 1996, pp. 423–424.
2. Hara, TJ. Olfaction and gustation in fish: an overview. Acta Physiol Scand. 1994 Oct;152(2):207-17. Review.
3. Brennan PA, Kendrick KM. Mammalian social odours: attraction and individual recognition. Philos Trans R Soc Lond B Biol Sci. 2006 Dec 29;361(1476):2061-78. Review.
4. Vickers, NJ. Mechanisms of animal navigation in odor plumes. Biol Bull. 2000 Apr;198(2):203-12. Review.
5. Mendoza, AS. Morphological studies on the rodent main and accessory olfactory systems: the regio olfactoria and vomeronasal organ.Ann Anat. 1993 Oct;175(5):425-46.
6. Beites CL, Kawauchi S, Crocker CE, Calof AL. Identification and molecular regulation of neural stem cells in the olfactory epithelium. Exp Cell Res. 2005 Jun 10;306(2):309-16. Epub 2005 Apr 21. Review.
7. Malnic B, Hirono J, Sato T, Buck LB. Combinatorial receptor codes for odors. Cell. 1999 Mar 5;96(5):713-23.
8. Serizawa S, Ishii T, Nakatani H, Tsuboi A, Nagawa F, Asano M, Sudo K, Sakagami J, Sakano H, Ijiri T, Matsuda Y, Suzuki M, Yamamori T, Iwakura Y, Sakano H. Mutually exclusive expression ofodorant receptor transgenes. Nat Neurosci. 2000 Jul;3(7):687-93.
9. Serizawa S, Miyamichi K, Nakatani H, Suzuki M, Saito M, Yoshihara Y, Sakano H. Negative feedback regulation ensures the one receptor-one olfactory neuron rule in mouse. Science. 2003 Dec 19;302(5653):2088-94. Epub 2003 Oct 30.
10. Vogalis F, Hegg CC, Lucero MT. Ionic conductances in sustentacular cells of the mouse olfactory epithelium. J Physiol. 2005 Feb 1;562(Pt 3):785-99. Epub 2004 Dec 20.
11. Vogalis F, Hegg CC, Lucero MT. Electrical coupling in sustentacular cells of the mouse olfactory epithelium. J Neurophysiol. 2005 Aug;94(2):1001-12. Epub 2005 Mar 23.
12. Rafols JA, Getchell TV. Morphological relations between the receptor neurons, sustentacular cells and Schwann cells in the olfactory mucosa of the salamander. Anat Rec. 1983May;206(1):87-101

13. Menco, B. PH. M. & Morrison, E. E. (2003) Morphology of the mammalian olfactory epithelium: Form, fine structure, function, and pathology. In: *Handbook of olfaction and gustation* (edited by Doty, R. L.), pp. 17–49. New York: Marcel Dekker.
14. Yu TT, McIntyre JC, Bose SC, Hardin D, Owen MC, McClintock TS. Differentially expressed transcripts from phenotypically identified olfactory sensory neurons. J Comp Neurol. 2005 Mar 14;483(3):251-62.
15. Okano M, Weber AF, Frommes SP. Electron microscopic studies on the distal border of the canine olfactory epithelium. J Ultrastruct Res. 1967 Mar;17(5):487-502.
16. Kaluza JF, Gussing F, Bohm S, Breer H, Strotmann J. Olfactory receptors in the mouse septal organ. J Neurosci Res. 2004 May 15;76(4):442-52.
17. Breer H, Fleischer J, Strotmann J. The sense of smell: multiple olfactory subsystems. Cell Mol Life Sci. 2006 Jul;63(13):1465-75. Review.
18. J. Brechbuhl, M. Klaey, and M. C. Broillet. Grueneberg ganglion cells mediate alarm pheromone detection in mice. *Science* 321 (5892):1092-1095, 2008.
19. Buck L, Axel R. A novel multigene family may encode odorant receptors: a molecular basis for odor recognition. Cell. 1991 Apr 5;65(1):175-87.
20. Niimura Y, Nei M. Comparative evolutionary analysis of olfactory receptor gene clusters between humans and mice. Gene. 2005 Feb 14;346:13-21. Epub 2005 Jan 7.
21. Yoshihito Niimura. Extensive Gains and Losses of Olfactory Receptor Genes in Mammalian Evolution. *PLoS ONE* 2 (8):e708, 2007.
22. B. M. Shykind. Regulation of odorant receptors: one allele at a time. *Hum.Mol.Genet.* 14 Spec No 1:R33-R39, 2005.
23. M. Q. Nguyen, Z. Zhou, C. A. Marks, N. J. Ryba, and L. Belluscio. Prominent roles for odorant receptor coding sequences in allelic exclusion. *Cell* 131 (5):1009-1017, 2007.
24. H. Breer, J. Fleischer, and J. Strotmann. The sense of smell: multiple olfactory subsystems. *Cell Mol.Life Sci.* 63 (13):1465-1475, 2006.
25. S. Firestein. How the olfactory system makes sense of scents. *Nature* 413 (6852):211-218, 2001.
26. T. Abaffy, A. Malhotra, and C. W. Luetje. The molecular basis for ligand specificity in a mouse olfactory receptor: a network of functionally important residues. *J Biol Chem.* 282 (2):1216-1224, 2007.
27. D. Schild and D. Restrepo. Transduction mechanisms in vertebrate olfactory receptor cells. *Physiol Rev.* 78 (2):429-466, 1998.

28. H. R. Matthews and J. Reisert. Calcium, the two-faced messenger of olfactory transduction and adaptation. *Curr.Opin.Neurobiol.* 13 (4):469-475, 2003.
29. F. Zufall and S. Firestein. Divalent cations block the cyclic nucleotide-gated channel of olfactory receptor neurons. *J.Neurophysiol.* 69 (5):1758-1768, 1993.
30. C. Dzeja, V. Hagen, U. B. Kaupp, and S. Frings. Ca2+ permeation in cyclic nucleotide-gated channels. *EMBO J.* 18 (1):131-144, 1999.
31. T. Kurahashi and K. W. Yau. Olfactory transduction. Tale of an unusual chloride current. *Curr.Biol.* 4 (3):256-258, 1994.
32. S. J. Kleene and R. C. Gesteland. Calcium-activated chloride conductance in frog olfactory cilia. *J.Neurosci.* 11 (11):3624-3629, 1991.
33. G. Lowe and G. H. Gold. Nonlinear amplification by calcium-dependent chloride channels in olfactory receptor cells. *Nature* 366 (6452):283-286, 1993.
34. J. Reisert, J. Lai, K. W. Yau, and J. Bradley. Mechanism of the excitatory Cl- response in mouse olfactory receptor neurons. *Neuron* 45 (4):553-561, 2005.
35. H. Kaneko, I. Putzier, S. Frings, U. B. Kaupp, and T. Gensch. Chloride accumulation in mammalian olfactory sensory neurons. *J.Neurosci.* 24 (36):7931-7938, 2004.
36. W. T. Nickell, N. K. Kleene, R. C. Gesteland, and S. J. Kleene. Neuronal chloride accumulation in olfactory epithelium of mice lacking NKCC1. *J.Neurophysiol.* 95 (3):2006.
37. T. Y. Chen and K. W. Yau. Direct modulation by Ca(2+)-calmodulin of cyclic nucleotide-activated channel of rat olfactory receptor neurons. *Nature* 368 (6471):545-548, 1994.
38. T. Kurahashi and A. Menini. Mechanism of odorant adaptation in the olfactory receptor cell. *Nature* 385 (6618):725-729, 1997.
39. J. Bradley, D. Reuter, and S. Frings. Facilitation of calmodulin-mediated odor adaptation by cAMP-gated channel subunits. *Science* 294 (5549):2176-2178, 2001.
40. J. Wei, A. Z. Zhao, G. C. Chan, L. P. Baker, S. Impey, J. A. Beavo, and D. R. Storm. Phosphorylation and inhibition of olfactory adenylyl cyclase by CaM kinase II in Neurons: a mechanism for attenuation of olfactory signals. *Neuron* 21 (3):495-504, 1998.
41. T. Leinders-Zufall, M. Ma, and F. Zufall. Impaired odor adaptation in olfactory receptor neurons after inhibition of Ca2+/calmodulin kinase II. *J.Neurosci.* 19 (14):RC19, 1999.
42. V. Bhandawat, J. Reisert, and K. W. Yau. Elementary response of olfactory receptor neurons to odorants. *Science* 308 (5730):1931-1934, 2005.
43. F. F. Borisy, G. V. Ronnett, A. M. Cunningham, D. Juilfs, J. Beavo, and S. H. Snyder. Calcium/calmodulin-activated phosphodiesterase expressed in olfactory receptor neurons. *J.Neurosci.* 12 (3):915-923, 1992.

44. C. Yan, A. Z. Zhao, J. K. Bentley, K. Loughney, K. Ferguson, and J. A. Beavo. Molecular cloning and characterization of a calmodulin-dependent phosphodiesterase enriched in olfactory sensory neurons. *Proc.Natl.Acad.Sci.U.S.A* 92 (21):9677-9681, 1995.
45. J. Reisert and H. R. Matthews. Na+-dependent Ca2+ extrusion governs response recovery in frog olfactory receptor cells. *J.Gen.Physiol* 112 (5):529-535, 1998.
46. S. D. Weeraratne, M. Valentine, M. Cusick, R. Delay, and J. L. Van Houten. Plasma membrane calcium pumps in mouse olfactory sensory neurons. *Chem.Senses* 31 (8):725-730, 2006.
47. Rachel I. Wilson and Zachary F. Mainen. Early events in olfactory processing. *Annual Review of Neuroscience* 29 (1):163-201, 2006.
48. G. M. Shepherd. Perspectives on olfactory processing, conscious perception, and orbitofrontal cortex. *Ann.N.Y.Acad.Sci.*, 2007.
49. K. J. Ressler, S. L. Sullivan, and L. B. Buck. A zonal organization of odorant receptor gene expression in the olfactory epithelium. *Cell* 73 (3):597-609, 1993.
50. C. L. Iwema, H. Fang, D. B. Kurtz, S. L. Youngentob, and J. E. Schwob. Odorant receptor expression patterns are restored in lesion-recovered rat olfactory epithelium. *J.Neurosci.* 24 (2):356-369, 2004.
51. K. Miyamichi, S. Serizawa, H. M. Kimura, and H. Sakano. Continuous and overlapping expression domains of odorant receptor genes in the olfactory epithelium determine the dorsal/ventral positioning of glomeruli in the olfactory bulb. *J.Neurosci.* 25 (14):3586-3592, 2005.
52. G. A. Schwarting, D. Raitcheva, J. E. Crandall, C. Burkhardt, and A. W. Puschel. Semaphorin 3A-mediated axon guidance regulates convergence and targeting of P2 odorant receptor axons. *Eur.J.Neurosci.* 19 (7):1800-1810, 2004.
53. T. Cutforth, L. Moring, M. Mendelsohn, A. Nemes, N. M. Shah, M. M. Kim, J. Frisen, and R. Axel. Axonal ephrin-As and odorant receptors: coordinate determination of the olfactory sensory map. *Cell* 114 (3):311-322, 2003.
54. J. Freitag, J. Krieger, J. Strotmann, and H. Breer. Two classes of olfactory receptors in Xenopus laevis. *Neuron* 15 (6):1383-1392, 1995.
55. M. Mezler, J. Fleischer, and H. Breer. Characteristic features and ligand specificity of the two olfactory receptor classes from Xenopus laevis. *J.Exp.Biol.* 204 (Pt 17):2987-2997, 2001.

56. H. J. Fulle, R. Vassar, D. C. Foster, R. B. Yang, R. Axel, and D. L. Garbers. A receptor guanylyl cyclase expressed specifically in olfactory sensory neurons. *Proc.Natl.Acad.Sci.U.S.A* 92 (8):3571-3575, 1995.
57. D. M. Juilfs, H. J. Fulle, A. Z. Zhao, M. D. Houslay, D. L. Garbers, and J. A. Beavo. A subset of olfactory neurons that selectively express cGMP-stimulated phosphodiesterase (PDE2) and guanylyl cyclase-D define a unique olfactory signal transduction pathway. *Proc.Natl.Acad.Sci.U.S.A* 94 (7):3388-3395, 1997.
58. M. R. Meyer, A. Angele, E. Kremmer, U. B. Kaupp, and F. Muller. A cGMP-signaling pathway in a subset of olfactory sensory neurons. *Proc.Natl.Acad.Sci.U.S.A* 97 (19):10595-10600, 2000.
59. T. Leinders-Zufall, R. E. Cockerham, S. Michalakis, M. Biel, D. L. Garbers, R. R. Reed, F. Zufall, and S. D. Munger. Contribution of the receptor guanylyl cyclase GC-D to chemosensory function in the olfactory epithelium. *Proc.Natl.Acad.Sci.U.S.A* 104 (36):14507-14512, 2007.
60. J. Hu, C. Zhong, C. Ding, Q. Chi, A. Walz, P. Mombaerts, H. Matsunami, and M. Luo. Detection of near-atmospheric concentrations of CO2 by an olfactory subsystem in the mouse. *Science* 317 (5840):953-957, 2007.
61. G. S. Suh, A. M. Wong, A. C. Hergarden, J. W. Wang, A. F. Simon, S. Benzer, R. Axel, and D. J. Anderson. A single population of olfactory sensory neurons mediates an innate avoidance behaviour in Drosophila. *Nature* 431 (7010):854-859, 2004.
62. C. Thom, P. G. Guerenstein, W. L. Mechaber, and J. G. Hildebrand. Floral CO2 reveals flower profitability to moths. *J.Chem.Ecol.* 30 (6):1285-1288, 2004.
63. W. D. Jones, P. Cayirlioglu, I. G. Kadow, and L. B. Vosshall. Two chemosensory receptors together mediate carbon dioxide detection in Drosophila. *Nature* 445 (7123):86-90, 2007.
64. S. D. Liberles and L. B. Buck. A second class of chemosensory receptors in the olfactory epithelium. *Nature* 442 (7103):645-650, 2006.
65. M. A. Paulos and R. E. Tessel. Excretion of beta-phenethylamine is elevated in humans after profound stress. *Science* 215 (4536):1127-1129, 1982.
66. A. M. Snoddy, D. Heckathorn, and R. E. Tessel. Cold-restraint stress and urinary endogenous beta-phenylethylamine excretion in rats. *Pharmacol.Biochem.Behav.* 22 (3):497-500, 1985.
67. J. Grimsby, M. Toth, K. Chen, T. Kumazawa, L. Klaidman, J. D. Adams, F. Karoum, J. Gal, and J. C. Shih. Increased stress response and beta-phenylethylamine in MAOB-deficient mice. *Nat.Genet.* 17 (2):206-210, 1997.

68. C. L. Gavaghan McKee, I. D. Wilson, and J. K. Nicholson. Metabolic phenotyping of nude and normal (Alpk:ApfCD, C57BL10J) mice. *J.Proteome.Res.* 5 (2):378-384, 2006.
69. K. Nishimura, K. Utsumi, M. Yuhara, Y. Fujitani, and A. Iritani. Identification of puberty-accelerating pheromones in male mouse urine. *J.Exp.Zool.* 251 (3):300-305, 1989.
70. W. Lin, R. Margolskee, G. Donnert, S. W. Hell, and D. Restrepo. Olfactory neurons expressing transient receptor potential channel M5 (TRPM5) are involved in sensing semiochemicals. *Proc.Natl.Acad.Sci.U.S.A* 104 (7):2471-2476, 2007.
71. C. Dulac and R. Axel. A novel family of genes encoding putative pheromone receptors in mammals. *Cell* 83 (2):195-206, 1995.
72. N. J. Ryba and R. Tirindelli. A new multigene family of putative pheromone receptors. *Neuron* 19 (2):371-379, 1997.
73. G. Herrada and C. Dulac. A novel family of putative pheromone receptors in mammals with a topographically organized and sexually dimorphic distribution. *Cell* 90 (4):763-773, 1997.
74. H. Matsunami and L. B. Buck. A multigene family encoding a diverse array of putative pheromone receptors in mammals. *Cell* 90 (4):775-784, 1997.
75. E. Pantages and C. Dulac. A novel family of candidate pheromone receptors in mammals. *Neuron* 28 (3):835-845, 2000.
76. M. Halpern and A. Martinez-Marcos. Structure and function of the vomeronasal system: an update. *Prog.Neurobiol.* 70 (3):245-318, 2003.
77. C. Dulac and A. T. Torello. Molecular detection of pheromone signals in mammals: from genes to behaviour. *Nat Rev.Neurosci* 4 (7):551-562, 2003.
78. P. Mombaerts. Genes and ligands for odorant, vomeronasal and taste receptors. *Nat Rev.Neurosci* 5 (4):263-278, 2004.
79. X. Zhang, X. Zhang, and S. Firestein. Comparative genomics of odorant and pheromone receptor genes in rodents. *Genomics* 89 (4):441-450, 2007.
80. I. Rodriguez. Pheromone receptors in mammals. *Horm.Behav.* 46 (3):219-230, 2004.
81. P. Shi and J. Zhang. Comparative genomic analysis identifies an evolutionary shift of vomeronasal receptor gene repertoires in the vertebrate transition from water to land. *Genome Res.* 17 (2):166-174, 2007.
82. T. Ishii, J. Hirota, and P. Mombaerts. Combinatorial coexpression of neural and immune multigene families in mouse vomeronasal sensory neurons. *Curr.Biol.* 13 (5):394-400, 2003.
83. J. Loconto, F. Papes, E. Chang, L. Stowers, E. P. Jones, T. Takada, A. Kumanovics, Lindahl K. Fischer, and C. Dulac. Functional expression of murine V2R pheromone receptors

involves selective association with the M10 and M1 families of MHC class Ib molecules. *Cell* 112 (5):607-618, 2003.

84. T. Ishii and P. Mombaerts. Expression of nonclassical class I major histocompatibility genes defines a tripartite organization of the mouse vomeronasal system. *J.Neurosci.* 28 (10):2332-2341, 2008.
85. L. Silvotti, A. Moiani, R. Gatti, and R. Tirindelli. Combinatorial co-expression of pheromone receptors, V2Rs. *J Neurochem.*, 2007.
86. D. Krautwurst. Human olfactory receptor families and their odorants. *Chem.Biodivers.* 5 (6):842-852, 2008.
87. I. Rodriguez, C. A. Greer, M. Y. Mok, and P. Mombaerts. A putative pheromone receptor gene expressed in human olfactory mucosa. *Nat.Genet.* 26 (1):18-19, 2000.
88. M. Witt, B. Georgiewa, M. Knecht, and T. Hummel. On the chemosensory nature of the vomeronasal epithelium in adult humans. *Histochem.Cell Biol.* 117 (6):493-509, 2002.
89. M. Witt and T. Hummel. Vomeronasal versus olfactory epithelium: is there a cellular basis for human vomeronasal perception? *Int.Rev.Cytol.* 248:209-259, 2006.
90. E. R. Liman, D. P. Corey, and C. Dulac. TRP2: a candidate transduction channel for mammalian pheromone sensory signaling. *Proc.Natl.Acad.Sci.U.S.A* 96 (10):5791-5796, 1999.
91. L. Stowers, T. E. Holy, M. Meister, C. Dulac, and G. Koentges. Loss of sex discrimination and male-male aggression in mice deficient for TRP2. *Science* 295 (5559):1493-1500, 2002.
92. B. G. Leypold, C. R. Yu, T. Leinders-Zufall, M. M. Kim, F. Zufall, and R. Axel. Altered sexual and social behaviors in trp2 mutant mice. *Proc.Natl.Acad.Sci.U.S.A* 99 (9):6376-6381, 2002.
93. K. Inamura, M. Kashiwayanagi, and K. Kurihara. Blockage of urinary responses by inhibitors for IP3-mediated pathway in rat vomeronasal sensory neurons. *Neurosci.Lett.* 233 (2-3):129-132, 1997.
94. I. Rodriguez, P. Feinstein, and P. Mombaerts. Variable patterns of axonal projections of sensory neurons in the mouse vomeronasal system. *Cell* 97 (2):199-208, 1999.
95. L. Belluscio, G. Koentges, R. Axel, and C. Dulac. A map of pheromone receptor activation in the mammalian brain. *Cell* 97 (2):209-220, 1999.
96. P. A. Brennan and F. Zufall. Pheromonal communication in vertebrates. *Nature* 444 (7117):308-315, 2006.
97. M. Sam, S. Vora, B. Malnic, W. Ma, M. V. Novotny, and L. B. Buck. Neuropharmacology. Odorants may arouse instinctive behaviours. *Nature* 412 (6843):142, 2001.

98. K. Trinh and D. R. Storm. Vomeronasal organ detects odorants in absence of signaling through main olfactory epithelium. *Nat.Neurosci.* 6 (5):519-525, 2003.

99. O. Levai, T. Feistel, H. Breer, and J. Strotmann. Cells in the vomeronasal organ express odorant receptors but project to the accessory olfactory bulb. *J.Comp Neurol.* 498 (4):476-490, 2006.

100. B. Schaal, G. Coureaud, D. Langlois, C. Ginies, E. Semon, and G. Perrier. Chemical and behavioural characterization of the rabbit mammary pheromone. *Nature* 424 (6944):68-72, 2003.

101. R. Hudson and H. Distel. Pheromonal release of suckling in rabbits does not depend on the vomeronasal organ. *Physiol Behav.* 37 (1):123-128, 1986.

102. K. M. Dorries, E. Adkins-Regan, and B. P. Halpern. Sensitivity and behavioral responses to the pheromone androstenone are not mediated by the vomeronasal organ in domestic pigs. *Brain Behav.Evol.* 49 (1):53-62, 1997.

103. D. Y. Lin, S. Z. Zhang, E. Block, and L. C. Katz. Encoding social signals in the mouse main olfactory bulb. *Nature* 434 (7032):470-477, 2005.

104. W. Lin, J. Arellano, B. Slotnick, and D. Restrepo. Odors detected by mice deficient in cyclic nucleotide-gated channel subunit A2 stimulate the main olfactory system. *J.Neurosci.* 24 (14):3703-3710, 2004.

105. S. Takigami, Y. Mori, and M. Ichikawa. Projection pattern of vomeronasal neurons to the accessory olfactory bulb in goats. *Chem.Senses* 25 (4):387-393, 2000.

106. S. Takigami, Y. Mori, Y. Tanioka, and M. Ichikawa. Morphological evidence for two types of Mammalian vomeronasal system. *Chem.Senses* 29 (4):301-310, 2004.

107. Y. Wakabayashi, Y. Mori, M. Ichikawa, K. Yazaki, and K. Hagino-Yamagishi. A putative pheromone receptor gene is expressed in two distinct olfactory organs in goats. *Chem.Senses* 27 (3):207-213, 2002.

108. Y. Wakabayashi, S. Ohkura, H. Okamura, Y. Mori, and M. Ichikawa. Expression of a vomeronasal receptor gene (V1r) and G protein alpha subunits in goat, Capra hircus, olfactory receptor neurons. *J.Comp Neurol.* 503 (2):371-380, 2007.

109. A. Date-Ito, H. Ohara, M. Ichikawa, Y. Mori, and K. Hagino-Yamagishi. Xenopus V1R vomeronasal receptor family is expressed in the main olfactory system. *Chem.Senses* 33 (4):339-346, 2008.

110. D. K. Karunadasa, C. Chapman, and R. J. Bicknell. Expression of pheromone receptor gene families during olfactory development in the mouse: expression of a V1 receptor in the main olfactory epithelium. *Eur.J.Neurosci.* 23 (10):2563-2572, 2006.

111. A. R. Genazzani, F. Bernardi, P. Monteleone, S. Luisi, and M. Luisi. Neuropeptides, neurotransmitters, neurosteroids, and the onset of puberty. *Ann.N.Y.Acad.Sci.* 900:1-9, 2000.

112. T. J. Wu, M. J. Gibson, M. C. Rogers, and A. J. Silverman. New observations on the development of the gonadotropin-releasing hormone system in the mouse. *J.Neurobiol.* 33 (7):983-998, 1997.

113. I. Merchenthaler, G. Setalo, P. Petrusz, A. Negro-Vilar, and B. Flerko. Identification of hypophysiotropic luteinizing hormone-releasing hormone (LHRH) neurons by combined retrograde labeling and immunocytochemistry. *Exp.Clin.Endocrinol.* 94 (1-2):133-140, 1989.

114. H. Yoon, L. W. Enquist, and C. Dulac. Olfactory inputs to hypothalamic neurons controlling reproduction and fertility. *Cell* 123 (4):669-682, 2005.

115. K. R. Kelliher, M. Spehr, X. H. Li, F. Zufall, and T. Leinders-Zufall. Pheromonal recognition memory induced by TRPC2-independent vomeronasal sensing. *Eur.J.Neurosci.* 23 (12):3385-3390, 2006.

116. P. B. Singh, R. E. Brown, and B. Roser. MHC antigens in urine as olfactory recognition cues. *Nature* 327 (6118):161-164, 1987.

117. W. C. Jordan and M. W. Bruford. New perspectives on mate choice and the MHC. *Heredity* 81 (Pt 3):239-245, 1998.

118. K. Yamazaki, G. K. Beauchamp, M. Curran, J. Bard, and E. A. Boyse. Parent-progeny recognition as a function of MHC odortype identity. *Proc.Natl.Acad.Sci.U.S.A* 97 (19):10500-10502, 2000.

119. E. A. Boyse, G. K. Beauchamp, and K. Yamazaki. Critical review: the sensory perception of genotypic polymorphism of the major histocompatibility complex and other genes: some physiological and phylogenetic implications. *Hum.Immunol.* 6 (4):177-183, 1983.

120. T. Leinders-Zufall, P. Brennan, P. Widmayer, S. PC, A. Maul-Pavicic, M. Jager, X. H. Li, H. Breer, F. Zufall, and T. Boehm. MHC class I peptides as chemosensory signals in the vomeronasal organ. *Science* 306 (5698):1033-1037, 2004.

121. M. Spehr, K. R. Kelliher, X. H. Li, T. Boehm, T. Leinders-Zufall, and F. Zufall. Essential role of the main olfactory system in social recognition of major histocompatibility complex peptide ligands. *J.Neurosci.* 26 (7):1961-1970, 2006.

122. D. Penn and W. K. Potts. Untrained mice discriminate MHC-determined odors. *Physiol Behav.* 64 (3):235-243, 1998.

123. P. Carninci, T. Kasukawa, S. Katayama, J. Gough, M. C. Frith, N. Maeda, R. Oyama, T. Ravasi, B. Lenhard, C. Wells, R. Kodzius, K. Shimokawa, V. B. Bajic, S. E. Brenner, S. Batalov, A. R. Forrest, M. Zavolan, M. J. Davis, L. G. Wilming, V. Aidinis, J. E. Allen, A. Ambesi-Impiombato, R. Apweiler, R. N. Aturaliya, T. L. Bailey, M. Bansal, L. Baxter, K. W. Beisel, T. Bersano, H. Bono, A. M. Chalk, K. P. Chiu, V. Choudhary, A. Christoffels, D. R. Clutterbuck, M. L. Crowe, E. Dalla, B. P. Dalrymple, B. de Bono, Gatta G. Della, D. di Bernardo, T. Down, P. Engstrom, M. Fagiolini, G. Faulkner, C. F. Fletcher, T. Fukushima, M. Furuno, S. Futaki, M. Gariboldi, P. Georgii-Hemming, T. R. Gingeras, T. Gojobori, R. E. Green, S. Gustincich, M. Harbers, Y. Hayashi, T. K. Hensch, N. Hirokawa, D. Hill, L. Huminiecki, M. Iacono, K. Ikeo, A. Iwama, T. Ishikawa, M. Jakt, A. Kanapin, M. Katoh, Y. Kawasawa, J. Kelso, H. Kitamura, H. Kitano, G. Kollias, S. P. Krishnan, A. Kruger, S. K. Kummerfeld, I. V. Kurochkin, L. F. Lareau, D. Lazarevic, L. Lipovich, J. Liu, S. Liuni, S. McWilliam, Babu M. Madan, M. Madera, L. Marchionni, H. Matsuda, S. Matsuzawa, H. Miki, F. Mignone, S. Miyake, K. Morris, S. Mottagui-Tabar, N. Mulder, N. Nakano, H. Nakauchi, P. Ng, R. Nilsson, S. Nishiguchi, S. Nishikawa, F. Nori, O. Ohara, Y. Okazaki, V. Orlando, K. C. Pang, W. J. Pavan, G. Pavesi, G. Pesole, N. Petrovsky, S. Piazza, J. Reed, J. F. Reid, B. Z. Ring, M. Ringwald, B. Rost, Y. Ruan, S. L. Salzberg, A. Sandelin, C. Schneider, C. Schonbach, K. Sekiguchi, C. A. Semple, S. Seno, L. Sessa, Y. Sheng, Y. Shibata, H. Shimada, K. Shimada, D. Silva, B. Sinclair, S. Sperling, E. Stupka, K. Sugiura, R. Sultana, Y. Takenaka, K. Taki, K. Tammoja, S. L. Tan, S. Tang, M. S. Taylor, J. Tegner, S. A. Teichmann, H. R. Ueda, E. van Nimwegen, R. Verardo, C. L. Wei, K. Yagi, H. Yamanishi, E. Zabarovsky, S. Zhu, A. Zimmer, W. Hide, C. Bult, S. M. Grimmond, R. D. Teasdale, E. T. Liu, V. Brusic, J. Quackenbush, C. Wahlestedt, J. S. Mattick, D. A. Hume, C. Kai, D. Sasaki, Y. Tomaru, S. Fukuda, M. Kanamori-Katayama, M. Suzuki, J. Aoki, T. Arakawa, J. Iida, K. Imamura, M. Itoh, T. Kato, H. Kawaji, N. Kawagashira, T. Kawashima, M. Kojima, S. Kondo, H. Konno, K. Nakano, N. Ninomiya, T. Nishio, M. Okada, C. Plessy, K. Shibata, T. Shiraki, S. Suzuki, M. Tagami, K. Waki, A. Watahiki, Y. Okamura-Oho, H. Suzuki, J. Kawai, and Y. Hayashizaki. The transcriptional landscape of the mammalian genome. *Science* 309 (5740):1559-1563, 2005.

124. D. Kampa, J. Cheng, P. Kapranov, M. Yamanaka, S. Brubaker, S. Cawley, J. Drenkow, A. Piccolboni, S. Bekiranov, G. Helt, H. Tammana, and T. R. Gingeras. Novel RNAs identified from an in-depth analysis of the transcriptome of human chromosomes 21 and 22. *Genome Res.* 14 (3):331-342, 2004.

125. J. Cheng, P. Kapranov, J. Drenkow, S. Dike, S. Brubaker, S. Patel, J. Long, D. Stern, H. Tammana, G. Helt, V. Sementchenko, A. Piccolboni, S. Bekiranov, D. K. Bailey, M. Ganesh, S. Ghosh, I. Bell, D. S. Gerhard, and T. R. Gingeras. Transcriptional maps of 10 human chromosomes at 5-nucleotide resolution. *Science* 308 (5725):1149-1154, 2005.

126. R. Kodzius, M. Kojima, H. Nishiyori, M. Nakamura, S. Fukuda, M. Tagami, D. Sasaki, K. Imamura, C. Kai, M. Harbers, Y. Hayashizaki, and P. Carninci. CAGE: cap analysis of gene expression. *Nat.Methods* 3 (3):211-222, 2006.

127. T. Shiraki, S. Kondo, S. Katayama, K. Waki, T. Kasukawa, H. Kawaji, R. Kodzius, A. Watahiki, M. Nakamura, T. Arakawa, S. Fukuda, D. Sasaki, A. Podhajska, M. Harbers, J. Kawai, P. Carninci, and Y. Hayashizaki. Cap analysis gene expression for high-throughput analysis of transcriptional starting point and identification of promoter usage. *Proc.Natl.Acad.Sci.U.S.A* 100 (26):15776-15781, 2003.

128. M. Harbers and P. Carninci. Tag-based approaches for transcriptome research and genome annotation. *Nat.Methods* 2 (7):495-502, 2005.

129. P. Carninci. Tagging mammalian transcription complexity. *Trends Genet.* 22 (9):501-510, 2006.

130. X. Zhang, M. Rogers, H. Tian, X. Zhang, D. J. Zou, J. Liu, M. Ma, G. M. Shepherd, and S. J. Firestein. High-throughput microarray detection of olfactory receptor gene expression in the mouse. *Proc.Natl.Acad.Sci.U.S.A* 101 (39):14168-14173, 2004.

131. E. Feldmesser, T. Olender, M. Khen, I. Yanai, R. Ophir, and D. Lancet. Widespread ectopic expression of olfactory receptor genes. *BMC.Genomics* 7:121, 2006.

132. X. Zhang, Cruz O. De la, J. M. Pinto, D. Nicolae, S. Firestein, and Y. Gilad. Characterizing the expression of the human olfactory receptor gene family using a novel DNA microarray. *Genome Biol.* 8 (5):R86, 2007.

133. N. Sammeta, T. T. Yu, S. C. Bose, and T. S. McClintock. Mouse olfactory sensory neurons express 10,000 genes. *J.Comp Neurol.* 502 (6):1138-1156, 2007.

134. P. S. Choi, L. Zakhary, W. Y. Choi, S. Caron, E. Alvarez-Saavedra, E. A. Miska, M. McManus, B. Harfe, A. J. Giraldez, R. H. Horvitz, A. F. Schier, and C. Dulac. Members of the miRNA-200 family regulate olfactory neurogenesis. *Neuron* 57 (1):41-55, 2008.

135. R. Elsaesser and J. Paysan. Morituri te salutant? Olfactory signal transduction and the role of phosphoinositides. *J.Neurocytol.* 34 (1-2):97-116, 2005.

136. S. J. Kleene. Origin of the chloride current in olfactory transduction. *Neuron* 11 (1):123-132, 1993.

137. K. Yu, Z. Qu, Y. Cui, and H. C. Hartzell. Chloride channel activity of bestrophin mutants associated with mild or late-onset macular degeneration. *Invest Ophthalmol.Vis.Sci.* 48 (10):4694-4705, 2007.

138. H. Sun, T. Tsunenari, K. W. Yau, and J. Nathans. The vitelliform macular dystrophy protein defines a new family of chloride channels. *Proc.Natl.Acad.Sci.U.S.A* 99 (6):4008-4013, 2002.

139. T. Tsunenari, H. Sun, J. Williams, H. Cahill, P. Smallwood, K. W. Yau, and J. Nathans. Structure-function analysis of the bestrophin family of anion channels. *J.Biol.Chem.* 278 (42):41114-41125, 2003.

140. F. Jourdan. [Ultrastructure of the olfactory epithelium of the rat: polymorphism of the receptors]. *C.R.Acad.Sci.Hebd.Seances Acad.Sci.D.* 280 (4):443-446, 1975.

141. E. Asan and D. Drenckhahn. Immunocytochemical characterization of two types of microvillar cells in rodent olfactory epithelium. *Histochem.Cell Biol.* 123 (2):157-168, 2005.

142. D. T. Moran, J. C. Rowley, III, and B. W. Jafek. Electron microscopy of human olfactory epithelium reveals a new cell type: the microvillar cell. *Brain Res.* 253 (1-2):39-46, 1982.

143. J. C. Rowley, III, D. T. Moran, and B. W. Jafek. Peroxidase backfills suggest the mammalian olfactory epithelium contains a second morphologically distinct class of bipolar sensory neuron: the microvillar cell. *Brain Res.* 502 (2):387-400, 1989.

144. V. M. Carr, A. I. Farbman, L. M. Colletti, and J. I. Morgan. Identification of a new non-neuronal cell type in rat olfactory epithelium. *Neuroscience* 45 (2):433-449, 1991.

145. R. Elsaesser, G. Montani, R. Tirindelli, and J. Paysan. Phosphatidyl-inositide signalling proteins in a novel class of sensory cells in the mammalian olfactory epithelium. *Eur.J.Neurosci.* 21 (10):2692-2700, 2005.

146. G. Montani, S. Tonelli, R. Elsaesser, J. Paysan, and R. Tirindelli. Neuropeptide Y in the olfactory microvillar cells. *Eur.J.Neurosci.* 24 (1):20-24, 2006.

147. P. Pro-Sistiaga, A. Mohedano-Moriano, I. Ubeda-Banon, M. Mar Arroyo-Jimenez, P. Marcos, E. Artacho-Perula, C. Crespo, R. Insausti, and A. Martinez-Marcos. Convergence of olfactory and vomeronasal projections in the rat basal telencephalon. *J.Comp Neurol.* 504 (4):346-362, 2007.

148. L. Lagostena and A. Menini. Whole-cell recordings and photolysis of caged compounds in olfactory sensory neurons isolated from the mouse. *Chem.Senses* 28 (8):705-716, 2003.

149. A. Boccaccio, L. Lagostena, V. Hagen, and A. Menini. Fast adaptation in mouse olfactory sensory neurons does not require the activity of phosphodiesterase. *J.Gen.Physiol* 128 (2):171-184, 2006.

150. A. Keller and F. L. Margolis. Immunological studies of the rat olfactory marker protein. *J.Neurochem.* 24 (6):1101-1106, 1975.

151. K. Schutze and G. Lahr. Identification of expressed genes by laser-mediated manipulation of single cells. *Nat.Biotechnol.* 16 (8):737-742, 1998.

152. T. Tsunenari, J. Nathans, and K. W. Yau. Ca2+-activated Cl- current from human bestrophin-4 in excised membrane patches. *J.Gen.Physiol* 127 (6):749-754, 2006.

153. B. Bakall, P. McLaughlin, J. B. Stanton, Y. Zhang, H. C. Hartzell, L. Y. Marmorstein, and A. D. Marmorstein. Bestrophin-2 is involved in the generation of intraocular pressure. *Invest Ophthalmol.Vis.Sci.* 49 (4):1563-1570, 2008.

154. S. J. Scheidl, S. Nilsson, M. Kalen, M. Hellstrom, M. Takemoto, J. Hakansson, and P. Lindahl. mRNA expression profiling of laser microbeam microdissected cells from slender embryonic structures. *Am.J.Pathol.* 160 (3):801-813, 2002.

155. J. Kawai, A. Shinagawa, K. Shibata, M. Yoshino, M. Itoh, Y. Ishii, T. Arakawa, A. Hara, Y. Fukunishi, H. Konno, J. Adachi, S. Fukuda, K. Aizawa, M. Izawa, K. Nishi, H. Kiyosawa, S. Kondo, I. Yamanaka, T. Saito, Y. Okazaki, T. Gojobori, H. Bono, T. Kasukawa, R. Saito, K. Kadota, H. Matsuda, M. Ashburner, S. Batalov, T. Casavant, W. Fleischmann, T. Gaasterland, C. Gissi, B. King, H. Kochiwa, P. Kuehl, S. Lewis, Y. Matsuo, I. Nikaido, G. Pesole, J. Quackenbush, L. M. Schriml, F. Staubli, R. Suzuki, M. Tomita, L. Wagner, T. Washio, K. Sakai, T. Okido, M. Furuno, H. Aono, R. Baldarelli, G. Barsh, J. Blake, D. Boffelli, N. Bojunga, P. Carninci, M. F. de Bonaldo, M. J. Brownstein, C. Bult, C. Fletcher, M. Fujita, M. Gariboldi, S. Gustincich, D. Hill, M. Hofmann, D. A. Hume, M. Kamiya, N. H. Lee, P. Lyons, L. Marchionni, J. Mashima, J. Mazzarelli, P. Mombaerts, P. Nordone, B. Ring, M. Ringwald, I. Rodriguez, N. Sakamoto, H. Sasaki, K. Sato, C. Schonbach, T. Seya, Y. Shibata, K. F. Storch, H. Suzuki, K. Toyo-oka, K. H. Wang, C. Weitz, C. Whittaker, L. Wilming, A. Wynshaw-Boris, K. Yoshida, Y. Hasegawa, H. Kawaji, S. Kohtsuki, and Y. Hayashizaki. Functional annotation of a full-length mouse cDNA collection. *Nature* 409 (6821):685-690, 2001.

156. M. C. Frith, E. Valen, A. Krogh, Y. Hayashizaki, P. Carninci, and A. Sandelin. A code for transcription initiation in mammalian genomes. *Genome Res.* 18 (1):1-12, 2008.

157. G. J. Faulkner, A. R. Forrest, A. M. Chalk, K. Schroder, Y. Hayashizaki, P. Carninci, D. A. Hume, and S. M. Grimmond. A rescue strategy for multimapping short sequence tags refines surveys of transcriptional activity by CAGE. *Genomics* 91 (3):281-288, 2008.

158. S. M. Fleming, N. A. Tetreault, C. K. Mulligan, C. B. Hutson, E. Masliah, and M. F. Chesselet. Olfactory deficits in mice overexpressing human wildtype alpha-synuclein. *Eur.J.Neurosci.* 28 (2):247-256, 2008.

159. A. Berghard and L. B. Buck. Sensory transduction in vomeronasal neurons: evidence for G alpha o, G alpha i2, and adenylyl cyclase II as major components of a pheromone signaling cascade. *J.Neurosci.* 16 (3):909-918, 1996.

160. C. A. Pfeiffer and R. E. Johnston. Hormonal and behavioral responses of male hamsters to females and female odors: roles of olfaction, the vomeronasal system, and sexual experience. *Physiol Behav.* 55 (1):129-138, 1994.

Acknowledgements

I want to warmly thank Prof. Stefano Gusitncich for agreeing to admit me as a Ph.D. student in his laboratory, for being a precious guide, for trusting my skills also when I doubted them, for his ability to look further than anyone else while firmly believing in what he looked at.

I would like to thank also all the people that have helped me in this path: PostDocs, Ph.D. colleagues, friends. Very special thanks go to a very special person, Dr. Dejan Lazarevic, for contributing to this thesis every single day with unvaluable critical comments.
My gratitude goes also to Dr. Silvia Zucchelli for her helpfulness and for her worthy training during my first months in Stefano's lab, to Dr. Zeno Scotto Lavina and Dr. Marta Biagioli for their patience and useful advices, to all people at RIKEN Institute for their irreplaceable work and to Prof. Anna Menini for her kindness.

I am particularly grateful to all of my Ph.D. comrades: Matteo, Dario, Silvia, Anil, Alessandra, Roberto, Milena, Sudhir, Claudia, Rossana, Paolo, Christina and Sandra for all the laughs and emotions we have shared and, of course, for their scientific suggestions.

In the end, I want to heartily and joyfully thank Marina for being so close to me in every single moment of these last months.

This thesis is dedicated to my family, with the deepest love.

Appendix A:

Publications.